NAVAL POSTGRADUATE SCHOOL

MONTEREY, CALIFORNIA

THESIS

FREQUENCY AND POLARIZATION DIVERSITY SIMULATIONS FOR URBAN UAV COMMUNICATION AND DATA LINKS

by

Fatih PALA

September 2004

Thesis Advisor:	David C. Jenn
Second Reader:	Daniel C. Schleher

Approved for public release, distribution is unlimited

THIS PAGE INTENTIONALLY LEFT BLANK

REPORT DOCUMENTATION PAGE			Form Approved OMB No. 0704-0188
Public reporting burden for this collection of information is estimated to average 1 hour per response, including the time for reviewing instruction, searching existing data sources, gathering and maintaining the data needed, and completing and reviewing the collection of information. Send comments regarding this burden estimate or any other aspect of this collection of information, including suggestions for reducing this burden, to Washington headquarters Services, Directorate for Information Operations and Reports, 1215 Jefferson Davis Highway, Suite 1204, Arlington, VA 22202-4302, and to the Office of Management and Budget, Paperwork Reduction Project (0704-0188) Washington DC 20503.			
1. AGENCY USE ONLY ***(Leave blank)***	**2. REPORT DATE** September 2004	**3. REPORT TYPE AND DATES COVERED** Master's Thesis	
4. TITLE AND SUBTITLE: Frequency and Polarization Diversity Simulations for Urban UAV Communication and Data Links			**5. FUNDING NUMBERS**
6. AUTHOR(S) Fatih PALA			
7. PERFORMING ORGANIZATION NAME(S) AND ADDRESS(ES) Naval Postgraduate School Monterey, CA 93943-5000			**8. PERFORMING ORGANIZATION REPORT NUMBER**
9. SPONSORING /MONITORING AGENCY NAME(S) AND ADDRESS(ES) N/A			**10. SPONSORING/MONITORING AGENCY REPORT NUMBER**
11. SUPPLEMENTARY NOTES The views expressed in this thesis are those of the author and do not reflect the official policy or position of the Department of Defense or the U.S. Government.			
12a. DISTRIBUTION / AVAILABILITY STATEMENT Approved for public release, distribution is unlimited			**12b. DISTRIBUTION CODE**

13. ABSTRACT (maximum 200 words)

The purpose of this research was to examine the effects of frequency, and polarization on radio wave propagation in urbanized areas for unmanned aerial vehicle (UAV) data links, and command and control.

The transmission from a UAV operating over a small city was simulated using the Urbana Wireless Toolset. Parameters that were varied include frequency, antenna polarization, UAV altitude, and building materials. Multiple reflections and diffractions were included in the simulation. In each case signal contours were generated at discrete frequencies over a 50 MHz bandwidth. It was observed that the signal levels varied up to over the bands at a fixed observation point due to frequency-dependent reflection and diffraction.

14. SUBJECT TERMS Unmanned aerial vehicles, Propagation models, Urbana wireless toolset, Frequency diversity, Polarization diversity, Communication and data links			**15. NUMBER OF PAGES** 135
			16. PRICE CODE
17. SECURITY CLASSIFICATION OF REPORT Unclassified	**18. SECURITY CLASSIFICATION OF THIS PAGE** Unclassified	**19. SECURITY CLASSIFICATION OF ABSTRACT** Unclassified	**20. LIMITATION OF ABSTRACT** UL

NSN 7540-01-280-5500 Standard Form 298 (Rev. 2-89)
Prescribed by ANSI Std. 239-18

THIS PAGE INTENTIONALLY LEFT BLANK

Approved for public release, distribution is unlimited

FREQUENCY AND POLARIZATION DIVERSITY SIMULATIONS FOR URBAN UAV COMMUNICATION AND DATA LINKS

Fatih PALA
1st. Lieutenant, Turkish Air Force
B.S., Turkish Air Force Academy, 1996

Submitted in partial fulfillment of the
requirements for the degree of

MASTER OF SCIENCE IN SYSTEMS ENGINEERING

from the

NAVAL POSTGRADUATE SCHOOL
September 2004

Author: Fatih PALA

Approved by: David C. Jenn
Thesis Advisor

Daniel C. Schleher
Second Reader

Dan Boger
Chairman, Department of Information Sciences

THIS PAGE INTENTIONALLY LEFT BLANK

ABSTRACT

The purpose of this research was to examine the effects of frequency, and polarization on radio wave propagation in urbanized areas for unmanned aerial vehicle (UAV) data links, and command and control.

The transmission from a UAV operating over a small city was simulated using the Urbana Wireless Toolset. Parameters that were varied include frequency, antenna polarization, UAV altitude, and building materials. Multiple reflections and diffractions were included in the simulation. In each case signal contours were generated at discrete frequencies over a 50 MHz bandwidth. It was observed that the signal levels varied up to ±5 dB over the bands at a fixed observation point due to frequency-dependent reflection and diffraction.

THIS PAGE INTENTIONALLY LEFT BLANK

TABLE OF CONTENTS

I. INTRODUCTION....1
A. APPLICATIONS OF UNMANNED AERIAL VEHICLES....1
B. PROPAGATION ISSUES FOR UAVS....4
C. OBJECTIVE....6
D. TECHNICAL APPROACH....6
E. THESIS OUTLINE....9

II. PROPAGATION AND ANTENNA FUNDAMENTALS....11
A. BASIC PROPAGATION MECHANISMS....11
1. Reflection....12
2. Diffraction and Geometric Theory of Diffraction....15
3. Diffuse Scattering and Rayleigh Scattering....17
4. Absorption....19
5. Path Loss....19
6. Fresnel Zones....21
B. ANTENNA FUNDAMENTALS....22
1. Radiation Pattern and Parameters....22
2. Polarization of Antennas....24
3. Smart Antennas....26
C. SUMMARY....27

III. PROPAGATION MODELS AND TOOLSETS....29
A. BASIC PROPAGATION MODELS....29
1. Theoretical Models....30
a. The Walfisch Model (Diffracting Screens Model)....30
b. The COST 231 Model (The COST-WI Model)....30
c. The Longley-Rice Model (The ITS Irregular Terrain Model)....31
2. Empirical Models....31
a. The Okumura Signal Prediction Model....32
b. The Hata and Modified Hata Model....32
c. Ibrahim and Parsons Model (The London Model)....34
B. URBANA WIRELESS TOOLSET....35
1. Basic Urbana Capability....35
a. Generating Input Data Files....38
b. Generating Urbana Input File (runname.ur_input)....39
c. Post Processing Steps....40
2. Urbana, XCell, and Cifer....40
3. Running Urbana on the Silicon Graphics (SGI) Workstations....40
4. Capturing, Converting, and Sending Files between SGIs and PCs....41
C. SUMMARY....41

IV. URBANA SIMULATION....43

A. GENERATING SIMULATION MODELS....43
1. Small City Model....43
2. Generating Observation Points....46
3. Converting Field Files with *f2f.x*....46
4. Antenna Parameters for Simulations....47
B. DIFFERENT ANTENNA ALTITUDES SCENARIO....48
1. Changing the Antenna Altitude....50
2. Conclusions Regarding Altitude....54
C. MATERIAL SELECTION SIMULATIONS....54
1. Generating Two-Building Simulation Environment....55
2. PEC, Wood, Concrete, and Glass Material Simulations....55
3. Material Simulation Conclusions....59
D. FREQUENCY SIMULATIONS....59
1. Differential Signal Plots with f2fd.x....60
2. Simulations of the 900 MHz Frequency Band....60
3. Simulations of the 2.4 GHz Frequency Band....66
4. Simulations of the 5.0 GHz Frequency Band....71
5. Frequency Simulation Conclusions....76
E. SIMULATIONS FOR DIFFERENT POLARIZATIONS....76
1. Polarization Difference Simulation for 900 MHz....77
2. Polarization Difference Simulations for 2.4 GHz....81
3. Polarization Difference Simulations for 5.0 GHz....85
F. NOISE BANDWIDTH AND EFFECTIVE BANDWIDTH....90
1. Noise Bandwidth Calculations....92
2. Effective Bandwidth Calculations....93

V. SUMMARY AND CONCLUSION....95
A. SUMMARY....95
B. CONCLUSIONS AND FUTURE WORK....95

APPENDIX....99
A. MATLAB CODES....99
B. URBANA INPUT SCRIPT FILE....105

LIST OF REFERENCES....113

INITIAL DISTRIBUTION LIST....117

LIST OF FIGURES

Figure 1. Multipath propagation due to reflection and diffraction. For clarity only a few reflections and diffractions are shown. 5
Figure 2. Hypothetical plot of transmission coefficient vs. frequency for an urban environment (the range dependency has been removed). 7
Figure 3. Horizontal and vertical polarizations generated by linearly polarized antennas 8
Figure 4. Illustration of propagation mechanisms. 12
Figure 5. (a) Perpendicular, and (b) parallel polarized incident wave on a boundary. (From Ref. [9].) 12
Figure 6. Reflection coefficients versus incident angle for some non-magnetic materials. 14
Figure 7. Reflection of a ray tube at a planar interface. (From Ref. [7]) 15
Figure 8. Geometry for three-dimensional wedge diffraction. 16
Figure 9. Reflection from an irregularity of height h (From Ref. [3]). 18
Figure 10. Free space propagation loss versus frequency. 20
Figure 11. Fresnel zone clearance. 22
Figure 12. (a) Ideal dipole. (b) H-plane radiation pattern (c) E-plane radiation pattern. 23
Figure 13. Normalized half-wave dipole power radiation pattern. 24
Figure 14. (a) Switched and (b) Adaptive beam antenna coverage (From Ref [16]). 27
Figure 15. Urbana suite of software codes. 37
Figure 16. Top view of the small city model. 44
Figure 17. Oblique view of the small city model. 44
Figure 18. Three-dimensional matched edge representation of the small city. 45
Figure 19. Small-city model with ground plane. 46
Figure 20. Small city with a vertical polarized antenna at $x = 0$ m, $y = -50$ m, $z = 30$ m 48
Figure 21. Signal contours for PEC buildings. An additional building was added to form an urban canyon along the y axis. 50
Figure 22. Signal levels for an antenna location of $(0\text{ m}, -50\text{ m}, 30\text{ m})$. 51
Figure 23. Signal levels for an antenna location of $(0\text{ m}, -50\text{ m}, 150\text{ m})$ 51
Figure 24. Signal levels for an antenna location of $(0\text{ m}, -50\text{ m}, 300\text{ m})$. 52
Figure 25. Signal levels for an antenna location of $(0\text{ m}, -50\text{ m}, 450\text{ m})$. 53
Figure 26. Signal levels for an antenna location of $(0\text{ m}, -50\text{ m}, 600\text{ m})$. 53
Figure 27. Three-dimensional representation of facets (left), edges (right), and antenna (top). 55
Figure 28. PEC material 56
Figure 29. Wood material 56
Figure 30. Concrete material 57
Figure 31. Glass material 58
Figure 32. Different wall materials: (a) PEC, (b) concrete, (c) wood, and (d) glass. 58
Figure 33. Vertical polarized antenna, 875 MHz 61

Figure 34. Vertical polarized antenna, 887.5 MHz 61
Figure 35. Vertical polarized antenna, 900 MHz 62
Figure 36. Vertical polarized antenna, 912.5 MHz 62
Figure 37. Vertical polarized antenna, 925 MHz 63
Figure 38. Frequency difference, 900 MHz - 875 MHz 64
Figure 39. Frequency difference, 900 MHz - 887.5 MHz 64
Figure 40. Frequency difference, 900 MHz - 912.5 MHz 65
Figure 41. Frequency difference, 900 MHz – 925 MHz 65
Figure 42. Vertical polarized antenna, 2.375 GHz 66
Figure 43. Vertical polarized antenna, 2.3875 GHz 67
Figure 44. Vertical polarized antenna, 2.4 GHz 67
Figure 45. Vertical polarized antenna, 2.4125 GHz 68
Figure 46. Vertical polarized antenna, 2.425 GHz 68
Figure 47. Frequency difference, 2.4 GHz – 2.375 GHz 69
Figure 48. Frequency difference, 2.4 GHz – 2.3875 GHz 69
Figure 49. Frequency difference, 2.4 GHz – 2.4125 GHz 70
Figure 50. Frequency difference, 2.4 GHz – 2.425 GHz 70
Figure 51. Vertical polarized antenna, 4.975 GHz 71
Figure 52. Vertical polarized antenna, 4.9875 GHz 72
Figure 53. Vertical polarized antenna, 5.0 GHz 72
Figure 54. Vertical polarized antenna, 5.0125 GHz 73
Figure 55. Vertical polarized antenna, 5.025 GHz 73
Figure 56. Frequency difference, 5.0 GHz – 4.975 GHz 74
Figure 57. Frequency difference, 5.0 GHz – 4.9875 GHz 74
Figure 58. Frequency difference, 5.0 GHz – 5.0125 GHz 75
Figure 59. Frequency difference, 5.0 GHz – 5.025 GHz 75
Figure 60. Horizontal polarized antenna, 900 MHz 78
Figure 61. Polarization comparison for 900 MHz (a) vertical and (b) horizontal 78
Figure 62. Polarization difference, 875 MHz 79
Figure 63. Polarization difference, 887.5 MHz 79
Figure 64. Polarization difference, 900 MHz 80
Figure 65. Polarization difference, 912.5 MHz 80
Figure 66. Polarization difference, 925 MHz 81
Figure 67. Vertical polarized antenna, 2.4 GHz 82
Figure 68. Polarization comparison for 2.4 GHz (a) vertical and (b) horizontal 82
Figure 69. Polarization difference, 2.375 GHz 83
Figure 70. Polarization difference, 2.3875 GHz 83
Figure 71. Polarization difference, 2.4 GHz 84
Figure 72. Polarization difference, 2.4125 GHz 84
Figure 73. Polarization difference, 2.425 GHz 85
Figure 74. Horizontal polarized antenna, 5.0 GHz 86
Figure 75. Polarization comparison for 5.0 GHz (a) vertical and (b) horizontal 86
Figure 76. Polarization difference, 4.975 GHz 87
Figure 77. Polarization difference, 4.9875 GHz 87
Figure 78. Polarization difference, 5.0 GHz 88

Figure 79. Polarization difference, 5.0125 GHz 88
Figure 80. Polarization difference, 5.025 GHz 89
Figure 81. Simulation area for noise and effective bandwidth, 2.4 GHz. 90
Figure 82. Magnitude of the total field values vs. observation points for 2.4 GHz frequency band. 91
Figure 83. E total values for 6^{th} and 14^{th} observation points. 92
Figure 84. Noise bandwidth values for every observation points. 93
Figure 85. Effective bandwidth values for every observation points. 94

THIS PAGE INTENTIONALLY LEFT BLANK

LIST OF TABLES

Table 1. Current UAV tier characteristics and applications. (After Ref. [2])....3
Table 2. Polarization mismatch loss between two linearly polarized antennas.(From Ref. [13])....25
Table 3. Applicable parameter ranges for Longley-Rice model (After Ref. [3]) 31
Table 4. Applicable parameter ranges for Okumura signal prediction model. 32
Table 5. Parameter ranges for the Hata model....33
Table 6. Height correction factor....33
Table 7. Ibrahim-Parsons model parameters (After Ref. [15]). 34
Table 8. Input parameters and responses for *f2f.x*....47
Table 9. Input parameters for simulation. 49
Table 10. Parameters for material slabs and graph ranges....54
Table 11. Frequency simulation parameters 59
Table 12. Input parameters and responses for *f2fd.x*....60
Table 13. Frequency difference results for 900 MHz. 66
Table 14. Frequency difference results for 2.4 GHz....71
Table 15. Frequency difference results for 5.0 GHz....76
Table 16. Horizontal polarization simulation parameters....77
Table 17. Polarization results for 900 MHz frequencies. 81
Table 18. Polarization results for 2.4 GHz frequencies. 85
Table 19. Polarization results for 5.0 GHz frequencies. 89

THIS PAGE INTENTIONALLY LEFT BLANK

ACKNOWLEDGMENTS

The author would like to extend his thanks to thesis advisor Professor David C. Jenn, Naval Postgraduate School, Monterey, CA for his patience, guidance, and flexibility throughout the thesis process. His insights, expert knowledge and candor on the issues were invaluable to this study. The author also would also like to thank to Professor Daniel C. Schleher for agreeing to be the second reader to the thesis. The precious time they took to educate me on the points of electromagnetism, antenna theory, and radar theory are sincerely appreciated.

The author is most grateful to his wife Aliye for her endless love, support, encouraging, and understanding to complete his Master's Degree and this thesis.

Additionally, the author would like to thank to his parents for their continuing love and support. Everything that the author has accomplished in his life is a direct result of their dedication and belief in him.

Finally, the author would like to express his sincere gratitude to his country Turkey and the Turkish Air Force for giving him the opportunity to undertake this study.

THIS PAGE INTENTIONALLY LEFT BLANK

I. INTRODUCTION

A. APPLICATIONS OF UNMANNED AERIAL VEHICLES

Unmanned aerial vehicles (UAVs) are powered aerial vehicles that do not carry a human operator. Unmanned aerial vehicles can fly autonomously or be piloted remotely, can carry cameras, sensors, lethal or nonlethal payloads, as well as communication equipment. Many nations' armed forces the world over have different types of UAVs for different types of missions, such as intelligence, surveillance, reconnaissance, and target acquisition. Due to their ability to perform multiple functions, UAVs have been rapidly expanding their missions and roles.

In civilian roles, UAVs can be very useful in monitoring traffic in cities, tracking suspicious ground vehicles, delivering critical medical supplies to various platforms, and gathering weather and other environmental information. They can also be used in agriculture to spray insecticide and to disinfect fields from hazardous insects. There are also numerous organizations that have used small UAVs for aerial photography. UAV systems research activities in the civilian arena are increasing significantly at some universities. One example of commercial UAV systems is the Yamaha RMAX/R-50 series that is used for crop spraying in Japan [1]. Other than this, UAVs can also be used in mineral exploration, when loaded with special equipment. Using UAVs in such areas will reduce the risk of human life compared to manned aerial vehicle platforms.

Within the civilian sector, there is a potential for significant growth in operational UAVs. The reason for current low levels of UAVs for civilian missions is the financial risk of an unproven system. Therefore, UAV platforms, as for most new technologies, have been adopted mostly by military tactical and strategic users.

In military applications, the need for the development of UAVs is more urgent than for the civilian case. They can have numerous benefits to operational ground forces trying to communicate with each other in a poor electromagnetic environment, and can be deployed to increase the quality of transmission. In an urban combat environment, the need for UAVs is critical for troops trying to collect data from the battlefield.

The success of UAVs in recent conflicts has demonstrated the potential of such remote controlled systems. The Air Force's MQ-1 Predator was armed with Hellfire missiles, and successfully attacked targets in Afghanistan, Yemen, and Iraq. Although the primary mission was airborne reconnaissance and target acquisition, the Predator can accomplish various types of missions with two electro-optical (E-O) cameras, an infrared (IR) camera, and synthetic aperture radar (SAR), which allows the UAV to operate in bad weather.

Pioneer is another type of UAV, which is tactical, and currently being launched from amphibious ships and land-based platforms. The mission of the Pioneer is to gather real time intelligence and reconnaissance for the command control unit. Operations in which Pioneer was used include Haiti, Somalia, and the Balkans [2].

The largest and the most expensive UAV produced is Global Hawk high altitude long endurance UAV, which provides near-real-time imagery of large areas. To accomplish this task, Global Hawk and the other types of UAVs need a good propagation environment, and reliable communication and sensing for command control and data links.

Other applications that UAVs are capable of include, counter narcotics, psychological operations, anti-submarine warfare, navigation, and all weather strike. In the future, large UAVs may also take on the aerial refueling mission now performed by tanker aircraft. Flying straight is the primary job in this mission, and therefore very suitable for unmanned aircraft, because they tend to fly far away from enemy air defense lines.

The unmanned combat air vehicle (UCAV) is a new concept that is a more sophisticated type UAV. They are expected to take over suppression of enemy air defense lines and electronic attack missions in electronic warfare. With a 34-feet long wingspan, a UCAV will be able to fly to a radius 500-1000 nmi and carry various types of weapon payloads. UCAVs will also be stealthy and have other survivability advantages. Boeing and Northrop Grumman are prime contractors for the X-46 and X-47 UCAVs, respectively. The Defense Advanced Research Projects Agency (DARPA) is trying to develop concepts for unmanned combat armed rotorcraft (UCAR) which will be capable of communicating with other manned and unmanned systems.

According to the type of application and technical specifications, UAVs can be classified into four different categories. Tier I is known as tactical UAV, Tier II as operative UAV, Tier II Plus as strategic UAV, and Tier III Minus as strategic low observable (LO) UAV. Current UAV programs are summarized in Table 1, according to this widely accepted classification for UAVs.

Category	Designation	Speed (kts)	Radius (nm)	Max. Alt. (ft)	Endurance (hours)	Payload (lbs)	Example	Producer
TierI	Interim-Middium Altitude,Endurance	60-100	100	15000	5-24	75	Pioneer, Searcher	AAI
TierII	Middium Altitude, Endurance	70	400	3000-25000	>24	450	Predator	General Atomics
TierII Plus	High Altitude, Endurance	350	5400	65000	32	1950	Global Hawk	Northdrop Grumman
TierIII Minus	Low Observable High Altitude, Endurance	300	350	45000-65000	12	1000	Darkstar (terminated)	Boeing

Table 1. Current UAV tier characteristics and applications. (After Ref. [2])

Airspace, weather, and frequency management are critical components of UAV support. In a real situation, UAVs will supply data to the combat troops as well as imagery and reconnaissance. UAVs will not necessarily have priority in the battlefield relative to manned air vehicles. Therefore, they have to establish a reliable data link with ground command and control units wherever they are positioned. Weather will also have a strong effect and will be a primary concern in flight operations. Bad weather conditions can reduce the quality of the data link, and thus communication and control. Frequency is another concern. In spite of a limited bandwidth, UAVs are expected to perform many different types of missions. Multiple UAVs operating close together may cause interference between links used for data transmission and control.

No matter the application of a UAV, its effectiveness is related to electromagnetic propagation issues. Many of them will be discussed in the following chapters, and their impact on the command, control and management of UAVs examined.

B. PROPAGATION ISSUES FOR UAVS

The propagation environment will influence UAV data links. Electromagnetic waves seldom propagate in an isolated free-space environment. The path between the transmitter and the receiver is often obstructed by several natural or man-made structures like buildings and foliage. The presence of these obstacles changes the quality of the signal, and results in additional path loss, distortion and spreading of the received signal [3]. Reflection, refraction, diffraction, attenuation, scattering, depolarization and absorption are some of the basic propagation mechanisms that affect electromagnetic waves. Reflection occurs when an electromagnetic wave is incident from one medium to another with different electrical properties. Diffraction occurs when the propagation path between transmitter and the receiver is obstructed by a surface that has sharp or curved irregularities like building edges and rounded hills. This is very significant in the propagation of electromagnetic waves in urban environments.

These mechanisms are dependent on the frequency of the incident wave. At high frequencies, diffraction and reflection depend on the geometry of the object as well as the amplitude, phase and polarization of the incident wave at the point of diffraction. Even though an obstacle blocks the transmitter, energy can be received because of the diffraction from the obstacles. These parameters will be discussed further in the following chapter.

In an urban or suburban environment there is rarely a direct path between transmitting and receiving antennas. There are usually multiple reflections, scattering and diffraction paths between a transmitter and receiver, and there are many propagation mechanisms by which signals can travel between the transmitter and the receiver. Except for line-of-sight (LOS) paths, their effectiveness is generally a strong function of the transmitter-receiver geometry and the frequency [5]. Direct path, direct plus earth reflections (or multipath), ground waves, terrain diffractions, low altitude surface ducts are some of the propagation mechanisms that vary with the frequency.

Multipath effect is generally the most severe channel impairment. Reflections of electromagnetic waves off objects interfere constructively and destructively with the transmitted wave and with each other. When the objects are large compared to the wavelength of the electromagnetic wave, such as buildings, and walls, geometrical optics

(GO) and the geometrical theory of diffraction (GTD) can be applied. An impenetrable object blocks the direct line-of-sight (LOS) path between the transmitter and the receiver, resulting in only reflected waves reaching the receiver. This effect (shadow fading), results in less signal power than expected from path loss computations [6]. These effects of multipath are depicted in Figure 1.

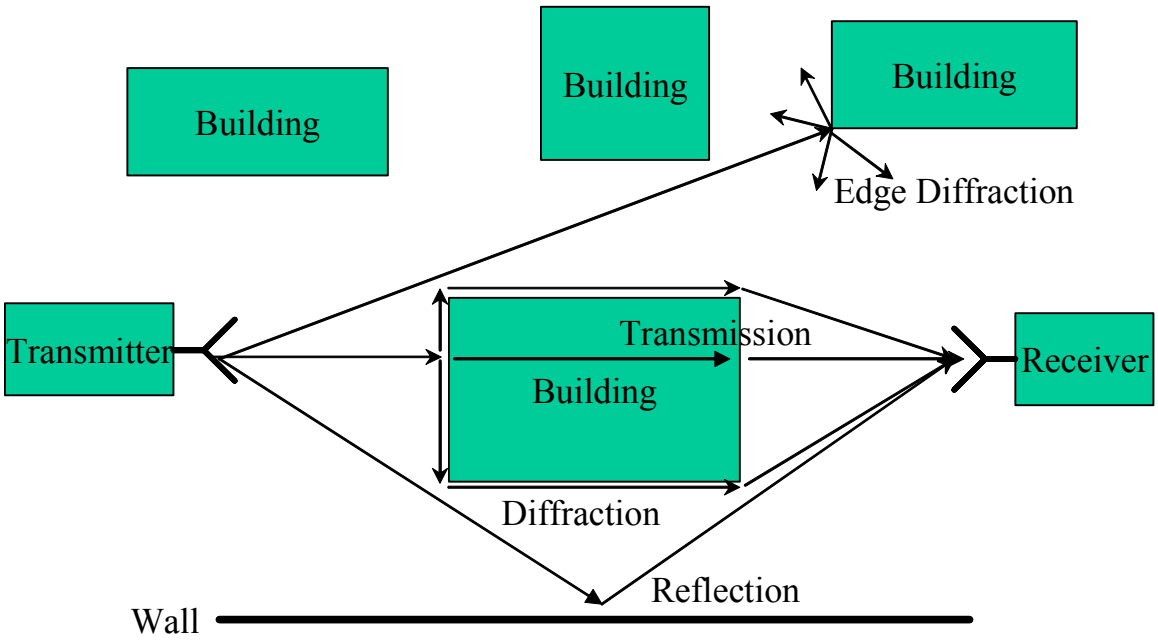

Figure 1. Multipath propagation due to reflection and diffraction. For clarity only a few reflections and diffractions are shown.

To handle the urban propagation problem, ray-tracing techniques based on three-dimensional implementations can provide accurate predictions. In reference [4], indoor narrowband and wideband measurements are compared using GO and GTD. System designers use ray tracing in the frequency domain to determine the received signal level for an indoor transmission at a certain point in time. Often designers use a simple four-ray model consisting of a direct ray, a ground-reflected ray, and two rays reflected off the walls. This computed number is only approximate, since it does not include all reflections and absorbers [6]. In this research, GO and GTD will be implemented to model the propagation of waves in the urban environment.

C. OBJECTIVE

Many of today's military operations are conducted in urban environments, where reliable communication and sensing is an extremely challenging problem. A variety of manned and unmanned platforms collect sensor data, and must communicate with each other and a command control center, or mobile users. The electronic systems may be subject to jamming by the enemy, but more fundamentally, poor propagation conditions may cause fading and lead to a reduction in the quality of transmission, or possibly even the complete loss of a link.

This research aims to simulate different types of urban propagation environments for UAV data links and determine the quality of transmission in the complex urban environment. Several possible methods of improving the performance of wireless systems in the frequency range 900 MHz to 5 GHz based on frequency and polarization diversity are also examined. The ultimate goal of this research is to provide useful guidelines for operating UAVs in urban areas.

D. TECHNICAL APPROACH

Frequency, polarization, and space diversity (or re-use) techniques are used for signal reception improvement.

A system with diversity can establish multiple channels between the transmitter and receiver through the selection various combinations of frequency, antenna beams, and antenna polarization. To exploit diversity it is important that the transmission characteristics at frequencies 900 MHz to 5 GHz be understood. Since the implementation of diversity techniques depends largely on the antenna capabilities, it is also important to access the state-of-the-art in multi-beam, polarization diverse antenna technology.

Frequency diversity involves sending the same information independently over several frequencies in a specific bandwidth. If the frequencies are separated enough it is unlikely that all the channels will be in fading at the same time. This diversity technique needs more bandwidth and possibly several transmitter antennas.

Figure 2 shows one possible implementation of frequency diversity, where a transmission channel is selected from several possible subbands in SHF (for example 500 MHz bands centered at 4.7, 7.5, and 15 GHz). At any particular time, the subband with the highest signal-to-noise ratio (SNR) is used.

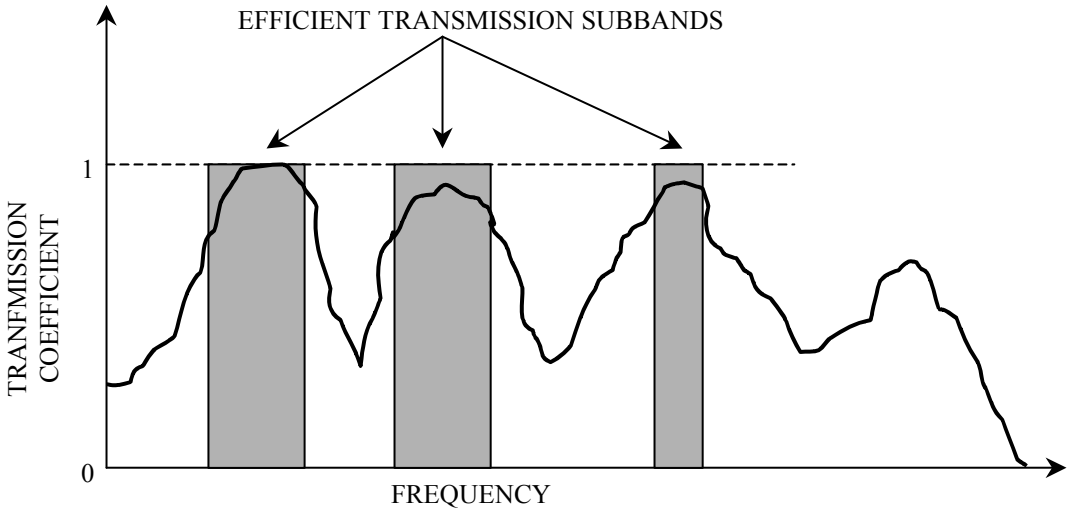

Figure 2. Hypothetical plot of transmission coefficient vs. frequency for an urban environment (the range dependency has been removed).

In addition to operating at a frequency where the SNR is optimum for the given environment, further improvement in performance can be achieved with the polarization diversity capabilities of digital antennas. Polarization diversity involves transmitting vertically and horizontally polarized waves simultaneously. Receiver antennas should be separate to receive each polarization signal. Received signals at the two polarizations are uncorrelated and therefore provide diversity [6]. The average signal levels of two polarizations are within ±3 dB most of the time. There will be a 3 dB reduction in power, because the power is split between two transmitting antennas. Polarization diversity techniques are thus attractive at data link and ground access point locations.

The efficiency of wireless transmission channels can also vary significantly with the polarization of the antenna. Generally horizontal and vertical are used as polarization references, as shown in Figure 3.

In the real world, signals are depolarized by multiple propagation mechanisms (reflections, diffractions, surface waves, etc.). Therefore, the paths between a transmitter

and receiver can be highly polarization dependent in an urban environment, and consequently, polarization is one means of filtering unwanted signals.

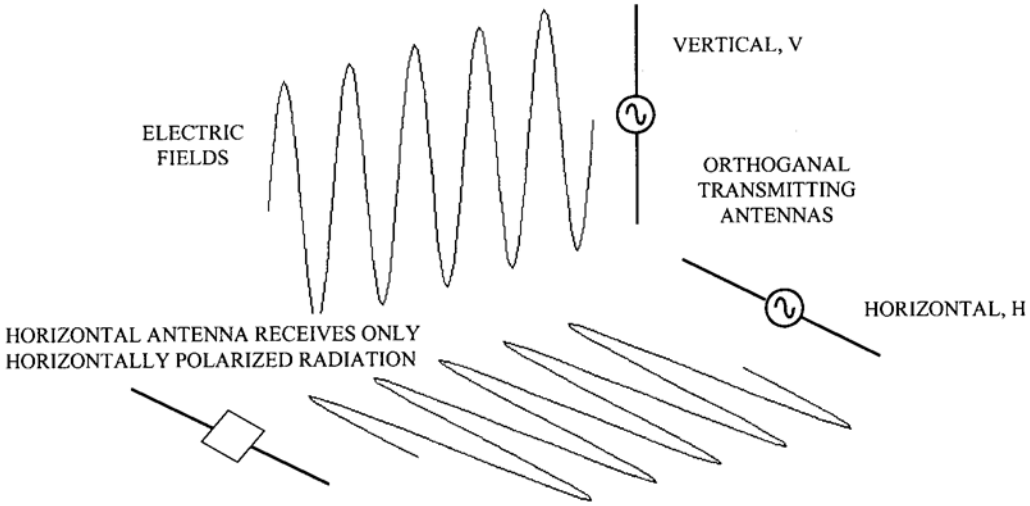

Figure 3. Horizontal and vertical polarizations generated by linearly polarized antennas

With frequency diversity, an operating frequency can be chosen where constructive interference occurs. With polarization diversity, the polarization that provides the most efficient propagation can be chosen.

In addition to frequency and polarization diversity, there is also spatial diversity that uses two or more antennas or beams in space. In the environment like cities, there are conditions that result in shadowed or blocked regions. It is possible that received signal level in the direction of the transmitter is very low, but in another direction the signal is higher. Several forms of diversity techniques are discussed in references [17] and [18].

Diversity gain is the improvement in SNR of the received signal from different receiver types. Diversity gain is a parameter that allows comparison between multiple antenna sensors and single antennas. Diversity gain for a given probability p is given by

$$G_{div}(p) = \gamma_{div}(p) - \gamma_1(p) \tag{0.1}$$

where, γ_{div} is the SNR with diversity, and γ_1 is the SNR of a single branch.

Diversity gain is maximized if the correlation of the envelopes of the signals received by each receiver is zero. Diversity gain decreases if correlation of the envelope of the received signal by each receiver increases [19].

The **Urbana** Wireless toolset is used to predict UAV data link performance in complex propagation environments such as major metropolitan cities. The **Urbana** Wireless Toolset offers two-dimensional (2-D) and three-dimensional (3-D) solutions for predicting multipath wireless propagation. The propagation model is a 3-D ray tracing process, which predicts the local mean power level received at any given point. The vector sum of multipath power is computed for each point. The model also accounts for diffraction effects like edge diffraction around corners, which may have significant contribution to power levels at shadowed observation points.

The efficiency of wireless transmission channels varies with operating frequency where SNR is the maximum for a particular environment. Additional improvement can also be achieved with polarization and space diversity capabilities of digital smart antennas. Therefore, this research attempts to analyze, model, simulate, and identify the effects of frequency, and polarization diversity of the wireless environment. The signal contour levels in simulated areas are used to evaluate the reliability of UAV data links.

E. THESIS OUTLINE

Chapter II discusses basic propagation and antenna fundamentals. Major propagation mechanisms that are reflection, diffraction, scattering, and absorption are discussed and briefly explained. The radiation pattern of a half-wave dipole antenna, and Fresnel zone clearance are described briefly.

Chapter III discusses both theoretical and empirical models that have been used to predict signal levels in a specific place or urban environment. **Urbana** as a propagation program is also mentioned in this chapter.

Chapter IV simulates UAV data and communication link in small city environment. Different frequency bands, different polarization, and different operation altitude are simulated with selected coating materials for walls. The parameters used for simulations are selected through logical deduction.

Chapter V summarizes the results of the simulations based on the data from Chapter IV, and makes suggestions for future research.

Appendix A lists the Matlab codes used in this thesis and Appendix B shows a sample **Urbana** input script file used for simulations.

II. PROPAGATION AND ANTENNA FUNDAMENTALS

In this Chapter, important relevant propagation issues for urban environments and basic antenna fundamentals will be discussed. Propagation of radiowave energy in urban areas is strongly influenced by the basic propagation mechanisms of reflection, diffraction and scattering. Fading occurs when several propagation components combine in a real situation. In other words, the actual received signal level is obtained by the vector sum of the all signals that are incident from all directions, weighted by the antenna pattern. In urban propagation modeling, it is important to consider these mechanisms in the signal calculations.

A. BASIC PROPAGATION MECHANISMS

Radio wave propagation can be very complex and diverse. Major propagation mechanisms are generally categorized as reflection, diffraction, scattering, and absorption [8]. Reflection occurs when a propagating electromagnetic wave hits a surface which has very large dimensions compared to the wavelength of the signal. Reflection can occur from the surface of the earth and from building and wall surfaces, and add constructively or destructively depending on the frequency. Diffraction occurs when an obstacle obstructs the communication path between the transmitter and receiver. Diffracted waves from the obstacle can maintain the communication channel when a line-of-sight (LOS) path does not exist. Scattering occurs when the obstacle dimensions are small compared to the wavelength. Absorption is energy dissipation inside of a material or medium such as a wall, or even a cloud. Figure 4 illustrates these propagation effects in the presence of an obstacle.

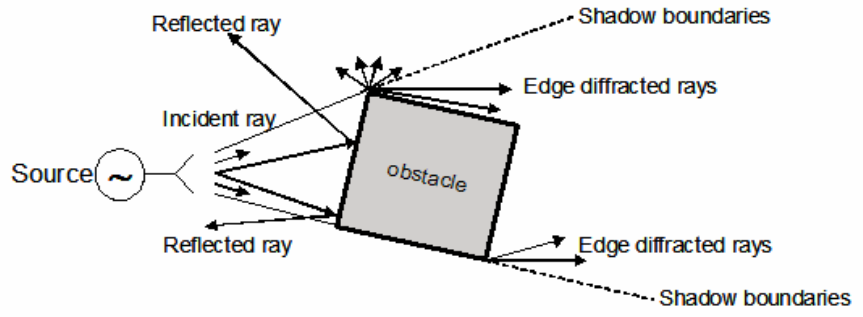

Figure 4. Illustration of propagation mechanisms.

1. Reflection

If a plane wave is incident on a medium with different dielectric properties, part of the energy is transmitted into the second medium and part of the energy is reflected back into the first medium. For large flat surfaces (relative to the wavelength), the reflection angle of the wave is equal to the incidence angle. If the second medium is a perfect conductor, then all incident energy is reflected without any transmission into the second medium.

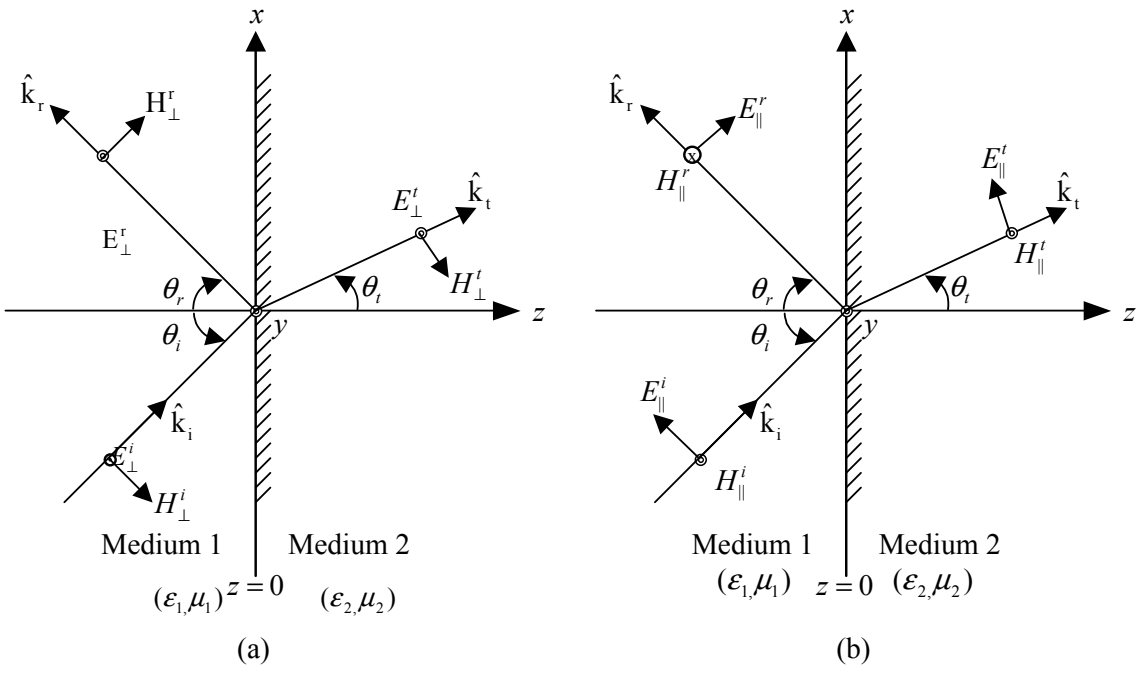

Figure 5. (a) Perpendicular, and (b) parallel polarized incident wave on a boundary. (From Ref. [9].)

An arbitrary polarization is decomposed into perpendicular and parallel components as shown in Figure 5. According to Snell's law of reflection

$$\theta_r = \theta_i \tag{2.1}$$

Thus, the reflection angle is equal to the incidence angle. Furthermore, according to the Snell's law of refraction

$$\frac{\sin\theta_t}{\sin\theta_i} = \frac{k_1}{k_2} = \frac{\sqrt{\varepsilon_2\mu_2}}{\sqrt{\varepsilon_1\mu_1}} = \frac{n_1}{n_2} \tag{2.2}$$

where k_1, k_2 are the wave numbers, μ_1 ,μ_2 are the media permeabilities, ε_1 ,ε_2 are the media permittivities, and n_1 ,n_2 are the indices of refraction.

The angle of the refraction of the transmitted wave depends on the ratio of the constitutive parameters of two media [7]. The reflection coefficient relates the magnitude of the reflected wave to the magnitude of the incident wave and for perpendicular polarization (when the electric field is perpendicular to the plane defined by $\hat{n}$ and $\hat{k}_i$) it can be found as

$$\Gamma_\perp = \frac{E^r_{\perp 0}}{E^i_{\perp 0}} = \frac{\eta_2\cos\theta_i - \eta_1\cos\theta_t}{\eta_2\cos\theta_i + \eta_1\cos\theta_t} \tag{2.3}$$

For parallel polarization (when the electric field vector is parallel to the plane defined by $\hat{n}$ and $\hat{k}_i$), the reflection coefficient can be found as

$$\Gamma_\parallel = \frac{E^r_{\parallel 0}}{E^i_{\parallel 0}} = \frac{\eta_2\cos\theta_t - \eta_1\cos\theta_i}{\eta_2\cos\theta_t + \eta_1\cos\theta_i} \tag{2.4}$$

where Γ = Fresnel reflection coefficient

E^r = Reflected electric field magnitude

E^i = Incident electric field magnitude

θ_t = Angle of refraction

η = Intrinsic impedance of medium 1 or 2.

For nonmagnetic materials ($\mu_1 = \mu_2 = \mu_0$) such as ground, ceramic, and water, the variation of the magnitudes of reflection coefficients of parallel and perpendicular polarized waves can be plotted according to their relative dielectric constants (ε_r). The expressions above were implemented in Matlab and the codes can be found in Appendix A. The reflection coefficient versus incident angle plot for these materials is shown in Figure 6. For each surface, $|\Gamma_{\parallel}| = 0$ at an angle that is called Brewster angle. At the Brewster angle, the parallel-polarized component of the incident wave is totally transmitted into medium 2 [9].

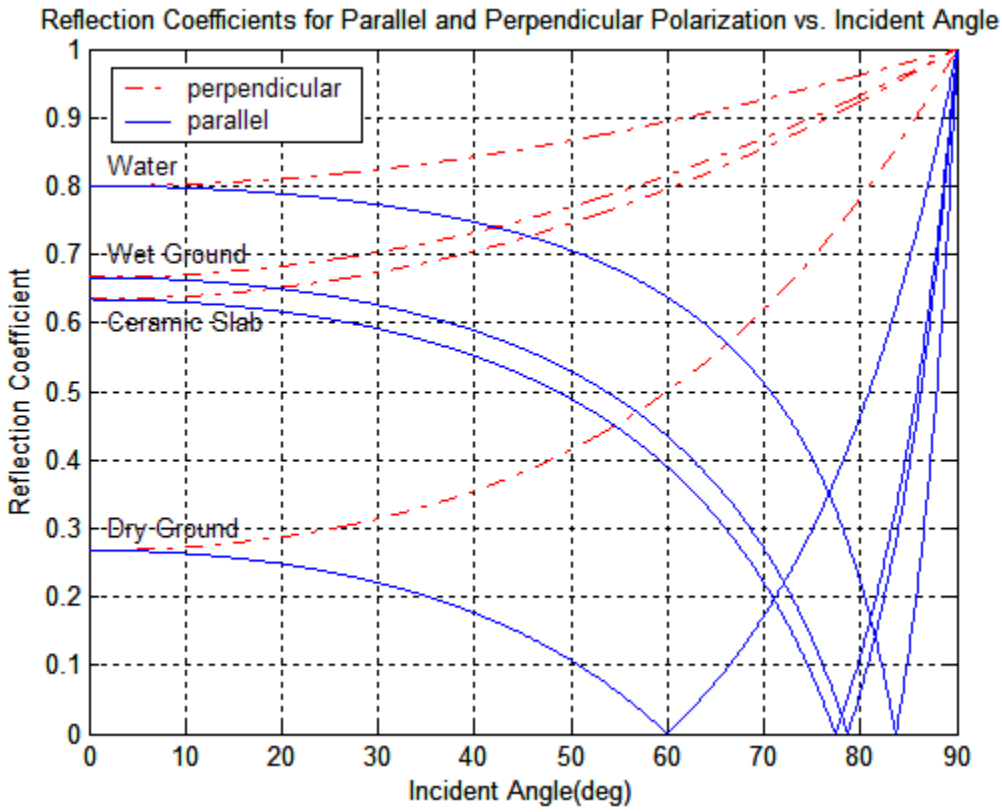

Figure 6. Reflection coefficients versus incident angle for some non-magnetic materials.

In urban propagation, most of the building walls and obstacles can be considered as large flat surfaces relative to the wavelength. Therefore, ray-tracing techniques can be used in urban propagation environments. The Fresnel reflection coefficient formulas are applicable away from edge regions of surfaces.

Geometrical optics (GO) is the most basic theory that describes wave behavior upon reflection or refraction at an interface between two materials. The curvature of the reflected wave R^r front determines how the power spreads as a function of distance and direction. It depends on the curvature of both the incident wave front R^i, and the reflecting surface, R^s as shown in the Figure 7. Thus the GO reflected field has the form

$$\vec{E}^r(p) = \vec{E}^i(R)\Gamma A(s)e^{-jks} \tag{2.5}$$

where s is the distance along the reflected ray to the observation point P, $\vec{E}^i(R)$ is the incident field at the reflection point, and $A(s)$ is a divergence factor that depends on R^r.

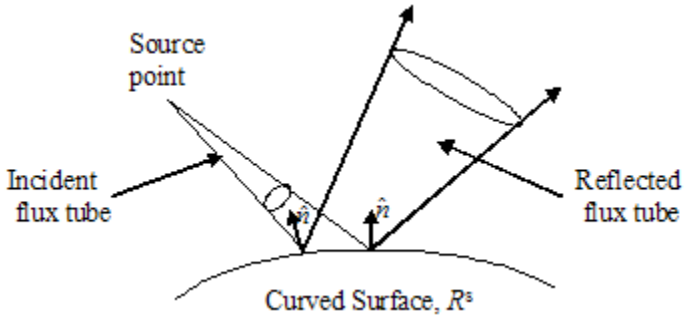

Figure 7. Reflection of a ray tube at a planar interface. (From Ref. [7])

GO consists of tracing the incident and reflected ray for a given geometry. The total field is then the sum of the direct and reflected fields. However, GO suffers from the drawback that it produces field discontinuities at the shadow boundaries and predicts a zero field in shadow regions [3].

2. Diffraction and Geometric Theory of Diffraction

The geometric theory of diffraction (GTD) is the supplementation of GO by the addition of diffraction. GTD eliminates some of the problems of GO. The total field at an observation point P can be found by sum of GO and diffracted components as:

$$\vec{E}_r(P) \equiv \vec{E}_{GO}(P) + \vec{E}_d(P) \tag{2.6}$$

If we define a local edge-fixed coordinate system along the edge (z-axis), with the x-axis on the surface pointing inward. The ray is incident onto the edge at an angle β' and a cone of diffracted rays emerges from diffraction point Q at an angle of β. The cone of diffracted rays is called Keller cone. Figure 8 is an illustration of this diffracted ray geometry and the Keller cone. Diffraction occurs when there is an obstacle with sharp edges in the line-of-sight between the transmitter and the receiver. Buildings can be considered as sharp edged obstacles. Because diffraction is a local phenomenon at high frequencies, the value of the field of a diffracted ray is proportional to the field value of the incident ray at the point of diffraction, multiplied by a coefficient called the diffraction coefficient. It is determined largely by the local properties of the field near the point of diffraction [10]. The matrix form of the diffracted field is:

$$\begin{bmatrix} E_{d\beta}(s) \\ E_{d\phi}(s) \end{bmatrix} = \begin{bmatrix} D_s & 0 \\ 0 & -D_h \end{bmatrix} \begin{bmatrix} E_{i\beta'}(s') \\ E_{i\phi'}(s') \end{bmatrix} A(s,s')e^{-jks} \tag{2.7}$$

where D_s is the parallel or soft polarization diffraction coefficient, and D_h is the perpendicular or hard polarization diffraction coefficient.

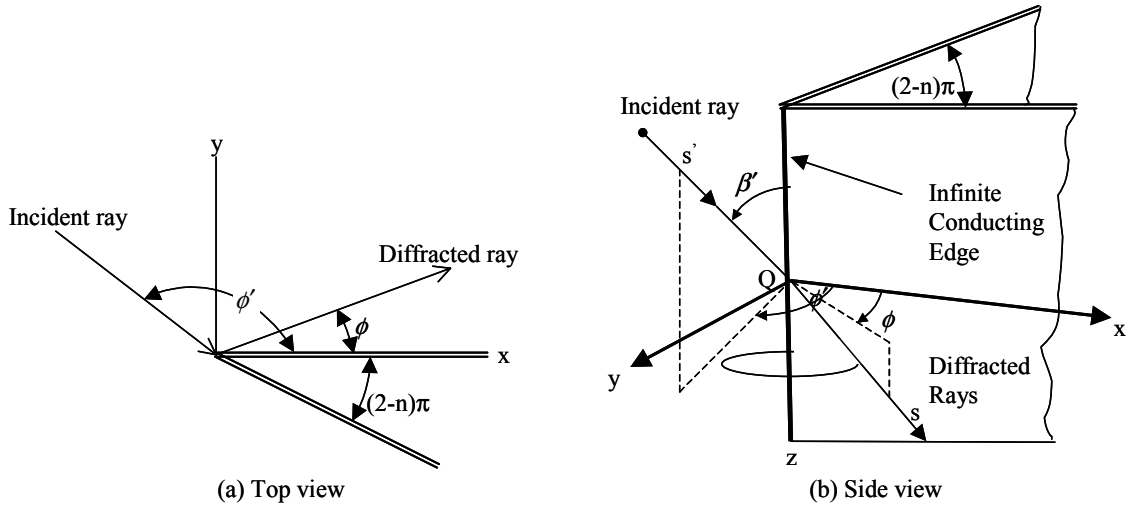

Figure 8. Geometry for three-dimensional wedge diffraction.

Diffraction coefficients for parallel and perpendicular polarized waves ($D_{\parallel}$ and $D_{\perp}$), can be found from Keller's diffraction formulas. If the field point is not

close to a shadow or reflection boundary and $\phi' \neq 0$ or $n\pi$ (grazing incidence), the scalar diffraction coefficients may be written as [10]

$$D_{\substack{\parallel \\ \perp}}(\phi,\phi';\beta') = \frac{e^{-j(\pi/4)}\sin(\pi/n)}{n\sqrt{2\pi k}\sin\beta'} \cdot \left[\frac{1}{\cos\frac{\pi}{n} - \cos\frac{\phi-\phi'}{n}} \mp \frac{1}{\cos\frac{\pi}{n} - \cos\frac{\phi+\phi'}{n}} \right] \tag{2.8}$$

This expression is valid for all types of incident waves like plane, cylindrical, conical, and spherical waves.

For the special case of a knife edge ($n = 2$), equation (2.8) can be expressed as

$$D_{\substack{\parallel \\ \perp}}(\phi,\phi';\beta') = -\frac{e^{-j(\pi/4)}}{2\sqrt{2\pi k}\sin\beta'} \cdot \left[\frac{1}{\cos\frac{1}{2}(\phi-\phi')} \mp \frac{1}{\cos\frac{1}{2}(\phi+\phi')} \right] \tag{2.9}$$

If the incident plane wave hits an edge, a diffracted ray arrives at an observation point, this is called single diffracted ray. If a diffracted wave travels along the surface and hits a second edge, it will be diffracted again. This case is a doubly diffracted ray. In an urban environment double diffraction can generally be ignored.

3. Diffuse Scattering and Rayleigh Scattering

Scattering occurs when there are obstacles or objects with small dimensions compared to the wavelength in the path of the electromagnetic wave. For small objects Rayleigh scattering occurs. Because of the small size relative to wavelength, the particles are isotropic scatterers. Energy is scattered uniformly in all directions. This mechanism allows energy to be scattered out of the antenna beam at all points along the path by large dust particles and raindrops. Larger objects, such as tree leaves can also contribute to Rayleigh scattering.

Diffuse scattering occurs when surfaces are not perfectly flat. The effect of small-scale roughness can be included qualitatively by modifying the reflection coefficient of the smooth surface. Surface roughness will cause diffuse scattering and a corresponding decrease in the amplitude of the specularly reflected wave as shown in Figure 9. According to the Rayleigh criterion, if h is the height of the irregularity of the surface

and ψ is the incident grazing angle, the path difference ΔR can be found as $\Delta R = 2h\sin\psi$, and the phase difference is

$$k\Delta R = 2kh\sin\psi \tag{2.10}$$

If this phase difference is small, the effect of the roughness is small, and the surface can be considered as smooth. Increasing kh or the grazing angle increases the path difference and weakens the reflected wave. When the phase difference is $k\Delta R = \pi/2$, and then $h\sin\psi < \pi/8$ is the condition for the surfaces to be considered smooth.

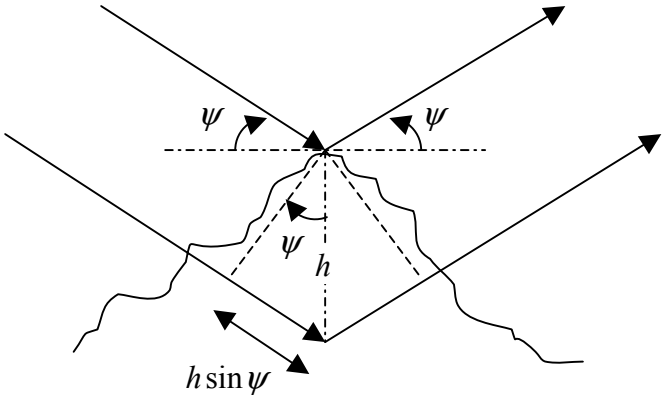

Figure 9. Reflection from an irregularity of height h (From Ref. [3]).

For a Gaussian rough surface having a standard deviation σ_h the reflection coefficient can be written as

$$\Gamma_r = \Gamma_s \rho_s = \Gamma_s e^{-2(k_0\sigma_h\sin\psi)^2} \tag{2.11}$$

where Γ_s is the reflection coefficient for smooth surface and ρ_s is the rough surface reduction factor.

For non-Gaussian surfaces the rough surface reduction factor, or scattering loss factor, can be obtained from the Fourier transform relation between ρ_s and the probability density function of the surface height [11]. The parameter ρ_s is then defined as

$$\rho_s = e^{-2(k_0\sigma_h\sin\psi)^2} I_0\left[2\left(k_0\sigma_h\sin\psi\right)^2\right] \tag{2.12}$$

where I_0 is the modified Bessel functions of the first kind of order zero.

4. Absorption

While propagating through a lossy medium, an electromagnetic wave will be attenuated. Absorption of a wave passing through a material is due to induced polarization and magnetization currents. Ohmic loss also occurs in an imperfect conductor. The attenuation constant of a lossy material can be computed from the material's complex permittivity, permeability, and conductivity. In reference [12], absorption in the atmosphere is handled in detail.

While simulating the urban propagation environment, buildings will be modeled with facets. Each facet will be assigned a coating parameter related to its attenuation characteristics.

5. Path Loss

The reduction in the signal power at the receiver relative to the transmitter in an unobstructed free space condition is called free space path loss [6]. The free space path loss factor L_p can be defined simply as

$$L_p = 20\log\left(\frac{4\pi d}{\lambda}\right) \tag{2.13}$$

where d is the distance from transmitter to the observer. At a fixed distance of $d = 1\,\text{km}$, the free space propagation loss factor versus frequency is shown in Figure 10. The Matlab code for this graph is in Appendix A.

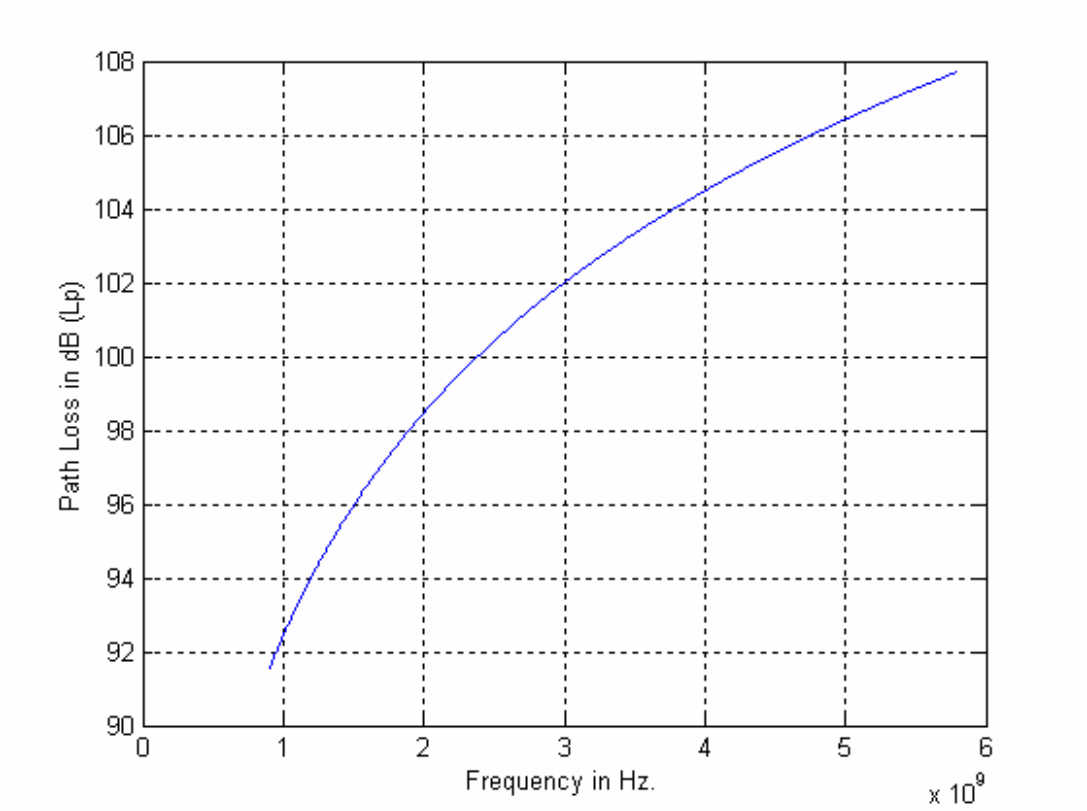

Figure 10. Free space propagation loss versus frequency.

The path loss in this plot includes only free space path loss. Other losses occurring along the path that reduce the signal are referred to as excess path loss. At the receiver antenna the average received power can be expressed by the Friis equation [6] as

$$P_r = P_t\left(\frac{\lambda}{4\pi d}\right)^n G_t G_r \tag{2.14}$$

where G_t, G_r are gains at the transmitter and the receiver, and n represents the path loss coefficient. For various obstructions the path loss coefficient varies from 2 to 6. If the transmitting and receiving antennas have different polarizations then Friis equation should be modified to include polarization loss factors [6] as

$$P_r = P_t\left(\frac{\lambda}{4\pi d}\right)^n G_t G_r \left(1-|\Gamma_t|^2\right)\left(1-|\Gamma_r|^2\right)\left|\rho_t \rho_r^*\right|^2 \tag{2.15}$$

where $|\rho_t \rho_r|$ is the polarization loss factor and Γ_t and Γ_r are the reflection coefficients of the transmitter and the receiver, respectively.

Large-scale path loss L_p can be defined [8] as

$$L_p(d) = L_p(d_o) + 10n \log\left(\frac{d}{d_0}\right) + \mathrm{X}_\sigma \tag{2.16}$$

For free space $n = 2$ can be used. For urban areas with multiple scatterers n must be chosen between 4 and 6. The $L_p(d_0)$ term gives the loss at distance d_0 (1 km for urban environments, 100 m for micro cell systems, and 1 m for indoor systems). X_σ is the zero mean Gaussian random variable that reflects the variation in average received power.

6. Fresnel Zones

While establishing a communication path between the transmitter and receiver, reflections from the ground are also important at low altitudes. Fresnel zones must be taken into consideration in such environments where direct and the reflected waves have a strong effect on the received signal level. If we consider a transmitter at a height H_t and a receiver at a height H_r, separated by a horizontal distance d, points on the earth's surface that bear a constant path difference relative to the direct wave are defined [3] as $\delta = R_2 - R_1$ as shown in Figure 11. R_1 is the direct path length, and R_2 is the reflected path length. Constant values of δ form ellipsoids. For a path length difference $\delta = n\lambda/2$, the Fresnel zone radius of any member ellipsoid can be obtained as

$$h_n = \sqrt{\frac{n\lambda}{(1/d_1) + (1/d_2)}} \tag{2.17}$$

where h_n = radius of n^{th} zone in meters

d_1 = transmitter direct path distance to obstacle

d_2 = receiver direct path to the obstacle

n = Fresnel zone number

λ = wavelength in meters.

To avoid diffraction loss by obstacles, antennas are placed so that at least the first Fresnel zone is cleared from the obstacles. For low-altitude missions, UAV links will be affected if there are significant obstacles in this region.

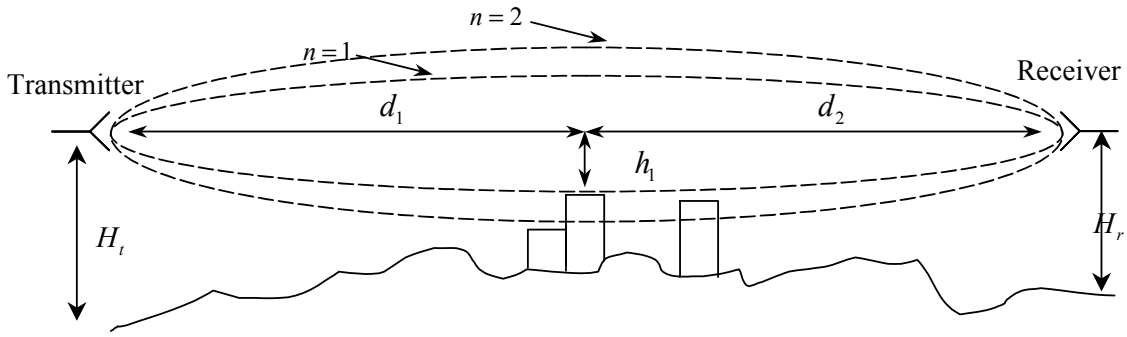

Figure 11. Fresnel zone clearance.

B. ANTENNA FUNDAMENTALS

Antennas are made in various shapes and sizes and used for transmitting and receiving purposes. A one-meter long dipole antenna operating at the wavelength 2 meters has the same properties as a 1 cm long dipole operating at 2 cm wavelength [9]. We can classify antennas as electrically small antennas, resonant antennas, broadband antennas and aperture antennas. Simulations in this research employ a resonant dipole antenna. This type of antenna operates well at a single frequency or selected narrow frequency bands.

1. Radiation Pattern and Parameters

A radiation pattern is a graphical representation of the far-field properties of the antenna. The complete polar radiation pattern for the ideal dipole resembles an omnidirectional pattern since it is uniform in the $x-y$ plane as shown in Figure 12. The E-plane and H-plane patterns of the ideal dipole are also shown.

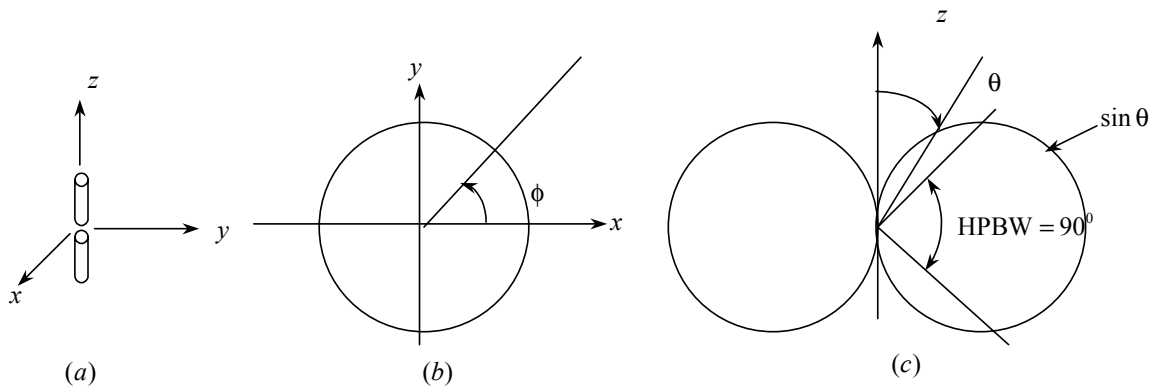

Figure 12. (a) Ideal dipole. (b) H-plane radiation pattern (c) E-plane radiation pattern.

The directivity of an antenna is defined as the ratio of its maximum normalized radiation intensity to the average value of radiation intensity over 4π space. The directivity of half-wave dipole can be found as $D = 1.64$. The input impedance of an infinitely thin half-wave dipole is $73 + j42.5\Omega$. If slightly reduced in length to achieve resonance, the input impedance is about $70 + j0\Omega$. The half-power beamwidth (HPBW) is defined as the angular separation of the points where the main beam of the power pattern equals half of the maximum power value. The HPBW can be written as

$$HPBW = \left|\theta_{HP\_left} - \theta_{HP\_right}\right| \tag{2.18}$$

The general normalized power pattern can be written as

$$P(\theta,\phi) = \left|F(\theta,\phi)\right|^2 \tag{2.19}$$

where F is the normalized voltage pattern function. The complete far-field pattern for half-wave dipole is given [10] as

$$F(\theta) = \frac{\cos[(\pi/2)\cos\theta]}{\sin\theta} \tag{2.20}$$

The power pattern plot and half-power beamwidth for half-wave dipole is shown in Figure 13. The Matlab code for this graph is in Appendix A.

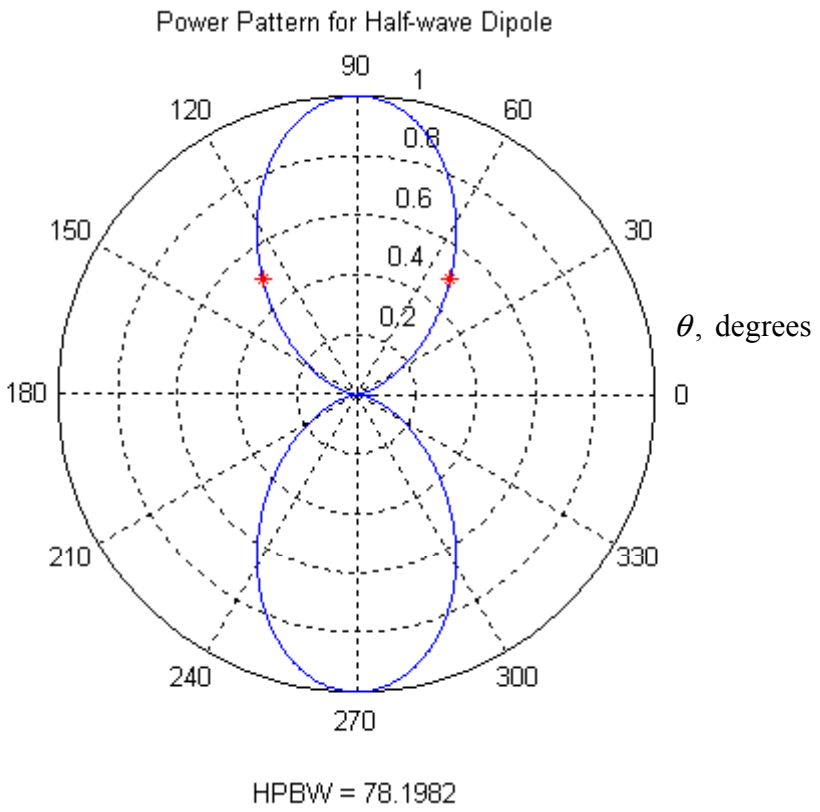

Figure 13. Normalized half-wave dipole power radiation pattern.

2. Polarization of Antennas

In most of the UAV data links and wireless communication channels, the transmitter and the receiver antennas are usually linearly polarized. The antennas at the base station or ground units are fixed, but moving platforms like UAVs and mobile platforms may be oriented so that they are no longer parallel with the antenna at the base station ground unit. These misalignments will cause polarization mismatch and therefore reduce the system efficiency. If the transmitting and receiving antennas are both linearly polarized, but not aligned, there will be a polarization mismatch loss (PML) that can be determined using the formula [13]

$$\text{PML (dB)} = 20\log(\cos\theta) \tag{2.21}$$

where θ is the misalignment angle between the two antennas. Table 2 illustrates some typical mismatch loss values for various angles. These values show the theoretical ratio

of power transmitted between antennas of different polarizations. In an urban environment, reflections from the obstacles such as buildings or trees result in a change of the polarization of the reflected or scattered wave. Multiple reflections and diffractions will make the polarization problem more significant.

Orientation Angle (Degrees)	Polarization Mismatch Loss (dB)
0.00	0.00
15.00	0.30
30.00	1.25
45.00	3.01
60.00	6.02
75.00	11.74
90.00	∞

Table 2. Polarization mismatch loss between two linearly polarized antennas.(From Ref. [13])

For circularly polarized antennas, radiation patterns are usually taken with a rotating linearly polarized reference antenna. The resulting antenna pattern is the linear polarized gain with a cyclic ripple. The peak-to-peak value is the axial ratio, and it represents the polarization quality for the circular polarized antenna. Taga reports [14] that, the mean equivalent gain (MEG) for a dipole inclined at 55 degrees from the vertical is –3 dBi, no matter what the cross-polarization coupling. The MEG is defined as

$$MEG = \int_0^{2\pi}\int_0^{\pi}\left[\frac{X}{1+X}G_\theta(\theta,\phi)P_\theta(\theta,\phi)+\frac{1}{1+X}G_\phi(\theta,\phi)P_\phi(\theta,\phi)\right]\sin(\theta)d\theta d\phi \qquad (2.22)$$

where X = Power ratio of horizontally to vertically polarized signal power

G_θ = Antenna power gain pattern for θ

G_ϕ = Antenna power gain pattern for ϕ

P_θ = Angular density function of the incoming plane wave for θ

P_ϕ = Angular density function of the incoming plane wave for ϕ

The best choice between using a circularly polarized antenna or dual linearly polarized antenna is really difficult to determine. As the axial ratio of the circularly polarized antenna increases, the dual linear polarized antenna will become the better choice [13].

3. Smart Antennas

Smart antenna technology provides very important system component for communication systems. Smart antennas have some signal or spatial processing capability embedded in them. Most smart antennas are capable of generating multiple beams. Multiple-beam antennas can generally be divided into two broad groups [15]. A fixed multiple-beam antenna system that is useful for transmitting and receiving applications is the first one. In reference [15] a Butler matrix-fed antenna is discussed as an example of this type. Processing the received signals of multiple antennas according to their angles of arrival is the second. This second group is usually suitable for receive-only conditions.

Most of the smart antenna systems form beams directed toward a desired target and nulls toward unwanted interferers or transmitters. This property of smart antennas improves the desired signal level and increases the signal-to-noise-ratio (SNR). Smart antennas can increase the range or coverage of a system because of the increased SNR. They can reject multipath interference and increase the bandwidth capacity.

Figure 14 is an illustration of typical multiple beam and smart antenna patterns. Switched beam antenna systems form multiple fixed beams with predefined sensitivity in particular directions. Switched beam systems can detect the second signal level and choose from one of several fixed beams, and switching from one beam to another as the UAV or mobile user passes throughout the coverage sector. Adaptive antennas represent the most advanced smart antenna approach to date. They use a variety of new signal-processing algorithms. The adaptive system can locate and track various types of signals to dynamically minimize interference and maximize intended signal reception.

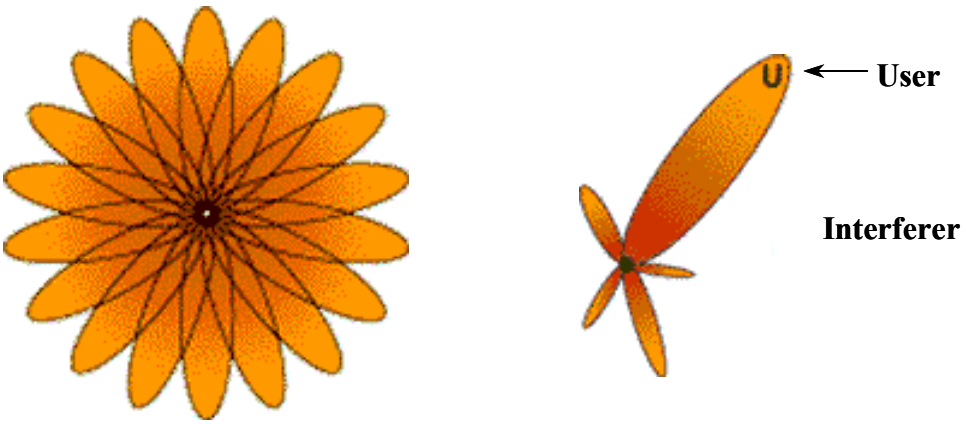

(a) (b)

Figure 14. (a) Switched and (b) Adaptive beam antenna coverage (From Ref [16]).

C. SUMMARY

In this chapter, important relevant propagation issues for urban environments and basic antenna fundamentals were discussed. Basic propagation mechanisms such as reflection, diffraction, scattering, and absorption are explained. Propagation of radio wave energy within specific places is strongly influenced by these basic propagation mechanisms. The radiation pattern of a half-wave dipole antenna, and Fresnel zone clearance are described briefly. In urban propagation modeling, it is important to consider these mechanisms in the link calculations.

In the next chapter, both theoretical and empirical models that have been used to predict signal levels in an urban environment are discussed. **Urbana** as a propagation prediction toll is also mentioned in the next chapter.

THIS PAGE INTENTIONALLY LEFT BLANK

III. PROPAGATION MODELS AND TOOLSETS

Propagation modeling for wireless systems has improved significantly over the last few decades. The improvement has been motivated by applications such as:

- Mobile communications systems
- Wireless local area networks
- GPS performance in urban environments
- Data links for UAVs flying in cities
- Command and control systems

Most of these systems operate at frequencies above 900 MHz. For the current research simulating data links over a small city, center frequencies of 900 MHz, 2.4 GHz, and 5 GHz are selected.

As discussed in Chapter II, propagation is decomposed into transmission, reflection, scattering, and diffraction. There are both theoretical and empirical models that have been implemented. These techniques are used both indoors and outdoors. Several of these models will be discussed in this chapter.

A. BASIC PROPAGATION MODELS

Urban propagation is relatively new area of study. It is very important in the design and development phase of the cellular networks as well as command control and data links for UAVs. The properties of the environment change from city to city and from building to building within the same city. Statistical models can be very effective and useful in an average sense in predicting propagation between operational units in this environment. Most of the time there is not a direct path between the transmitter and receiver. However multiple reflections and diffraction paths can possibly give the necessary connectivity.

Reflections from objects will cause multiple signals to add and cancel each other. Complete cancellation is called “deep fading.” Rayleigh statistics predict these small-scale variations in the signal strength [5].

1. Theoretical Models

Propagation problems are very difficult to implement because the field strength in the area is the superposition of the multiple scattering mechanisms. The signal level can change from a deep fade to a peak level (a difference of tens of dB). There are many models for this behavior, including the Longley-Rice model [21], the Bullington model [22], and Lee's model [23].

a. The Walfisch Model (Diffracting Screens Model)

Walfisch and Bertoni [20], proposed a theoretical model that is applicable to propagation in urban environments. This model assumes a simple representation of a city. To mathematically calculate the field at rooftop level, rows of buildings are replaced by an absorbing half-screen and the Kirchoff-Fresnel equation numerically evaluated for an incident plane wave. The field at rooftop height is found to obey the following expression to within 0.8 dB:

$$Q(\theta) = \begin{cases} 0.1\left[\dfrac{\theta}{0.03}\sqrt{\dfrac{d}{\lambda}}\right], & \theta\sqrt{d/\lambda} \le 0.3875 \\ 1.0\ , & \text{otherwise} \end{cases} \tag{3.1}$$

where, $Q(\theta)$ is the amplitude of the field at the roof top, θ is the incident wave angle on an array of building rows, d is the spacing between screens, and λ is the wavelength.

The field for receiver antenna heights below the roofline can be calculated by including a term to account for the diffraction over the final rooftop down to the antenna [20].

b. The COST 231 Model (The COST-WI Model)

The European Research Committee COST 231 created an urban propagation model based on the work of Walfisch and Bertoni and Ikegami [24]. The basic COST 231 model uses Walfisch-Bertoni results to calculate urban environment propagation prediction along with Ikegami's correction functions for taking into account the street orientation. The model was applied to the 800 MHz to 1.8 GHz bands and tested in the German cities Mannheim and Darmstadt. The street orientation influence was found to be minimal while it was found to require considerable improvements when

the antenna was at or below rooftop level. The accuracy of the COST-WI model is best for antenna heights much greater than the building heights, and deteriorates when the height of the antenna is less than the height of the building. The model becomes inaccurate when the terrain topography is non-flat or if the coating material of the land is inhomogeneous.

c. The Longley-Rice Model (The ITS Irregular Terrain Model)

This model is a path loss prediction model over irregular terrain that is suitable for coverage prediction in rural type environments. It is sometimes referred as the ITS irregular terrain model where ITS stands for Institute for Telecommunication Sciences. GO is used to compute the path loss, and Fresnel-Kirchoff knife-edge diffraction is used for horizon paths. It has been reported that the Longley-Rice model underestimates the transmission loss for most typical mobile propagation situations and has some discontinuities in the path loss between its two modes of operation. The model is applicable to parameters stated in Table 3.

Longley-Rice Model Parameter Ranges		
Parameters	**Min**	**Max**
Frequency	200 MHz	20 GHz
Range	1 km	2000 km
Antenna Heights	0.5 m	3 km
Polarization	Horizontal and Vertical	

Table 3. Applicable parameter ranges for Longley-Rice model (After Ref. [3])

2. Empirical Models

Most of the time, the direct path between transmitter and the receiver is obscured if a ground unit is below the roof level of the buildings. Propagation in urban and suburban environments is different from that of a direct path that has a single ground reflection. There are several empirical models developed to predict signal characteristics and to model propagation in the definable areas from measured data and curve-fit equations. Empirical models are city-specific and are tied to urban land-use maps. The London model of Ibrahim and Parsons [25], the Tokyo model of Okumura and his collaborators [26], and the Hata model [27] are well known empirical models for urban propagation.

a. The Okumura Signal Prediction Model

Okumura and his collaborators [26] measured signal strengths in the vicinity of Tokyo over a wide range of frequencies, with several mobile and fixed-site antenna heights and over irregular terrains and environments. They generated a set of curve-fits for these parameters. The model is applicable to the parameters in Table 4.

Okumura Model Parameter Ranges		
Parameters	**Min**	**Max**
Frequency	150 MHz	1920 MHz
Range	1 km	100 km
Antenna Heights	30 m	1000 m
Polarization	Horizontal and Vertical	

Table 4. Applicable parameter ranges for Okumura signal prediction model.

Curves were then generated that extracted various behaviors in several environments, including the distance dependence, frequency dependence, and urban to suburban differences. This gives a suburban correction factor, dependence of mobile antenna height on signal strength and variation of signal strength with fixed-station antenna height. Behavior of the curve was then extrapolated and interpolated to the frequencies between 100 MHz and 3 GHz. The completeness of the study has made the model a standard, but since the data are available only as curves, they are inconvenient to use. Formulas have been devised to fit the Okumura curves.

b. The Hata and Modified Hata Model

Hata [27] expressed the results of Okumura in terms of path loss between isotropic antennas and developed curve fitted formulas in the form of

$$\text{Loss} = A + B\log(d) \tag{3.2}$$

which have proven be very useful in system design and planning. A and B are functions of frequency, antenna heights, and terrain type, and d is the distance. There are also a number of modified Hata models that extend the range and the frequency spectrum. These models vary slightly from each other, and some of them are similar to Okumura's model. The Hata model is limited to the parameters in Table 5.

Hata Model Parameter Ranges		
Parameters	**Min**	**Max**
Frequency	100 MHz	1.5 GHz
Range	1 km	20 km
Mobile Ant. Heights	1 m	10 m
Antenna Heights	30 m	200 m

Table 5. Parameter ranges for the Hata model

The Hata model propagation loss is

$$L_p(\text{urban}) = [69.55 + 26.16\log(f) - 13.82\log(H_b) + \\ +[44.9 - 6.55\log(H_b)]\log(d) + a_x(H_m)] \tag{3.3}$$

where f = Frequency, MHz

d = Distance, km

H_b = Base station height, m.

Here, a mobile height correction factor $a_x(H_m)$ is applied for mobile antenna heights. Table 6 gives expressions for the correction factor.

The Mobile Height Correction Factor ($a_x(H_m)$)		
Frequency	**Large City**	**Medium/Small City**
$f \le 200$ MHz	$1.1 - 8.29\log^2[1.54H_m]$	$[0.7 - 1.1\log(f)]H_m + 1.56\log(f) - 0.8$ for all frequencies
$f \ge 400$ MHz	$4.97 - 3.2\log^2[11.75H_m]$	

Table 6. Height correction factor

Hata also provides expressions for median path losses in suburban and open areas as

$$L_p = \begin{cases} L_p(\text{urban}) - 2[\log(f/28)]^2 - 5.4 & \text{(Suburban)} \\ L_p(\text{urban}) - 4.78[\log f]^2 + 18.33\log f - 40.94 & \text{(Open Rural)} \end{cases} \tag{3.4}$$

Modifications can be made to the Hata formulas to improve accuracy relative to the Okumura model curves.

c. Ibrahim and Parsons Model (The London Model)

Ibrahim and Parsons [25] used the approach that propagation in urban areas depends on such things as the density of the buildings, the heights of the buildings, and the ground. The empirical behaviors were extracted from measured data as a function of various the factors such as land-usage factor, urbanization degree, and varying terrain height for the mobile. The data were collected 500 m squares. These were the same parameters that were available on land-use maps of London, England. This method can be applied to other cities as well as London. The parameter ranges for Ibrahim Parsons Model are given in Table 7.

Ibrahim-Parsons Model Parameter Ranges		
Parameters	**Min**	**Max**
Frequency	150 MHz	1 GHz
Range	0 m	10 km
Mobile Ant. Heights	0 m	3 m
Antenna Heights	30 m	300 m
Urbanization Factor	0-100	

Table 7. Ibrahim-Parsons model parameters (After Ref. [15]).

The "best fit" model based on measurements in London is

$$\begin{aligned} L_{ip} = -[&-20\log(0.7H_b) - 8\log(H_m) + \frac{f}{40} \\ &+ 26\log\left[\frac{f}{40}\right] - 86\log\left[\frac{f+100}{156}\right] \\ &+ \left[40 + 14.15\log\left[\frac{f+100}{156}\right]\right]\log(d1{,}000) \\ &+ 0.265L - 0.37H + 0.087U - 5.5\ ] \end{aligned} \tag{3.5}$$

where L_{ip} = Ibrahim and Parsons median propagation loss, dB

H_b = Base antenna height, m

H_m = Mobile antenna height, m

L = Land-use factor, percentage of grid covered by buildings

H = Height difference between grid containing the fixed site and grid containing the mobile, m

U = Urbanization factor, percentage of buildings in grid taller than three levels; outside city center $U = 63.2$

d = Range, km (not beyond radio horizon)

f = Frequency, MHz

Compared to measurements, the rms errors produced by this model are 2.1 dB at 168 MHz, 3.2 dB at 455 MHz, and 4.2 dB at 900 MHz.

B. URBANA WIRELESS TOOLSET

Science Applications International Corporation (SAIC), developed the **Urbana** Wireless Toolset. **Urbana** is a powerful computational electromagnetic (CEM) tool for simulating wireless propagation in complex environments [28]. The toolset uses a ray-tracing engine that includes GO and GTD to produce a high-fidelity three-dimensional (3-D) simulations. The ray-tracing process predicts the local mean power received at a given point in *x, y,* and *z*. For each point the vector sum of multipath power is computed. The calculations also include the effects of frequency, polarization, material properties, and varying antenna patterns. The model can include the effects of diffraction around corners of the scatterers. This property is very important in predicting the signal power in urban and indoor and outdoor environments.

1. Basic Urbana Capability

Urbana is a UNIX-based toolset and composed of the stand-alone components **XPatch, XCell, Cifer,** and **Urbana.** The collective toolset allows user to evaluate the effects of different material coatings of the buildings or other scatterer materials as well as the frequency, polarization and spatial diversity of the environment. Given the system parameters, antenna locations, and environment parameters, **Urbana** determines the power levels at specific predefined observation points.

Through the 3-D visualization interface, the user can study various simulation inputs and scenarios in a wide range of realistic scenes. The **Urbana** ray-tracing engine can account for multiple walls and other partially penetrable boundaries in all simulation environments. The key inputs to the **Urbana** code are:

- CAD facet models for terrain and buildings
- Observation regions that conform to the terrain and the buildings
- Surface material properties (Concrete, wood, glass, earth, dielectrics, etc.)
- Placements, strength, and vector polarized antenna patterns of transmitters and receivers
- Edge files of the surfaces to simulate diffraction from the edges
- Operating frequency of the transmitter and its physical properties
- Preference file *(*.xedge_pref)* to see signals and structures in **XCell**

The key output file is:

- Composite field level at each observation or coverage region sampling point

The **Urbana** process steps can be classified as:

- Generating geometry and edge files
- Generating the **Urbana** input file
- Executing the **Urbana**
- Post processing and data analysis

A brief description of each program and the processing steps is illustrated in Figure 15. There are some additional steps and programs used in this research that will be explained briefly in the following sections.

STEP 1: GENERATING INPUT DATA FILES

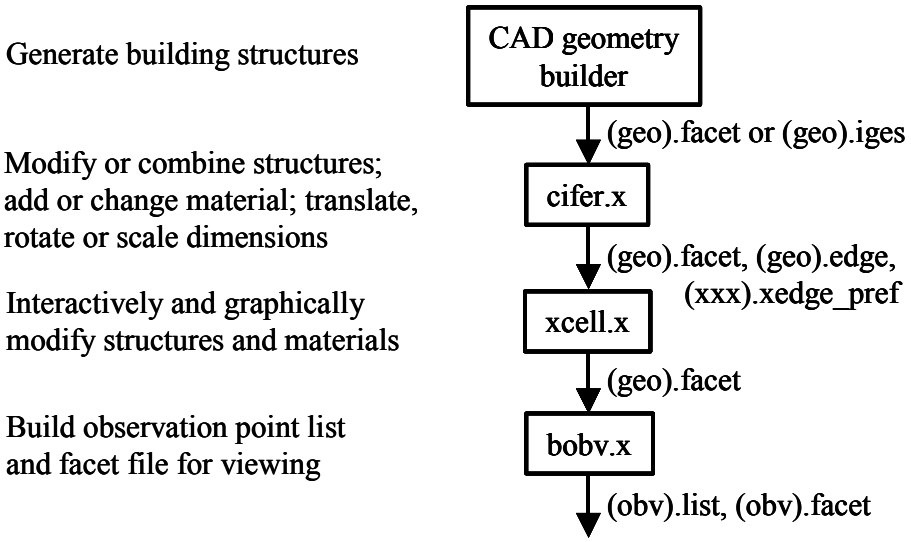

STEP 2: GENERATE URBANA INPUT FILE AND RUN URBANA

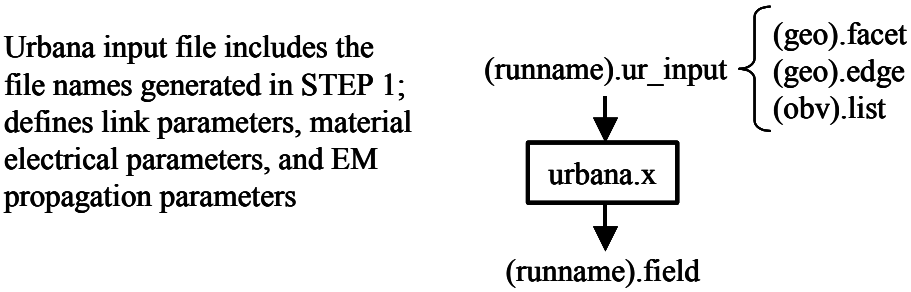

STEP 3: POST PROCESSING

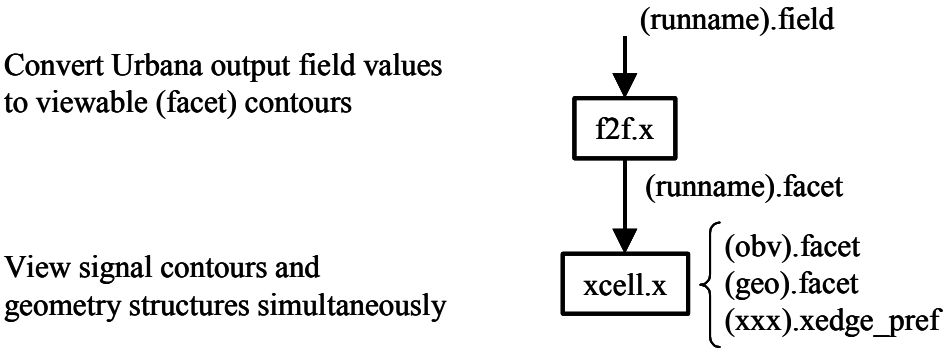

Figure 15. Urbana suite of software codes.

a. Generating Input Data Files

In **Urbana** simulations physical objects are represented by surfaces of triangular facets. Then the output files are converted to the DEMACO facet file format. To build the CAD model, software such as **AutoCad** and **ACADS** can be used. The CAD file should have a **.facet* extension. For simple objects, **Cifer** can be used. In **Cifer,** "The Facet Editor" menu allows simple shapes such as curves, boxes and planes to be built. **Cifer** was used to create the small city environment shown later by combining and resizing buildings with each other.

The material characteristics for each of the facets are specified by the coating material, and are defined by the input variable ICOAT. Each facet has a material variable that describes the type of material as defined in a master list of material properties. The next chapter explains how to specify some different material compositions like glass, wood, and concrete. In the simple city model, the ground plane has an ICOAT = 3, and the wall an ICOAT = 1 or 2. The PEC material simulations are done by changing to ICOAT = 0 in the simulations. **Cifer** is used to create the edge files needed for diffraction calculations of the simulation area. All files created should be in the same directory with the **Urbana** input file, unless the full path is used in the input file.

Observation points and planes can be created by ***bobv.x*** or by Matlab script. The purpose of this step is to build the two-dimensional array of observation points over the terrain or structure needed for the **Urbana** program. Generally the observation area of interest has the same dimensions as the ground plane. ***bobv.x*** requires a script file to create the observation plane. Below is the sample script for the observation points:

terrainname.facet
1.0
1 2 10
1
-300.0 300.0 -200.0 200.0 2.0 4.0

The first line indicates the name of the file describing the terrain. The second line specifies the length unit of the observation area. In this model, the observation units are 1 meter. The number in line three indicates the number of blocks, footprint size, and a dummy input variable that is ignored. The footprint size in this script file is 2 meters. In Line 4, "1" signifies that the observation area is a rectangular region. Line 5 consists of the x and y region limits, delta, and the offset. In this example $-300 \le x \le 300$, $-200 \le y \le 200$, delta is 2 and the offset is 4.

Once all the inputs are specified, the observation program ***bobv.x*** is executed. An observation list file (*terrainname.list*) and observation facet file are created. The list file is a simple table of *x, y, z* for each of the observation points. The facet file is used to view the observation points in **XCell**. The list file is read by **Urbana** upon execution. However, when using ***bobv.x,*** it creates observation points only outside of the building. By using the Matlab script, observation points can be specified at any location. In this research observation points are needed inside of the buildings so that the outdoor-to-indoor propagation can be assessed. A sample Matlab code for creating an observation plane is shown in Appendix A.

b. Generating Urbana Input File (runname.ur_input)

The **Urbana** input file is ASCII text with a specific set of input parameters and code words. These parameters are modified as needed for various simulation types. Some of the input parameters are:

- City geometry file, length and frequency units
- Antenna description and parameters
- Observation point parameters
- Theoretical considerations
- Coating materials
- Optional advanced features

After generating the input file, the code is executed in the shell window by typing "*urbana runname.ur_input 1*". The output includes an "**.field"* file that will be used to create signal contours.

c. Post Processing Steps

There are basically two steps in displaying the field file contours. One is translating the computational results into a color-coded facet file that can be viewed in **XCell.** The other is running **XCell** and viewing the facet file with the suitable preference file. The ***f2f.x*** program is used to convert **Urbana** output field files to viewable facet contours by **XCell.** A sample response table for ***f2f.x*** will be provided in the next chapter.

The ***f2fd.x*** program is used to take the difference of field files and to create a difference facet file for comparing the results of two different simulations. Observation plane and points should be identical in this process. Multiple field file differences can also be taken by using this program.

2. Urbana, XCell, and Cifer

Urbana is the computational engine that determines the signal levels for specified inputs. There are several selectable computational parameters for running **Urbana.** All of them are based on the high frequency assumption. There are comment lines describing the parameters and their range of values in the **Urbana** input file. The necessary parameters in the input file can be modified using any text editor application.

XCell displays a 3-D model and perspective views of signal strengths in and around buildings. The signal levels computed by **Urbana** can be plotted as color-coded pixels or cells. **XCell** can also be used to remove facets or change their material ICOAT numbers and, thus their properties. The details of the electrical properties of the material are defined near the end of the input file.

3. Running Urbana on the Silicon Graphics (SGI) Workstations

Several SGI machines are available for running **Urbana.** They range from a SGI

Indigo workstation with 325 MB main memory; 16 kB data cache size, and about 150 MHz CPU to newer SGI Octanes with up to 2 GB main memory; 32 kB data cache size, and about 400 MHz CPU.

4. Capturing, Converting, and Sending Files between SGIs and PCs

There are several ways to capture and use SGI displayed figures in personal computer (PC) documents. The best way to get images with high quality is to expand the figure on the screen and then capture images using **Media Recorder** or **Capture Galileo**. Captured images are saved in "rgb" format. This is an SGI image format. Then these "rgb" formatted files can be converted to "jpeg" using the **dmconvert** command:

dmconvert –f jfif <source.rgb> <target.jpg>

where **jfif** is the code for "jpeg" format.

To send converted "jpeg" files or any other file to a PC the **WS_FTP** program with a valid password can be used from a network PC. By using the full network address for the host name as "emag2.span.nps.navy.mil", files can be transferred to any PC on the network.

C. SUMMARY

In this chapter, some basic propagation mechanisms for urban environments are discussed. Theoretical and empirical models are examined briefly, and **Urbana** as a propagation toolset is mentioned. Additional tools and methods used in data processing are also explained. Key points and key inputs for the **Urbana** wireless toolset are shown, as well as selecting computational parameters to input file.

Frequency and polarization diversity properties of simulated UAV data links are examined in the next chapter. Selecting material coatings is also mentioned and simulation scenarios are prepared according to realistic UAV data link parameters.

THIS PAGE INTENTIONALLY LEFT BLANK

IV. URBANA SIMULATION

In this chapter, the steps involved in generating the simulation environment and models are explained step by step. A simple city environment is created, and simulations were performed for various parameter sets.

A. GENERATING SIMULATION MODELS

A small city was modified from an existing Urbana model. The small city is comprised of 23 buildings all having the same material properties. The small city model was extracted from a larger model of the city of Austin, Texas included in the Urbana package. The ground is modeled as flat with layers over a semi-infinite ground. This small city has 304 facets and the bounding box dimensions (i.e. maximum and minimum coordinate values) are:

$$(x_{\max}, y_{\max,} z_{\max}) = (255.59 \text{ m}, 177.90 \text{ m}, 150.00 \text{ m})$$

$$(x_{\min}, y_{\min,} z_{\min}) = (-255.59 \text{ m}, -177.90 \text{ m}, 0.00 \text{ m})$$

The transmitting antenna power is selected as 1 watt for all of the simulations. This is chosen as a conservative but also technologically possible power level for UAVs flying over a city. Contours for other power levels can be obtained by simple scaling. A combination of GO and GTD were used in computation of the signal contours. The ray launch method is a uniform angular distribution with 2 degrees angular separation. The maximum number of ray bounces is set to 7 as a compromise between simulation time and accuracy for a dense building environment. A dipole is used as the transmitting antenna in all simulations.

1. Small City Model

The propagation model for the small city environment was created with the help of **Cifer**. The existing Austin city model was clipped to give a smaller urban model. The tallest building has a height of 150 m and the average height of the buildings is 60 m. The ground plane dimensions are selected as 400 m by 600 m, with an observation plane

having the same dimensions. The ground plane is located at $z = 0$ m. Two-dimensional and three-dimensional views of the small city are shown in Figures 16 and 17.

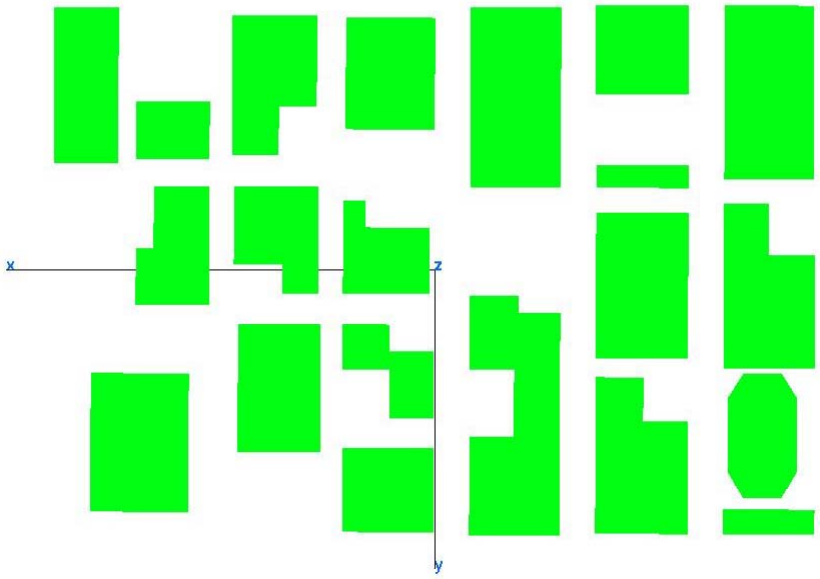

Figure 16. Top view of the small city model.

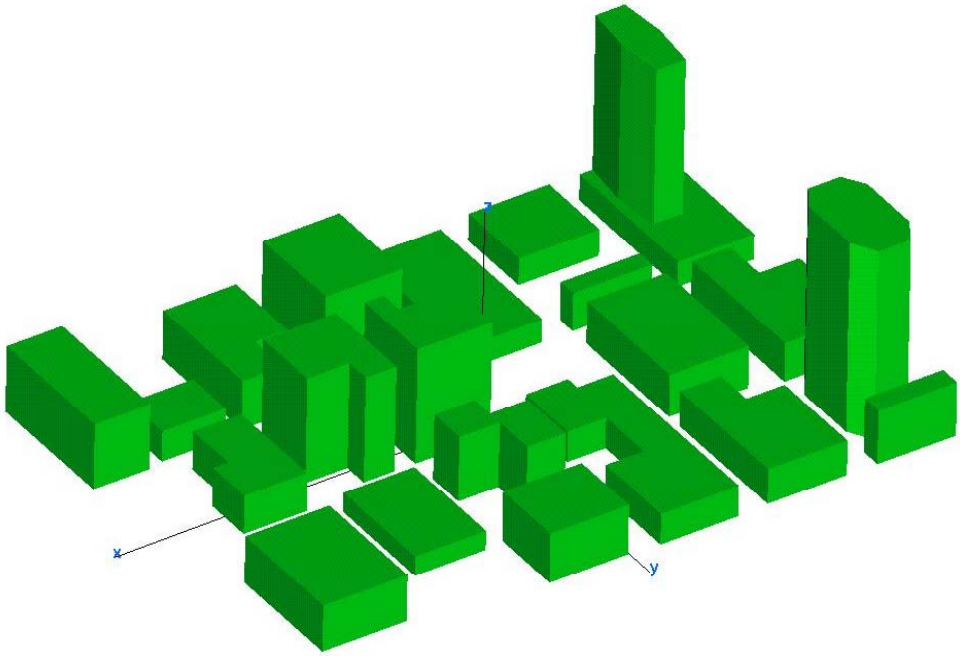

Figure 17. Oblique view of the small city model.

After creating the city buildings, edges are created with **Cifer**. Only matched edges are created. The extracted 3-D edge representation of the city is shown in Figure 18 and with the ground plane in Figure 19. Diffraction will be included for the edges shown in Figure 18.

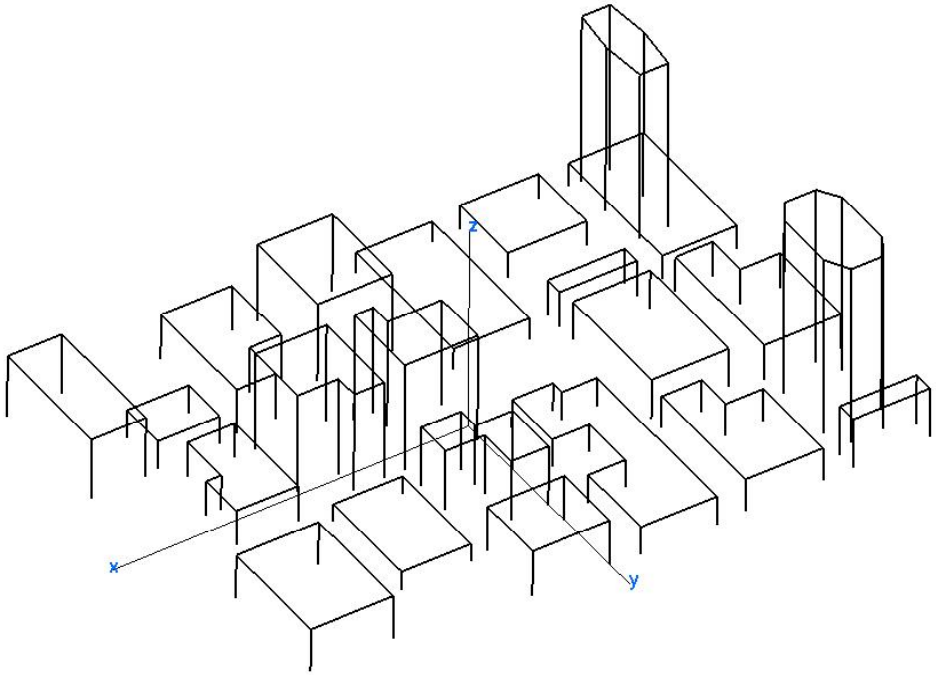

Figure 18. Three-dimensional matched edge representation of the small city.

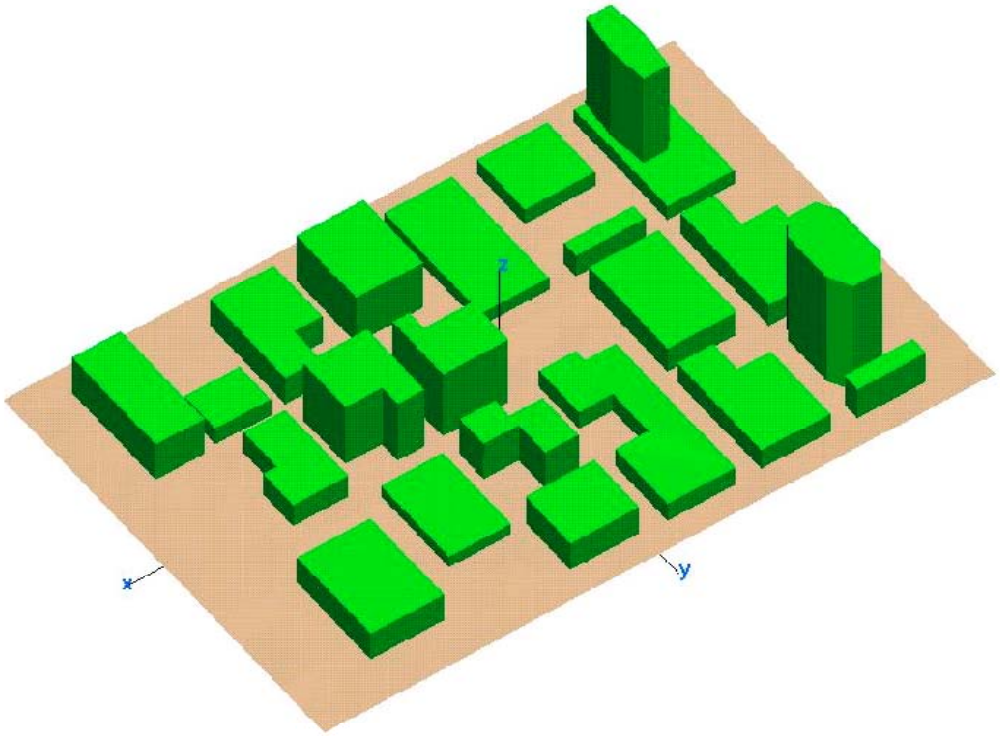

Figure 19. Small-city model with ground plane.

2. Generating Observation Points

The observation plane has the same dimensions as the ground plane. A height of $z = 4$ m is selected as the observation plane. The plane is an array of points at specified locations. To see the outdoor-to-indoor propagation, Matlab software is used for creating the observation plane. Using ***bobv.x*** does not give observation points inside of buildings. For an observation plane with the dimensions 600 m by 400 m, a cell size of 2 m is used. There are approximately 60501 observation points. Decreasing the distance between observation points (cell size) increases the resolution of the output contours. Too many observation points increase the running time or may require more CPU memory than available. A footprint (cell) size of 2 meters for the small city corresponds to about 60000 points. The Matlab code for creating the observation plane is listed in Appendix A.

3. Converting Field Files with *f2f.x*

The program ***f2f.x*** has to be executed to translate the field results into a color-coded facet file format that can be viewed in **XCell.** Table 8 shows a sample input response to the ***f2f.x*** program. This type of input sequence is kept constant for the entire

altitude test scenarios, except the range and clip values. Output files generated with this program are loaded into **XCell** to display the signal level contours.

Input Parameters	Response
Type of E-Field	*Magnitude of E-Total*
Number of Field Files	1
Name of Field File	*city.field*
Antenna Power Level	1
Histogram Interval	10 dB
Max. and Min. Clip Values	-200 dBm, 0 dBm
Max. and Min. Range Values	-200 dBm, 0 dBm
Number of Levels	25
Lowest Coating Code	1
Name of Output Facet File	*cityout.facet*
Side of Footprint Square	2
Shift According to Z-data	N
Enter z-offset footprint	0

Table 8. Input parameters and responses for *f2f.x*

4. Antenna Parameters for Simulations

All of the simulations employ a half-wave dipole antenna transmitting a power of 1 W. The antenna parameters are varied in the input file to change frequency and polarization. For different altitudes and material selection scenarios, a separate antenna file is used in the simulations. In Figure 20, the antenna location is $x = 0$ m, $y = -50$ m, $z = 30$ m. (The antenna image is magnified 3.5 times in **XCell** for ease of viewing). The antenna location in (*x, y*) is fixed for all of the small city simulations, but the polarization, frequency, and altitude (*z*) vary.

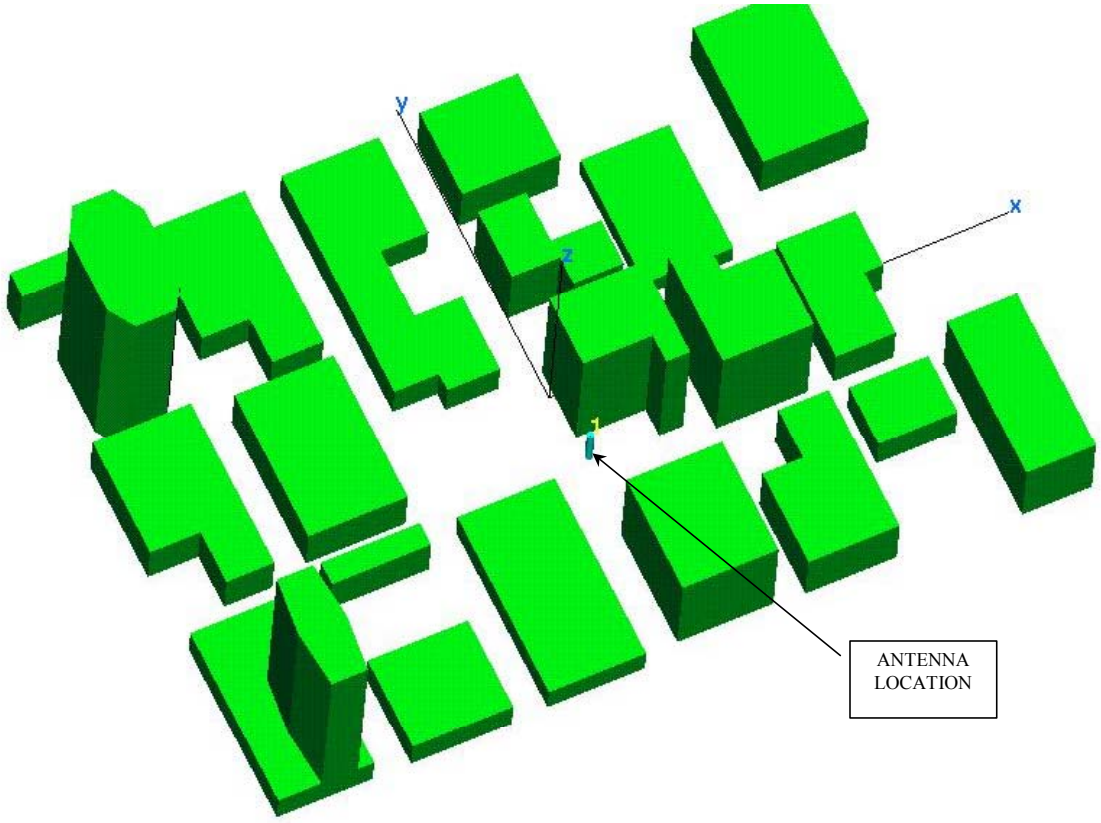

Figure 20. Small city with a vertical polarized antenna at $x = 0$ m, $y = -50$ m, $z = 30$ m.

B. DIFFERENT ANTENNA ALTITUDES SCENARIO

UAVs flying over a city will try to maintain links to ground command and control centers and other ground units. Obviously the UAV location affects the field strength at the observation points. To start with, PEC material is used for all walls of all buildings. The input file parameters used in this simulation are listed in Table 9.

Input Parameters	Response
Facet Model	*city.facet*
Unit Length	meters
Frequency	2.4 GHz
Antenna Description	from file:*city.antenna*
Antenna Type	Dipole
Antenna Polarization	Vertical X(1, 0, 0) and Z(0, 0, 1)
Observation Points	from file:*observ.obv*
Computation Method	Geometrical Optics
Edge Diffraction	UTD
Edge File	*city.edge*
Angular Interval	2.0 Degrees
Max Ray Bouncing	7
Coating Material	PEC
Advanced features	NO

Table 9. Input parameters for simulation.

The maximum number of bounces is limited to 7. Note that most of the propagation is limited to the area near the antenna location. For this simulation an additional building located at (-10 m, 0 m, 0 m) was added as seen in Figure 21. This building limits propagation to the corridor along y-axis like a waveguide. This configuration of a street bounded by high-rise building is referred to as an urban canyon. It effectively confines the signal to narrow paths along the street. This effect can be used to advantage when positioning a UAV for communications. The urban canyon effect is strongest when the UAV is at an altitude below the building height, in this case (0 m, 0 m, 5 m).

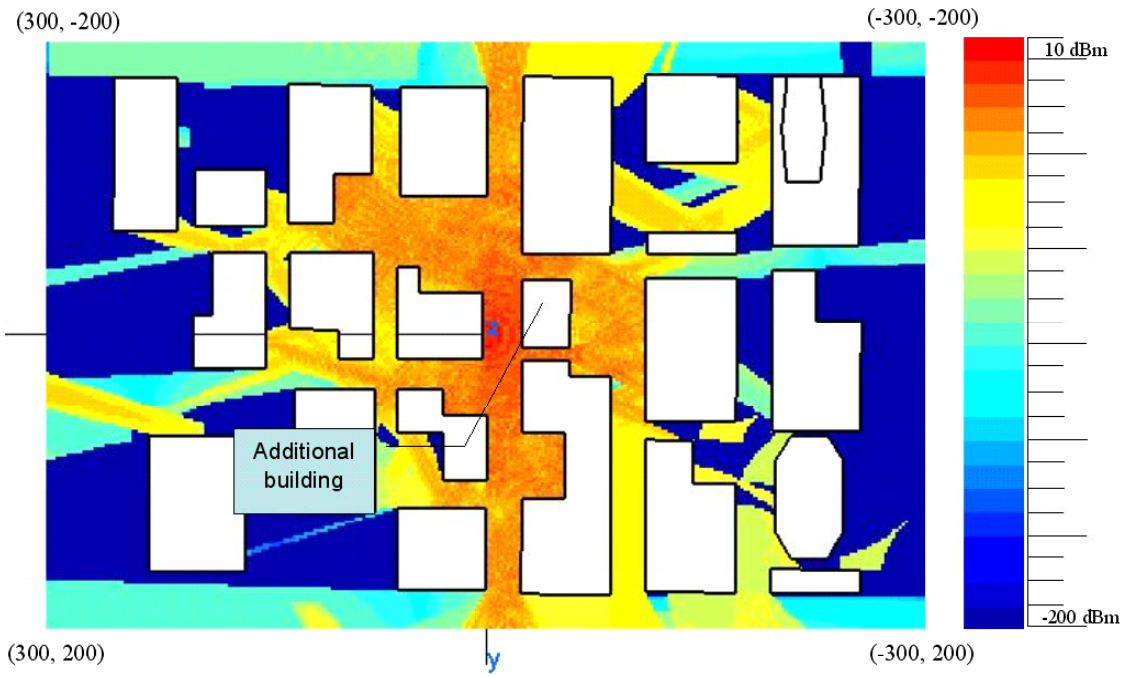

Figure 21. Signal contours for PEC buildings. An additional building was added to form an urban canyon along the *y* axis.

1. Changing the Antenna Altitude

In this simulation, the antenna is located at the point $(0\text{ m}, -50\text{ m}, 30\text{ m})$. The field values range between 0 and -200 dBm for 1 W powered vertical polarized antenna. All buildings are considered as PEC. PEC buildings will reflect all the incident waves coming toward it and multipath will be strong. Note that the small scale fluctuations (on the order of a wavelength) are not visible because of the large cell size. Within each cell the field may vary to 3 dB from the value plotted.

For UAV applications altitude has a significant effect on communication link reliability. These effects are apparent by comparing the data in Figures 22 to 26. The simulation parameters for this series are:

- PEC building material
- No ground plane
- 1 W transmitter antenna power
- Frequency = 2.4 GHz, half-wave dipole, vertical polarization

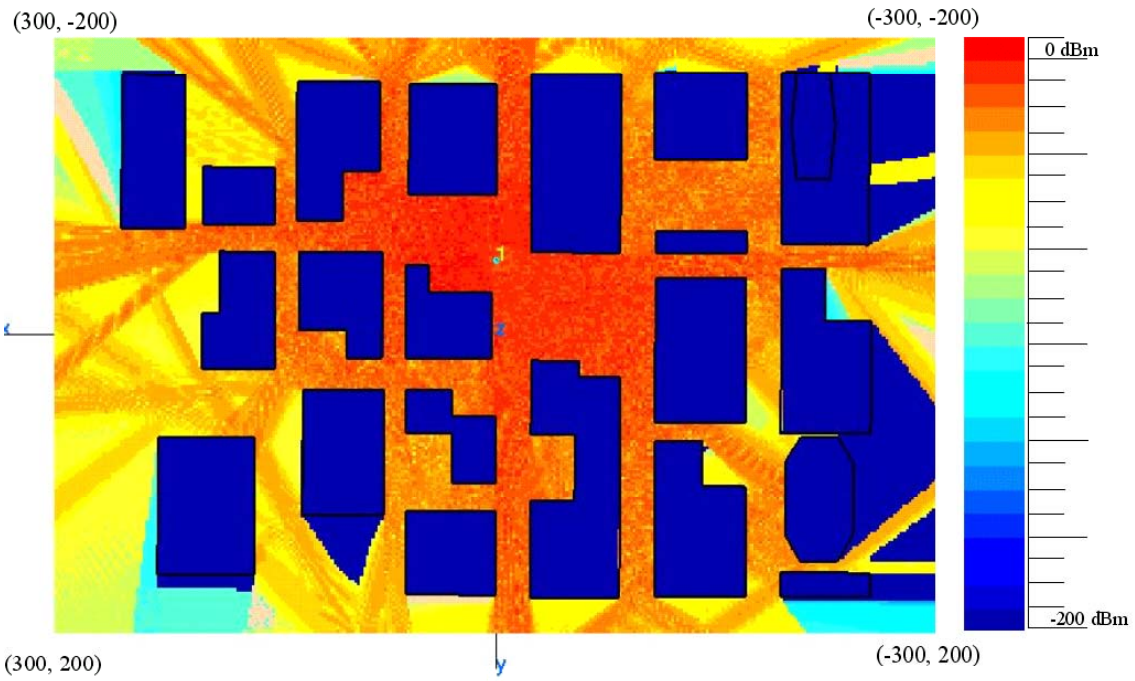

Figure 22. Signal levels for an antenna location of $(0\text{ m}, -50\text{ m}, 30\text{ m})$**.**

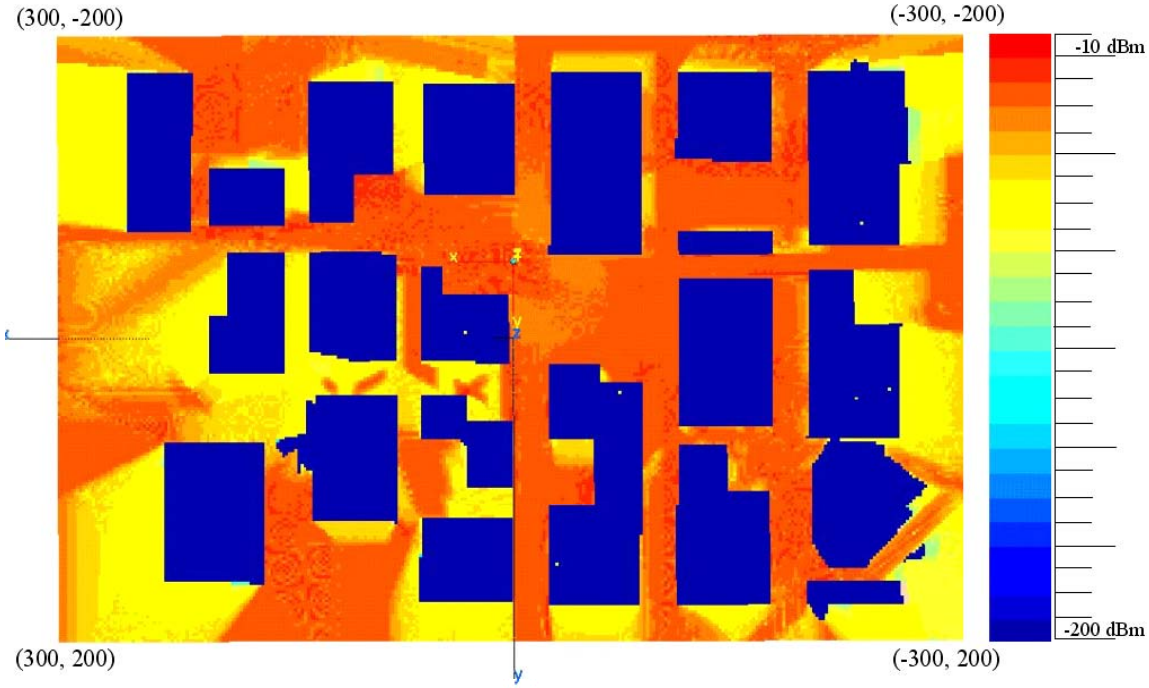

Figure 23. Signal levels for an antenna location of $(0\text{ m}, -50\text{ m}, 150\text{ m})$**.**

The height of the antenna is changed from 30 to 600 meters in steps of 150 m. The tallest building in the city environment is 150 m. When the UAV uses this elevation,

the maximum signal level dropped 10 dB, but the signal level is more uniform compared to the lower altitudes. This is expected, because of the increased free space path loss and decreased shadowing at higher altitudes.

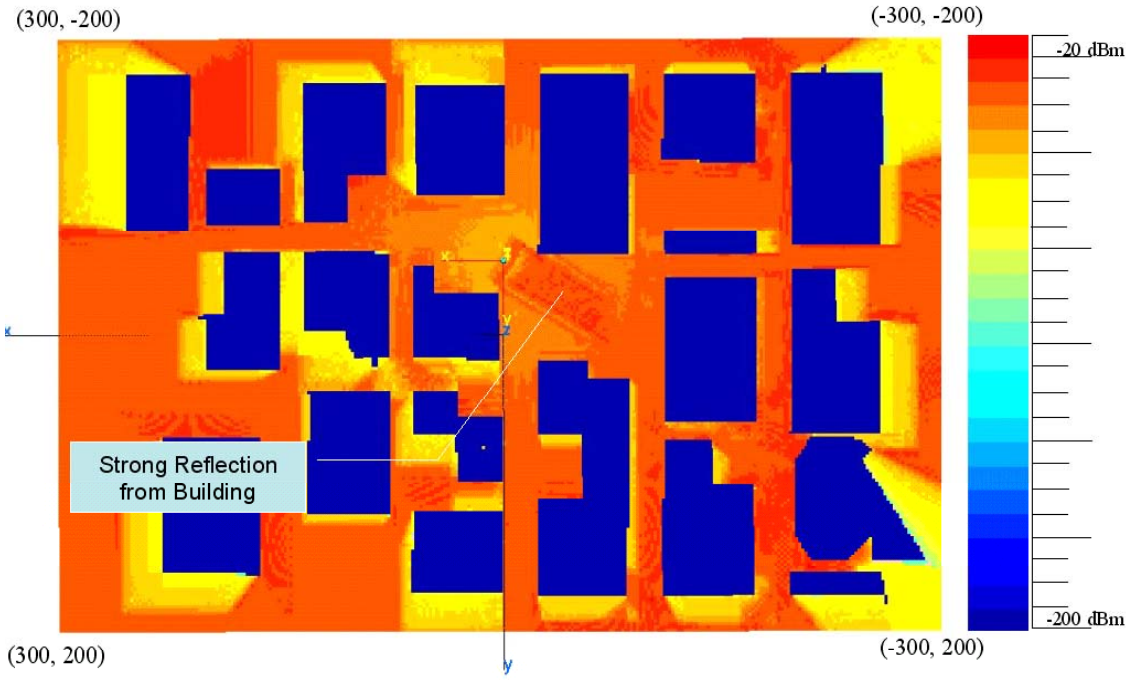

Figure 24. Signal levels for an antenna location of $(0\text{ m}, -50\text{ m}, 300\text{ m})$**.**

In Figure 24, the average signal level dropped another 10 dB. At 300 meters altitude, we expect to have a reflection from the tallest building at point (-250 m, 150 m). The building has a surface perpendicular to the antenna and the reflection is clearly seen in the figure. In general, most of the areas in the city have -30 to -40 dBm signal level.

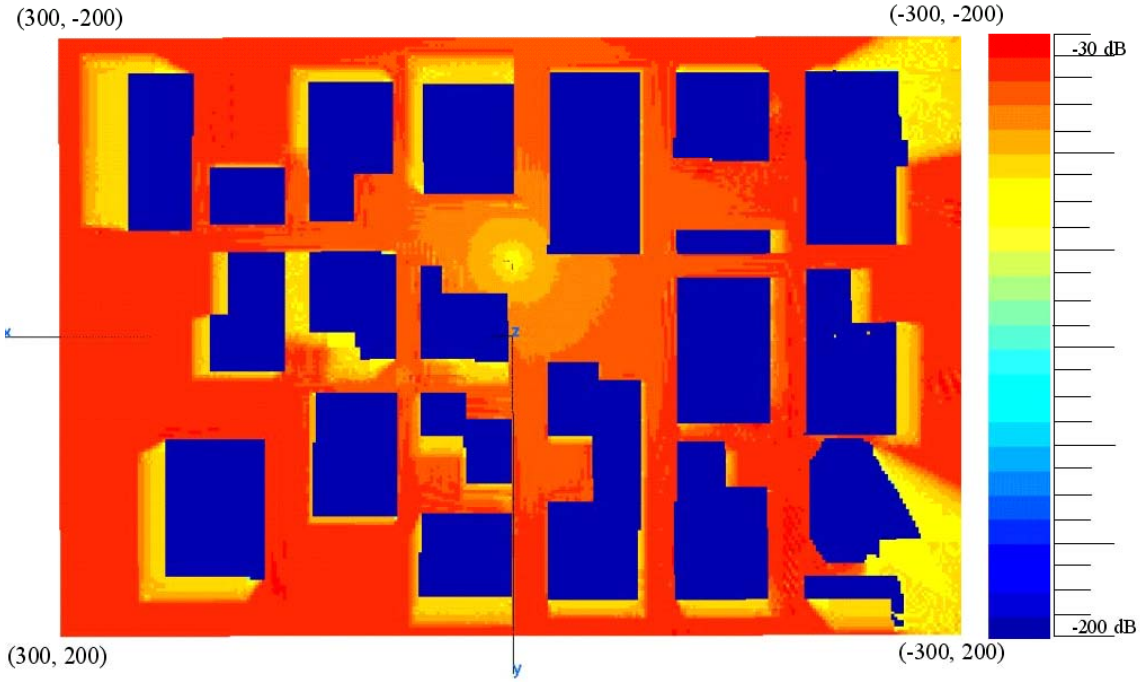

Figure 25. Signal levels for an antenna location of $(0\text{ m}, -50\text{ m}, 450\text{ m})$**.**

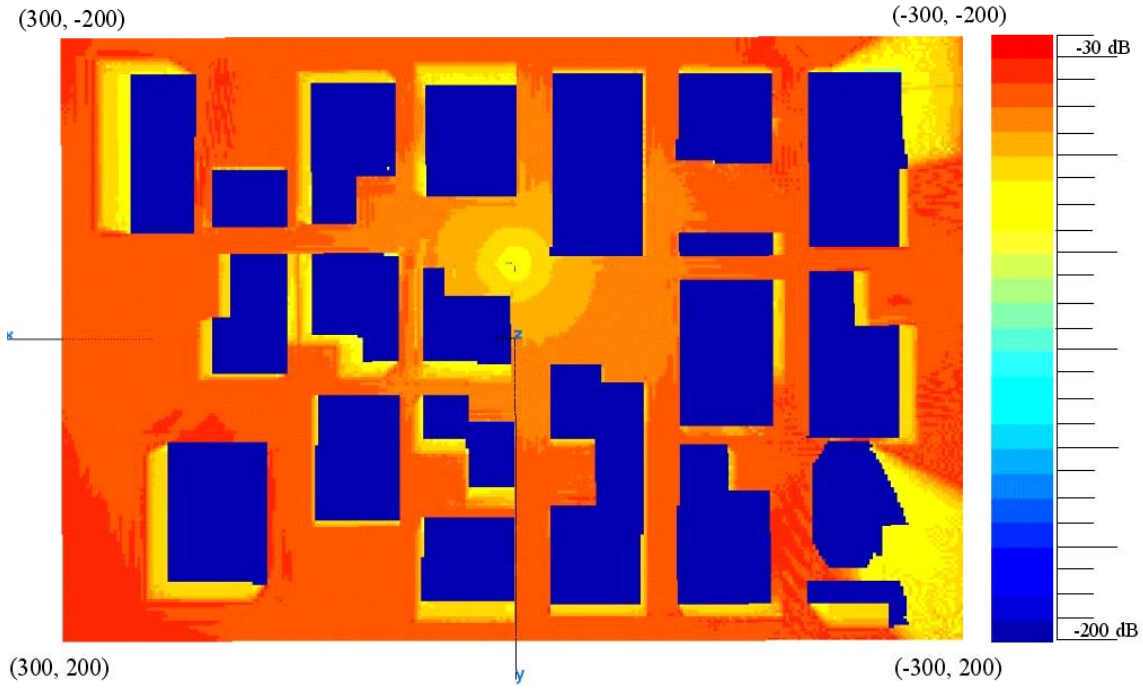

Figure 26. Signal levels for an antenna location of $(0\text{ m}, -50\text{ m}, 600\text{ m})$**.**

At the heights 450 m and 600 m, propagation through the city can be considered as uniform. This is due to the fact that the high antenna altitude casts very small building shadows. Under the antenna, the signal level is lower than for areas farther away because of the null of the pattern. At 600 meters from the ground the decrease in signal level due to the increasing free space loss is evident.

2. Conclusions Regarding Altitude

Increasing altitude generally gives more uniform coverage because building shadows are smaller. However, high altitudes make the UAV more visible and perhaps more vulnerable to fire. Also, more fuel may be consumed at higher altitudes.

The optimum altitude is about two or three times higher than the tallest building height, according to Lock [29]. That corresponds to between 300 m and 450 m for this city. To further study the effects of the antenna polarization and frequency, an altitude of 150 m will be used.

C. MATERIAL SELECTION SIMULATIONS

The material of the walls is the same for all buildings in the model. They are modeled as PEC, concrete, wood, and glass. To investigate the effect of materials in propagation, a simple two-building model is used. The same thickness value is used for all of the materials. For fixed antenna location, the simulation and display parameters are shown in Table 10.

Material Selection Simulations for fixed Antenna Location $(x, y, z) = (-30, -1, -1)$						
Coating Material	**Relative Permittivity** $(\varepsilon', \varepsilon'')$	**Relative Permeability** (μ', μ'')	**Resistivity (ohm)**	**Thickness (m)**	**Graph Range (dB)**	
					Min	**Max**
Concrete	10.1, 0.50	1.0, 0.0	10^{30}	0.3	-70	10
Wood	3, 0.67	1.0, 0.0	10^{30}	0.3	-70	10
Glass	6, 0.00	1.0, 0.0	10^{30}	0.3	-60	10

Table 10. Parameters for material slabs and graph ranges

1. Generating Two-Building Simulation Environment

The two building bounding box limits (in meters) are:

$$(x_{\max}, y_{\max,} z_{\max}) = (10\text{ m}, 60\text{ m}, 10\text{ m})$$

$$(x_{\min}, y_{\min,} z_{\min}) = (-10\text{ m}, 0.0\text{ m}, 0.0\text{ m})$$

There are 2 big parts and 20 facets for these two buildings. The same steps mentioned in Chapter III are used in creating the facet, antenna, and edge files. A 3-D representation of buildings and antenna are shown in Figure 27.

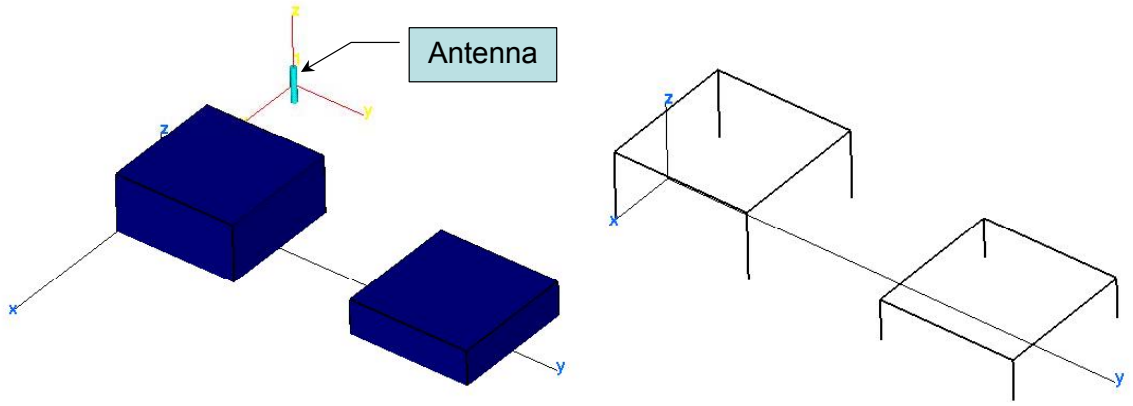

Figure 27. Three-dimensional representation of facets (left), edges (right), and antenna (top).

2. PEC, Wood, Concrete, and Glass Material Simulations

An antenna power of 1 W and a frequency of 2.4 GHz is used in these simulations. Here, the antenna is located at $(0\text{ m}, -50\text{ m}, 30\text{ m})$. The signal levels range from 0 to –200 dBm for 1 Watt transmitted with a vertical polarized antenna. All buildings are considered as PEC, and the field is shown in Figure 28. PEC building walls will reflect all the incident signals resulting in strong multipath propagation. However, with only two buildings, after two or three bounces, most reflections will exit the observation region. Therefore, deep fades (i.e., complete cancellation) are not as likely as they would be for a large city with many buildings.

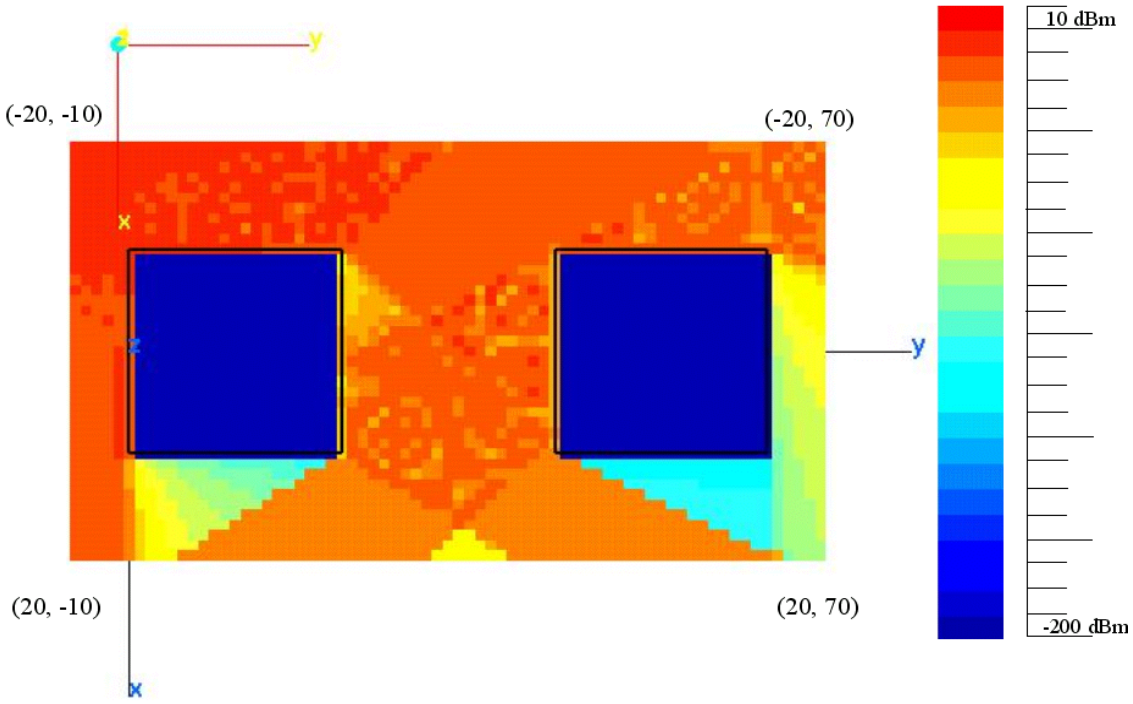

Figure 28. PEC material

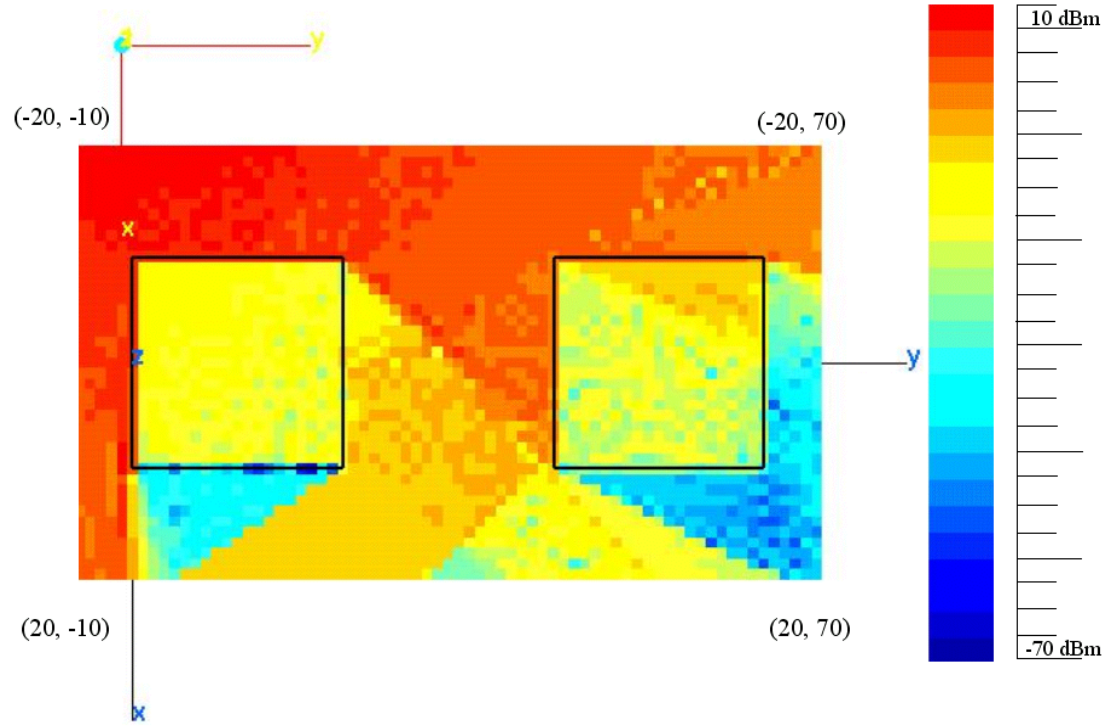

Figure 29. Wood material

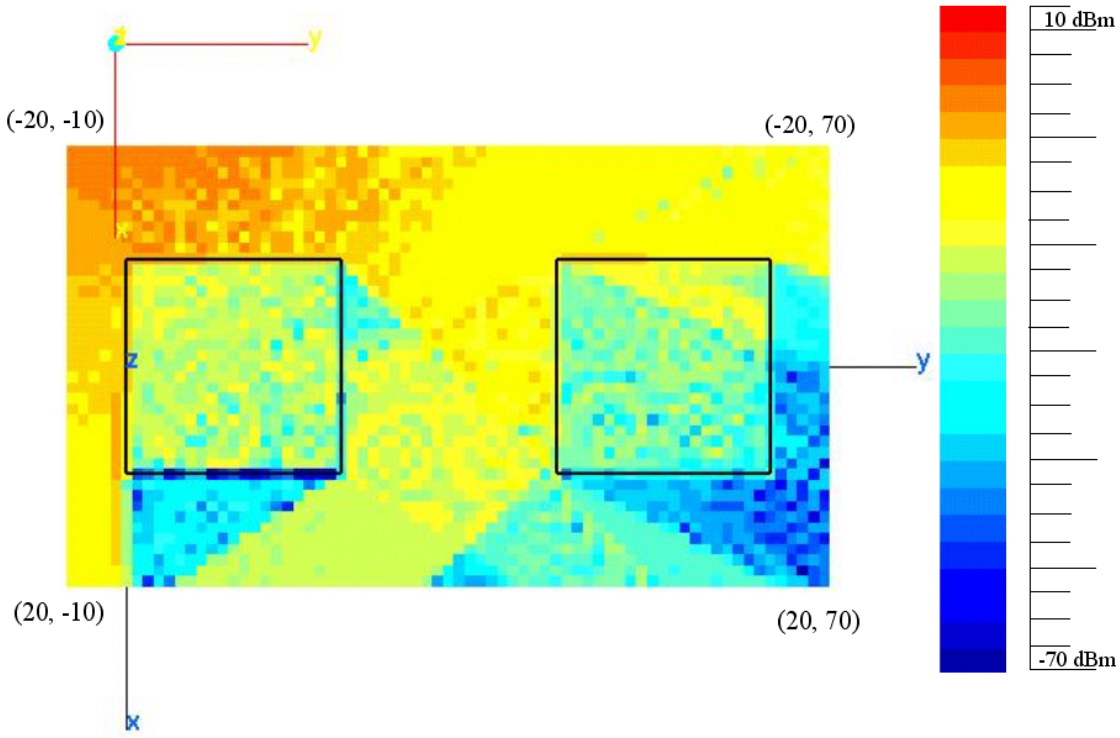

Figure 30. Concrete material

Diffraction from the edges and the reflection from the surfaces can be seen easily from this altitude (30 m). Figure 29 illustrates the signal distribution for wood walls. The signal levels are between 10 and -70 dBm values for 1 W powered vertical polarized antenna. Figure 30 illustrates the propagation for concrete walls and the graph values are again between 10 and –70 dBm. Figure 31 shows propagation for glass materials. Most of the incident waves are transmitted into the material and reflection from the glass surface is very low compared to the other materials used in this simulation.

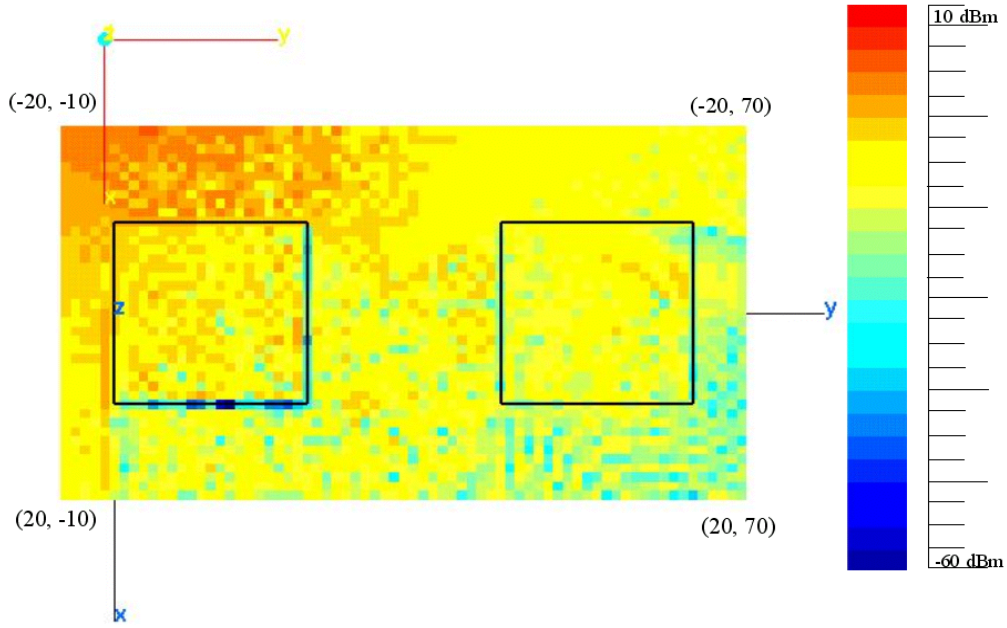

Figure 31. Glass material

The minimum signal level for the glass simulation is –60 dBm, which is 10 dBm greater than that of wood and concrete coated walls. A combined illustration of the different material simulations is shown in Figure 32.

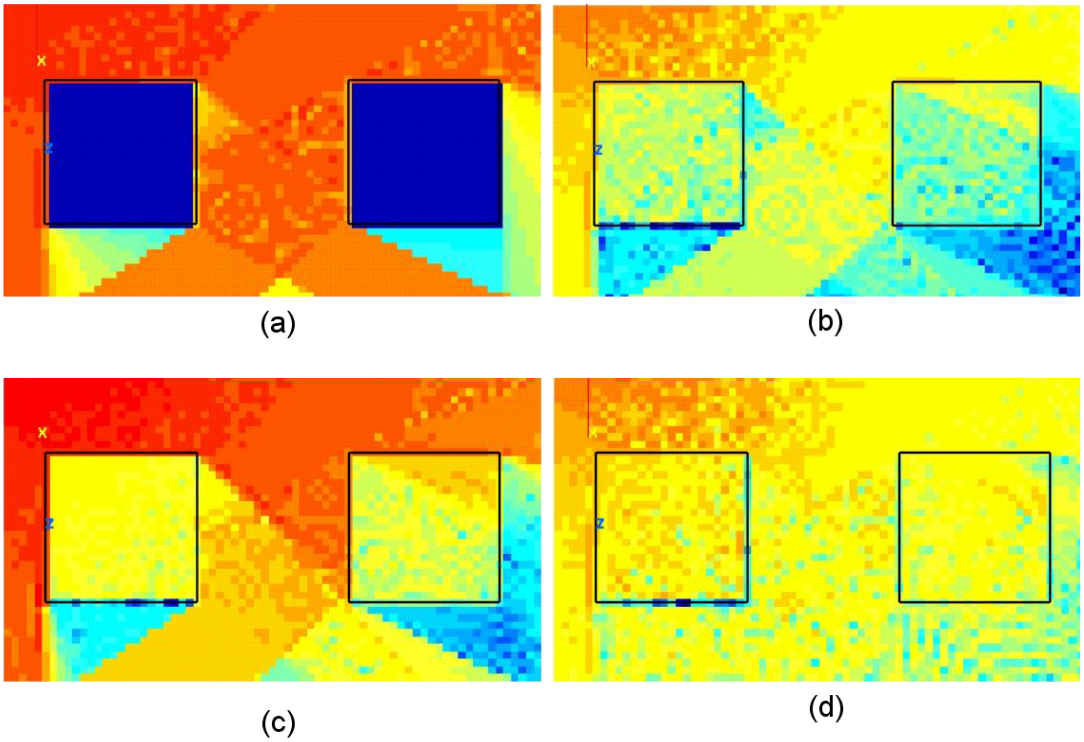

Figure 32. Different wall materials: (a) PEC, (b) concrete, (c) wood, and (d) glass.

3. Material Simulation Conclusions

Results clearly indicate that material coatings have a very strong effect on the signal contour levels. It is really difficult to predict the material characteristics of the building walls in a city. Most of the materials in a military installation are concrete while some of them have glass surfaces. In the concrete material simulation, large regions of the observation area are shadowed. However, in the glass and wood material simulations, the signal level is more uniform. For the remaining frequency and polarization simulations, concrete material will be used.

D. FREQUENCY SIMULATIONS

In this part, three center frequencies are chosen for the links: 900 MHz, 2.4 GHz, and 5.0 GHz. A bandwidth of 50 MHz is chosen as being typical of most data-links. In following simulations the antenna is located at point $(0\text{ m}, -50\text{ m}, 150\text{ m})$. This altitude is selected because of the high reflection and diffraction effects of the walls of city environment. Table 11 is a summary of the simulations and their maximum and minimum power levels.

Frequency Simulations for BW=50MHz.				
Center Frequency	Simulation Frequency (GHz)	Dipole Length (Half-wave) (m)	Power (dB)	
			Min	Max
900 MHz	0.875	0.17143	-94	-20
	0.8875	0.16901	-88	-20
	0.9	0.16667	-96	-20
	0.9125	0.16438	-90	-20
	0.925	0.16216	-98	-20
2.4 GHz	2.375	0.06316	-109	-22
	2.3875	0.06283	-112	-22
	2.4	0.06250	-111	-22
	2.4125	0.06218	-115	-22
	2.425	0.06186	-114	-22
5.0 Ghz	4.975	0.03015	-140	-22
	4.9875	0.03008	-138	-22
	5	0.03000	-144	-22
	5.0125	0.02993	-142	-22
	5.025	0.02985	-139	-22

Table 11. Frequency simulation parameters

All of the material coatings are set to concrete. Power in dBm can be read from the right columns in Table 11. Minimum power decreases when the frequency increases due to path loss, as expected.

1. Differential Signal Plots with f2fd.x

After generating the field files for different parameters ***f2fd.x*** is used to convert the field files to facet files that plot the power differences between the fields. Sample responses to ***f2fd.x*** are similar to ***f2f.x***. Input parameters and responses are shown in Table 12. The same observation plane is used in both files.

Input Parameters	Response
Type of E-Field	*Magnitude of E-Total (4)*
Take absolute value of dB Difference	No
Number of Field Files on (+) side	*1*
Name of Field File on (+) side	*cityfre1.field*
Antenna Power level Scale Factor	*1*
Number of Field Files on (-) side	*1*
Name of Field File on (-) side	*cityfre2.field*
Antenna Power level Scale Factor	*1*
Histogram Interval	10 dB
Max. and Min. Clip Values	-30 dBm, 30 dBm
Max. and Min. Range Values	-30 dBm, 30 dBm
Number of Levels	25
Lowest Coating Code	1
Name of Output Facet File	*citydiffout.facet*
Side of Footprint Square	2
Shift According to Z-data	N
Enter z-offset footprint	0

Table 12. Input parameters and responses for *f2fd.x*

2. Simulations of the 900 MHz Frequency Band

Figures 33 to 37 show the propagation contours from 875 MHz to 925 MHz. In these simulations a total bandwidth of 50 MHz is used, and the frequency stepped in 12.5 MHz increments. All other parameters are constant in order to detect the variations due solely to the frequency change.

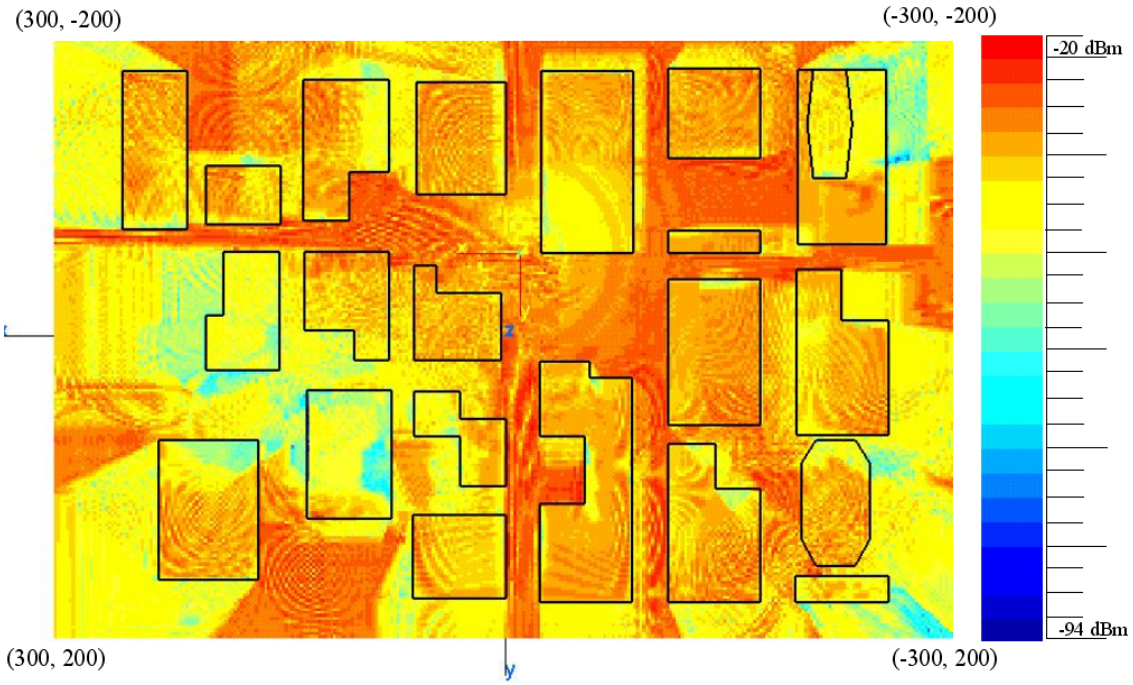

Figure 33. Vertical polarized antenna, 875 MHz

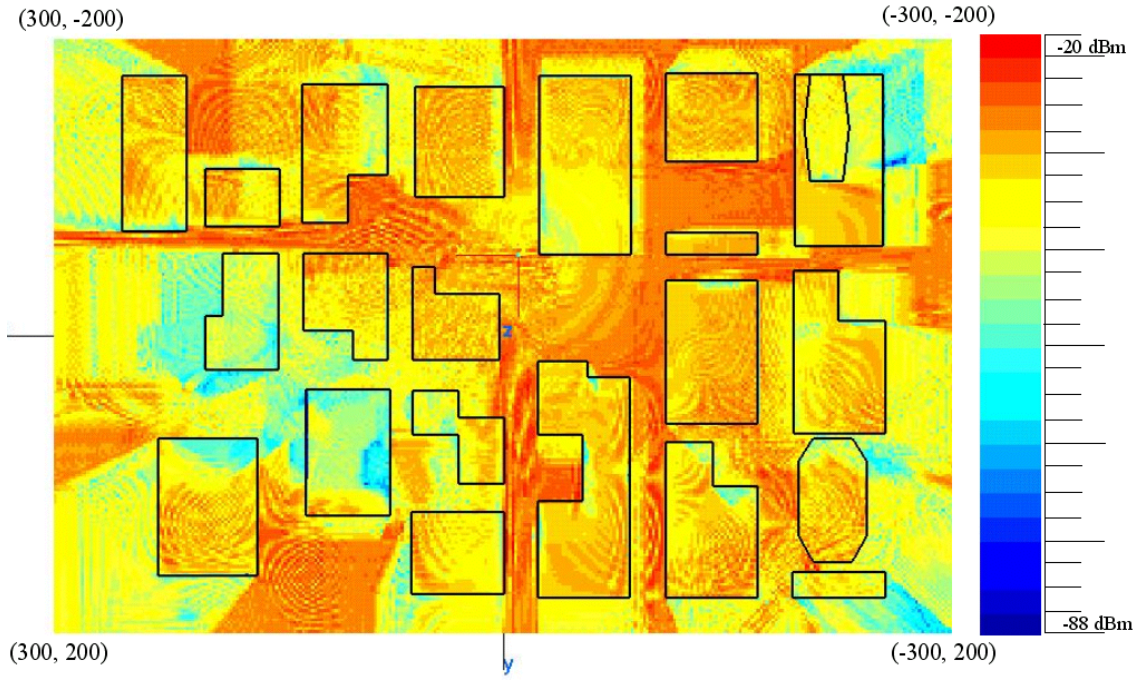

Figure 34. Vertical polarized antenna, 887.5 MHz

At a frequency of 875 MHz the levels are between -20 and -94 dBm while at the frequency 887.5 MHz, the levels are between –20 and –88 dBm for a 1 W powered vertical polarized antenna.

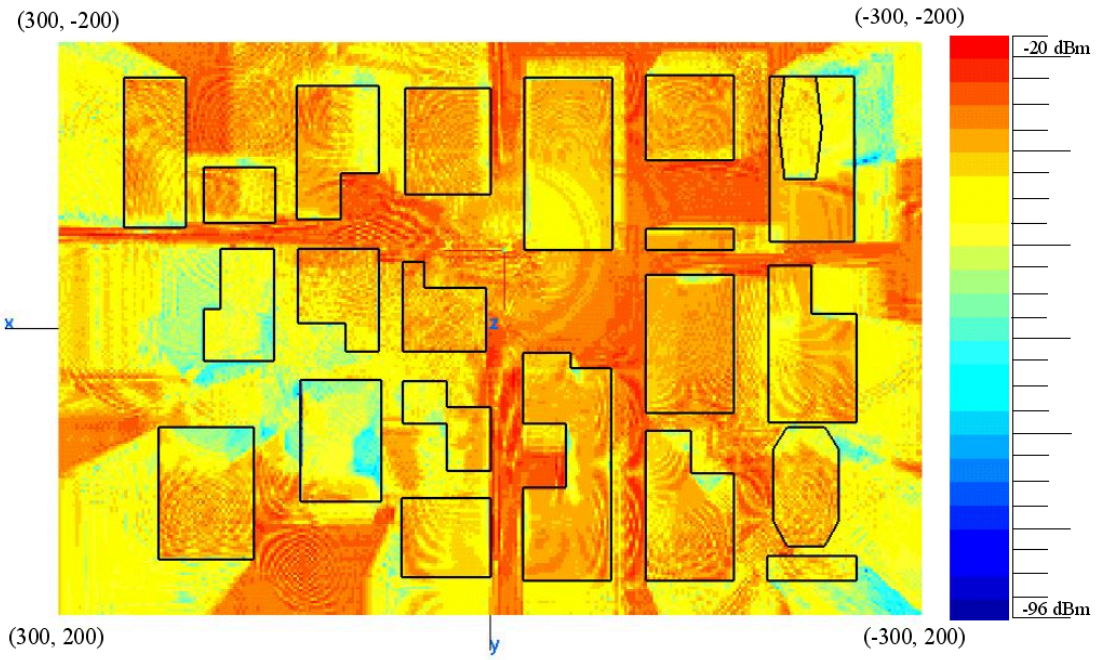

Figure 35. Vertical polarized antenna, 900 MHz

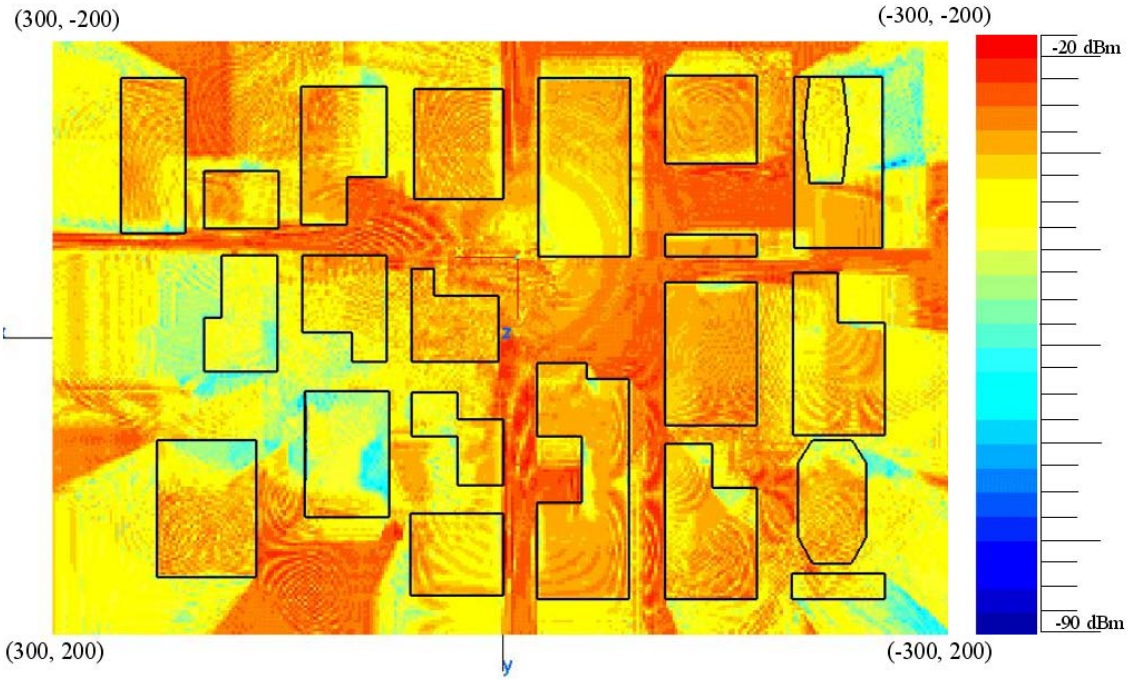

Figure 36. Vertical polarized antenna, 912.5 MHz

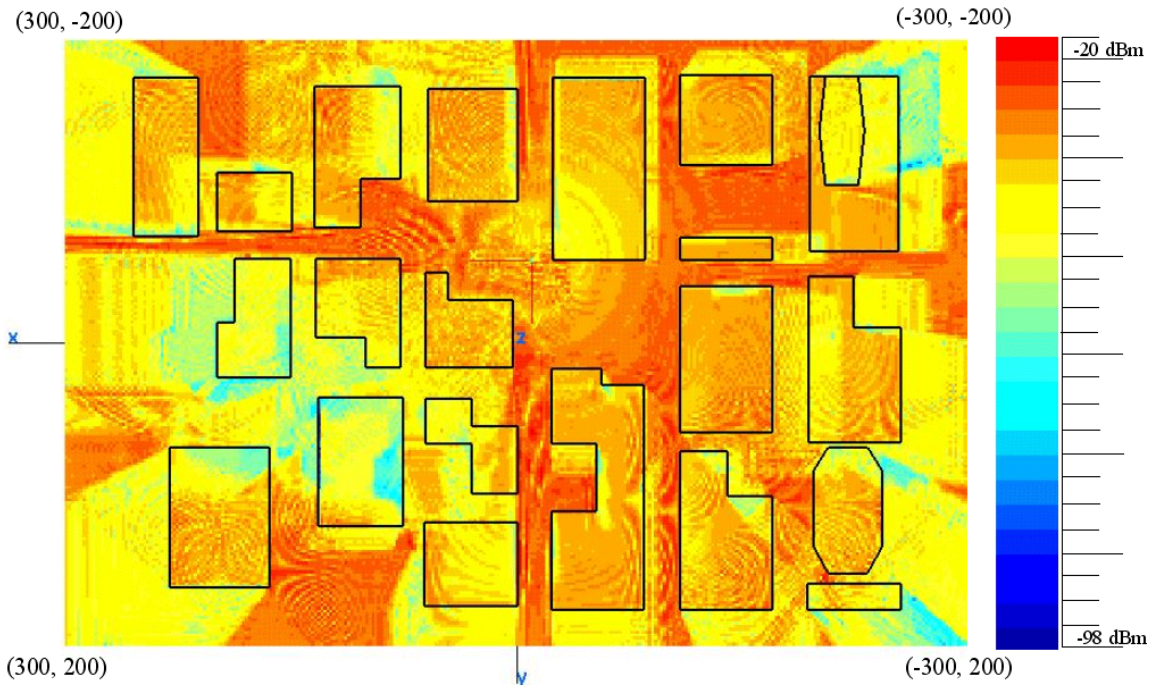

Figure 37. Vertical polarized antenna, 925 MHz

When the frequency of the transmitter is changed, there is a noticeable change in the signal contours. In particular, the location of the hot spots (localized areas of high signal level) changes with the frequency. Increasing the frequency results a decrease in outdoor-to-indoor propagation. Signal levels inside of the buildings decrease slightly. The diffraction patterns (rings and curves) are clearly seen in the figures. Shadow regions have lower signal levels compared to the direct path regions. However, some shadow regions have good signal strength due to reflections from surfaces and diffractions from edges.

The signal level differences are generated with the program ***f2fd.x***. The reference frequency is 900 MHz and steps of 12.5 MHz are taken over a 50 MHz band. The value shown is simply the difference in dB values between the signal levels for the two frequencies. Note that this may not be the best or most useful measure. Depending on the modulations used, a coherent difference that uses a common phase reference may be better. However, a dB difference does give insight into the change in signal level due to the propagation channel.

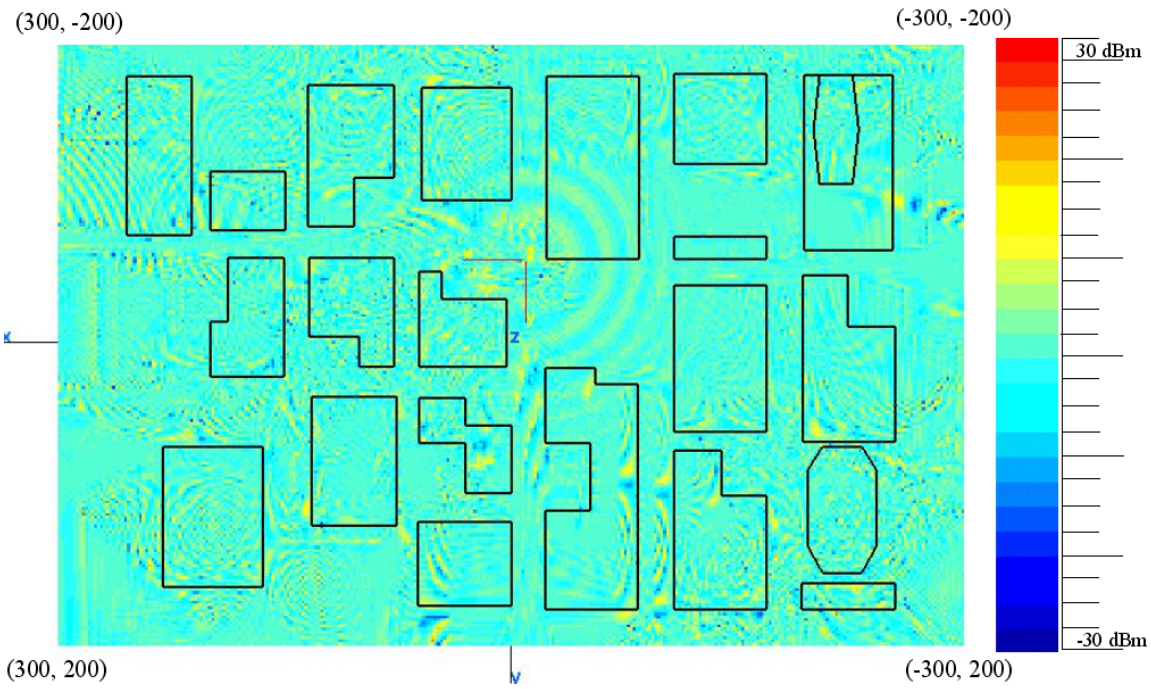

Figure 38. Frequency difference, 900 MHz - 875 MHz

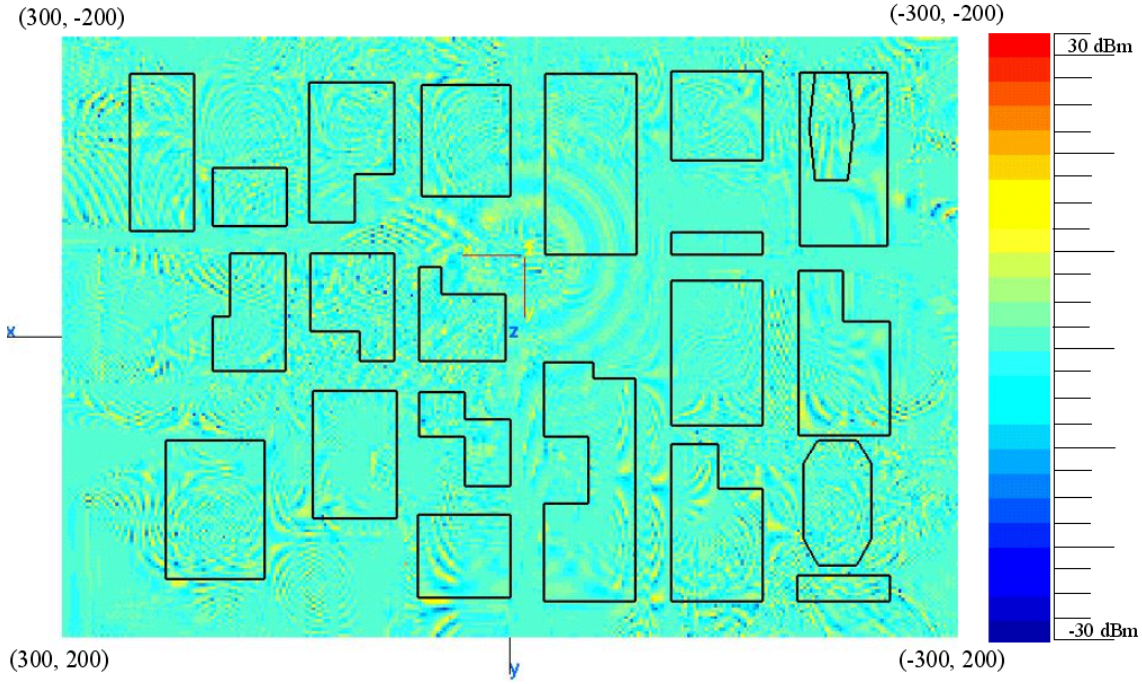

Figure 39. Frequency difference, 900 MHz - 887.5 MHz

Figures 38 to 41 are illustrations of frequency difference plots related to the center frequency of 900 MHz. Most of the variations are small (a couple of dB) compared to the

absolute signal levels. The majority of observation points show differences in the range of –5 to 5 dB but there are some hot spots where the difference of the graphs can reach 30 or –30 dB. A summary of the frequency difference simulation result for the 900 MHz band is shown in the Table 13.

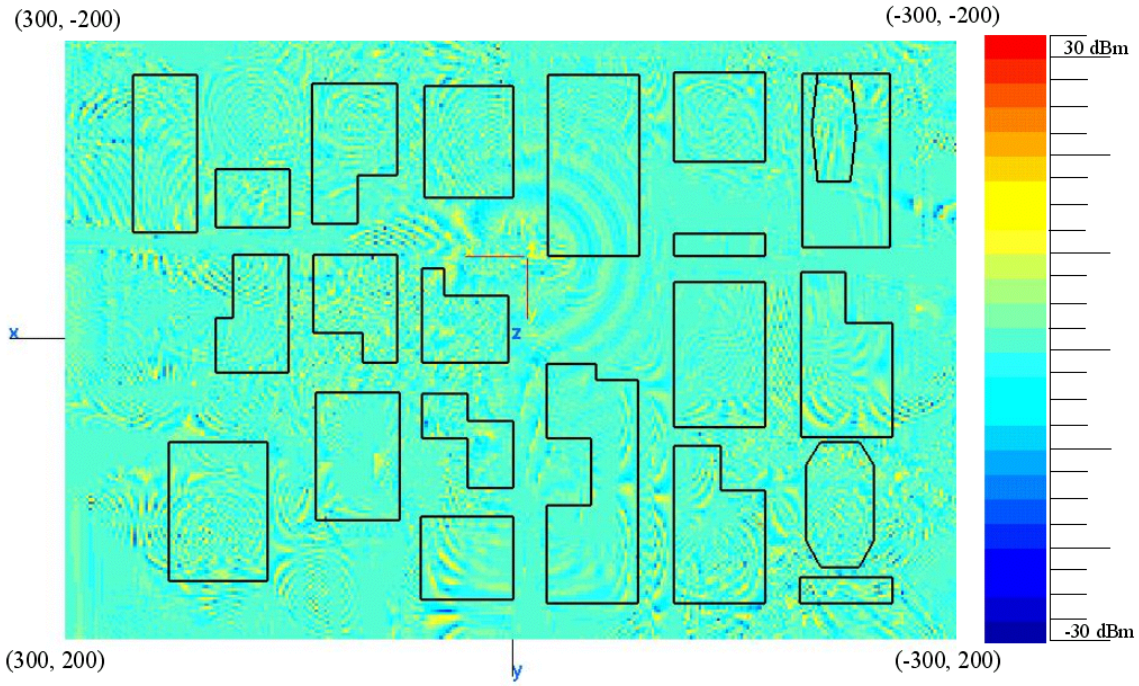

Figure 40. Frequency difference, 900 MHz - 912.5 MHz

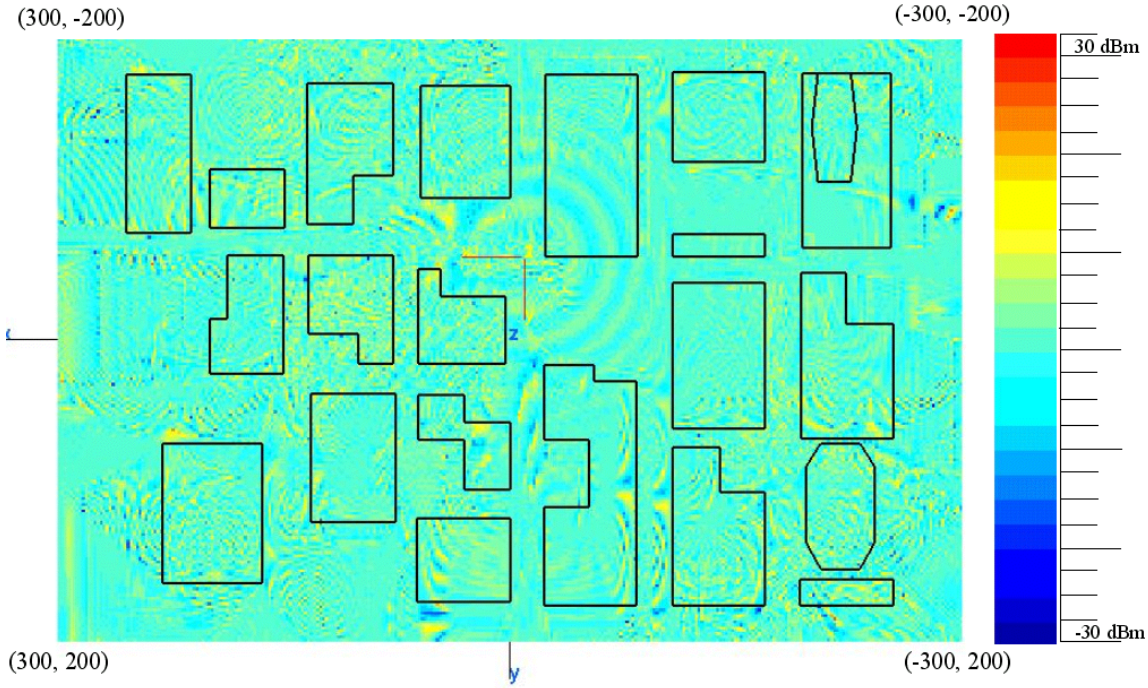

Figure 41. Frequency difference, 900 MHz – 925 MHz

Center Frequency	Simulation Frequency (GHz)	Power Difference (dB)		Graph Range (dB)	
		Min	Max	Min	Max
900 MHz	0.875	-27.0125	21.9001	-30	30
900 MHz	0.8875	-23.2860	24.9170	-30	30
900 MHz	0.9125	-21.8899	22.1050	-30	30
900 MHz	0.925	-22.9488	24.2161	-30	30

Table 13. Frequency difference results for 900 MHz.

3. Simulations of the 2.4 GHz Frequency Band

This section describes the results for a center frequency of 2.4 GHz. The bandwidth is 50 MHz. Figures 42 to 46 show the results starting at a frequency of 2.375 GHz and stepping in 12.5 MHz increments.

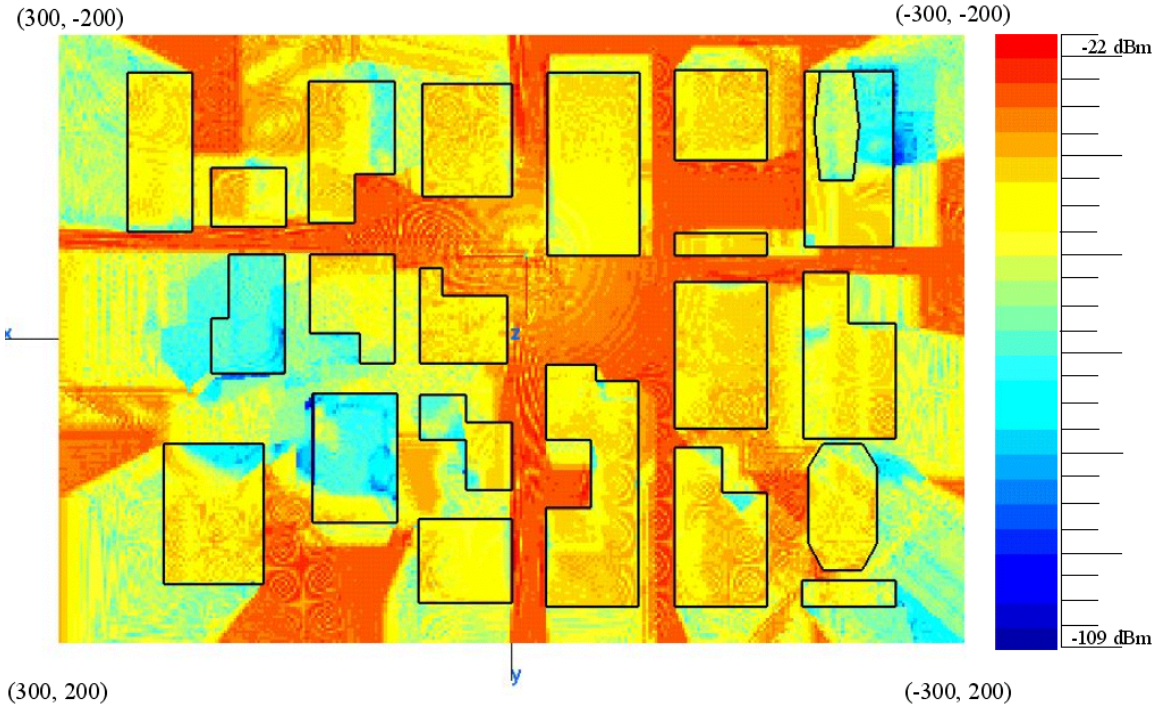

Figure 42. Vertical polarized antenna, 2.375 GHz

In these set of graphs outdoor-to-indoor propagation is decreased compared to the 900 MHz band. Also, the diffraction patterns are changing much more rapidly than at 900 MHz simulations due to the shorter wavelength.

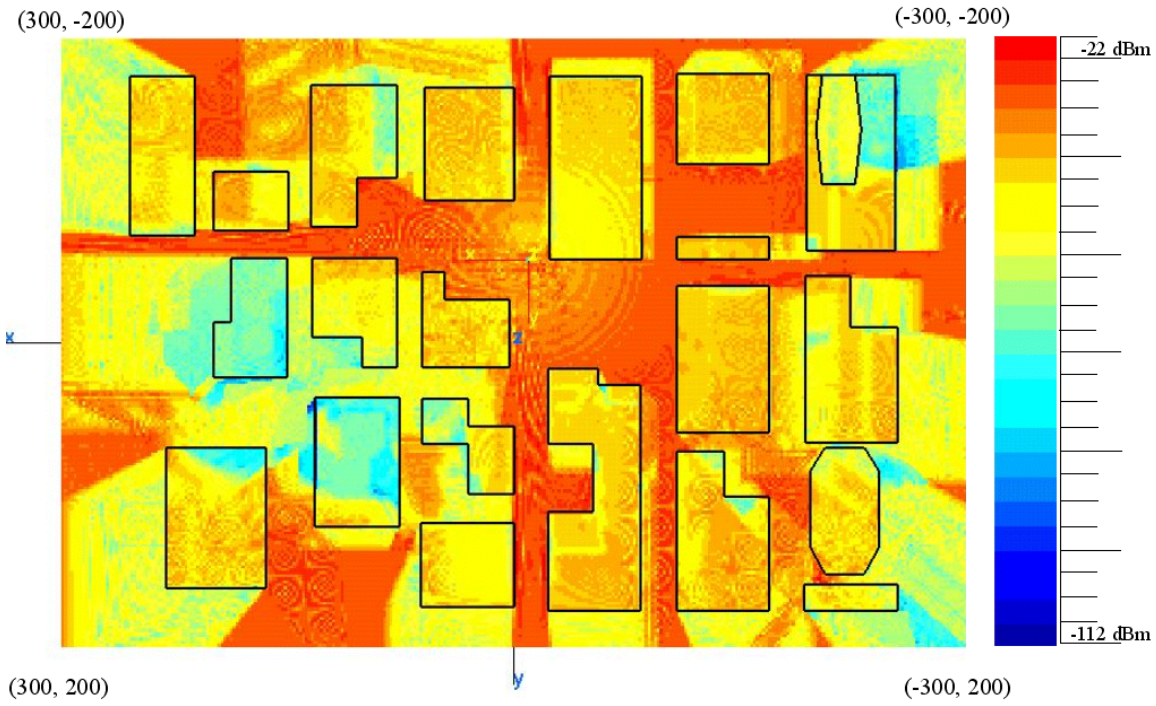

Figure 43. Vertical polarized antenna, 2.3875 GHz

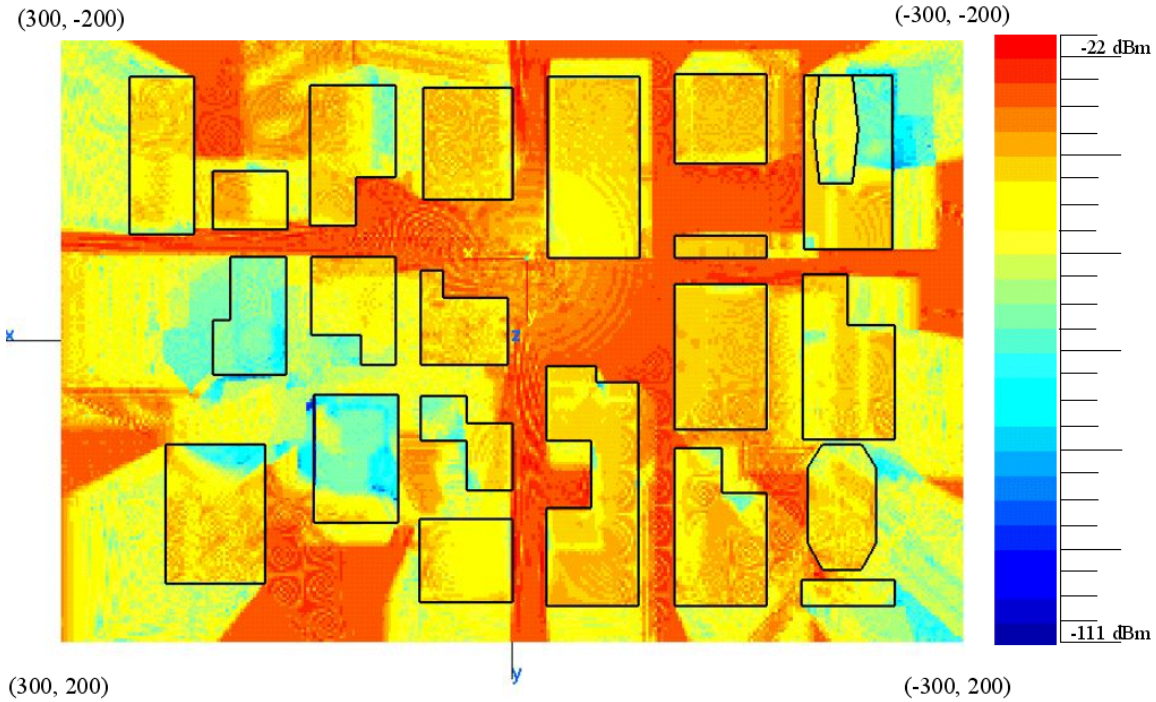

Figure 44. Vertical polarized antenna, 2.4 GHz

When we look at the area in the vicinity of (−20 m, 100 m), at the lower left, there are approximately five circular diffraction rings. At 900 MHz there were only two. These rings are due to many edge diffractions adding and canceling.

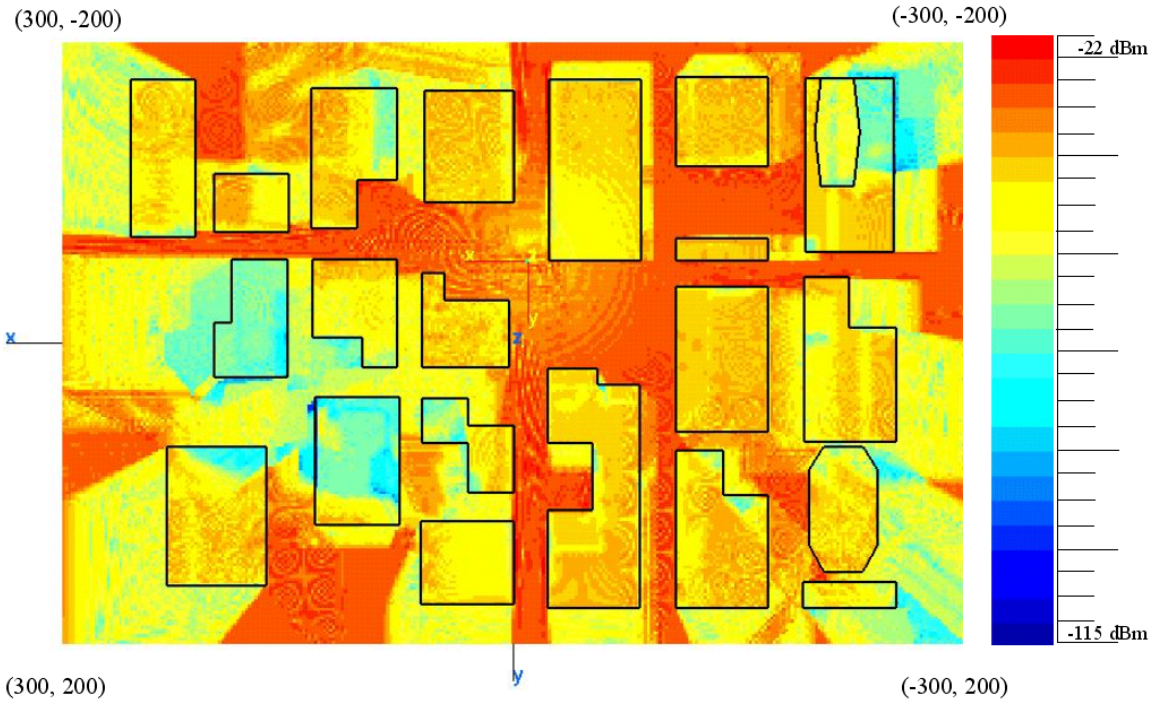

Figure 45. Vertical polarized antenna, 2.4125 GHz

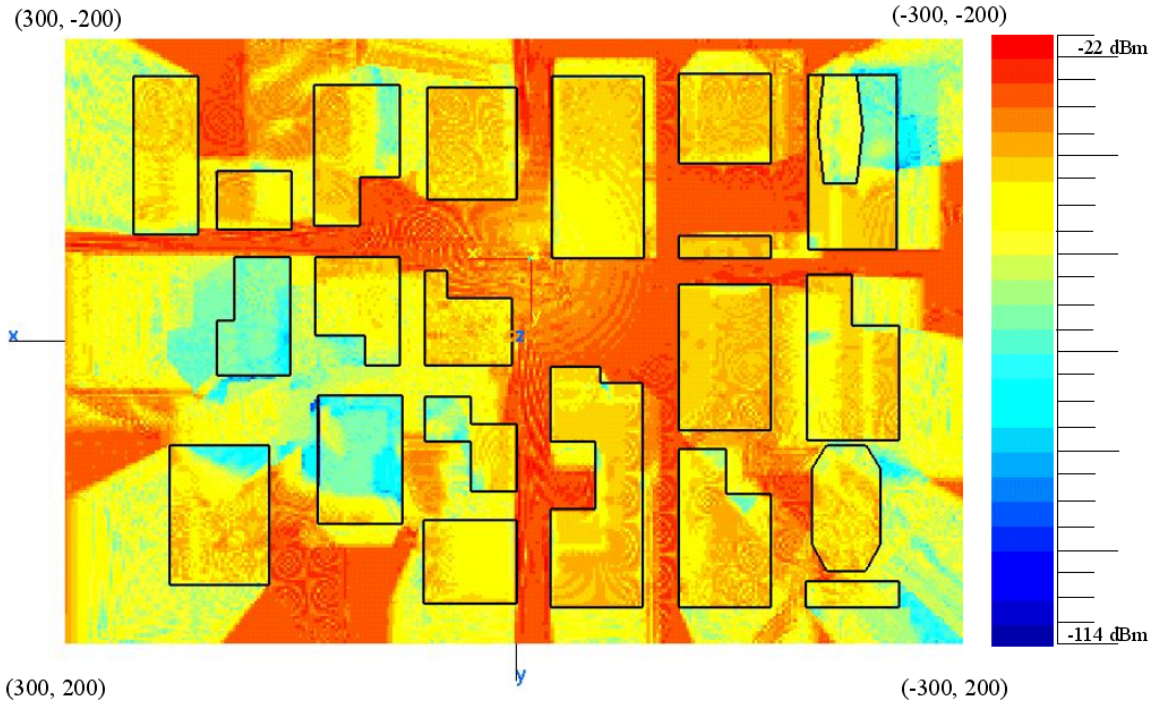

Figure 46. Vertical polarized antenna, 2.425 GHz

The differences between frequencies in the band relative to 2.4 GHz were created using ***f2fd.x***. The results are shown in Figures 47 to 50.

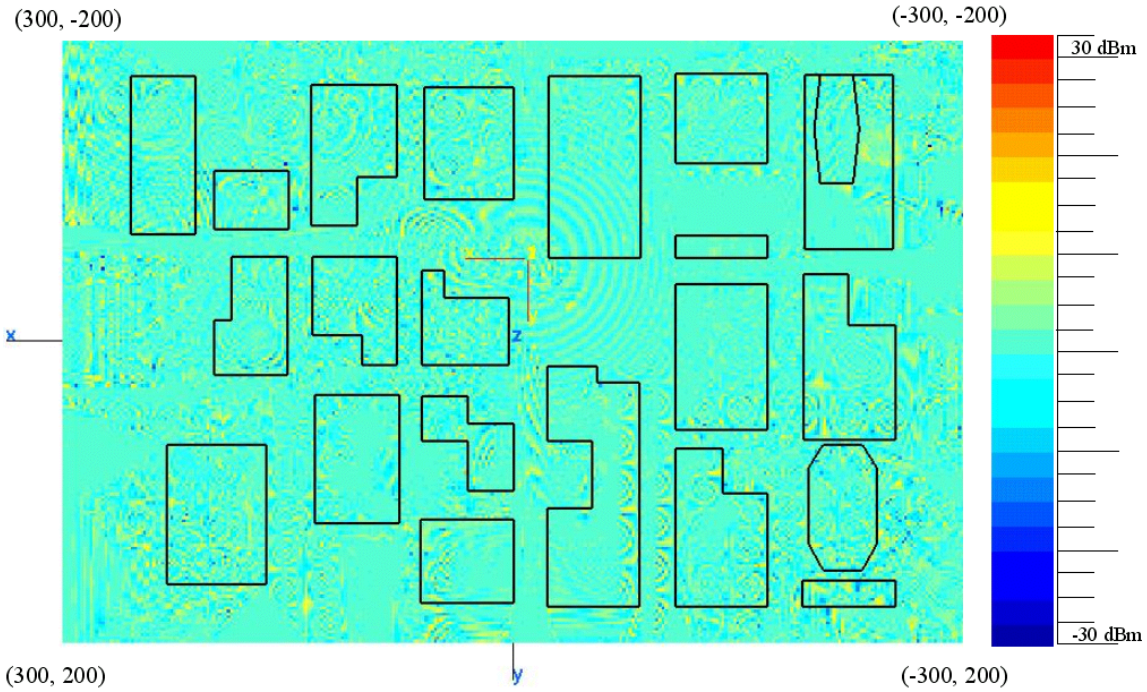

Figure 47. Frequency difference, 2.4 GHz – 2.375 GHz

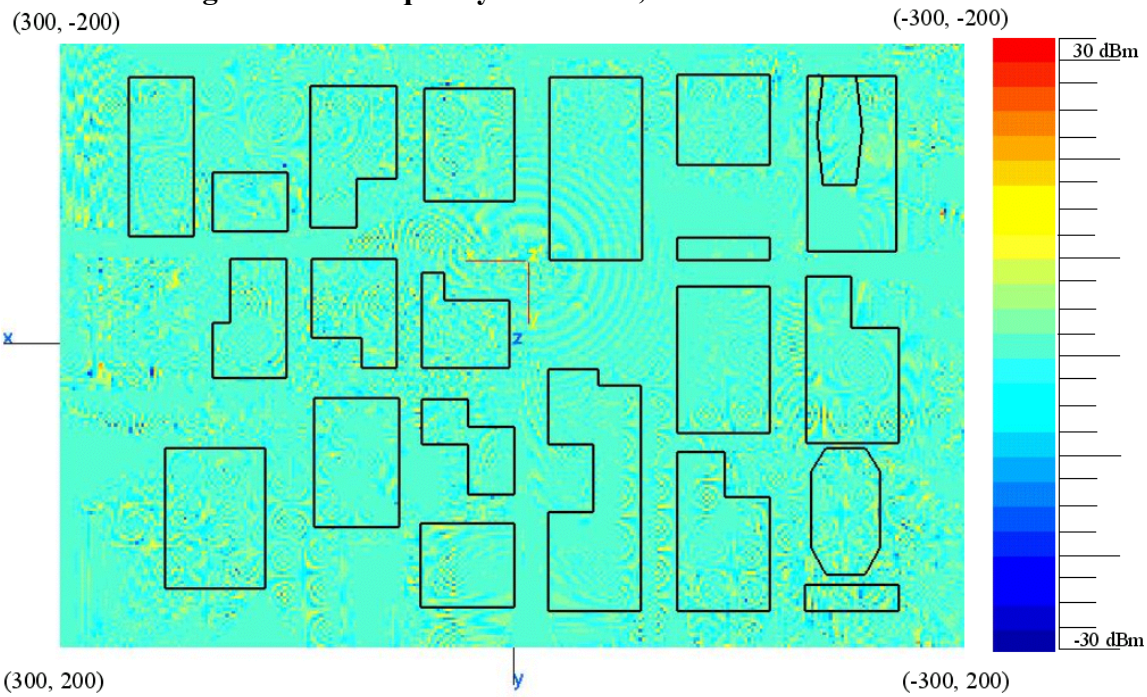

Figure 48. Frequency difference, 2.4 GHz – 2.3875 GHz

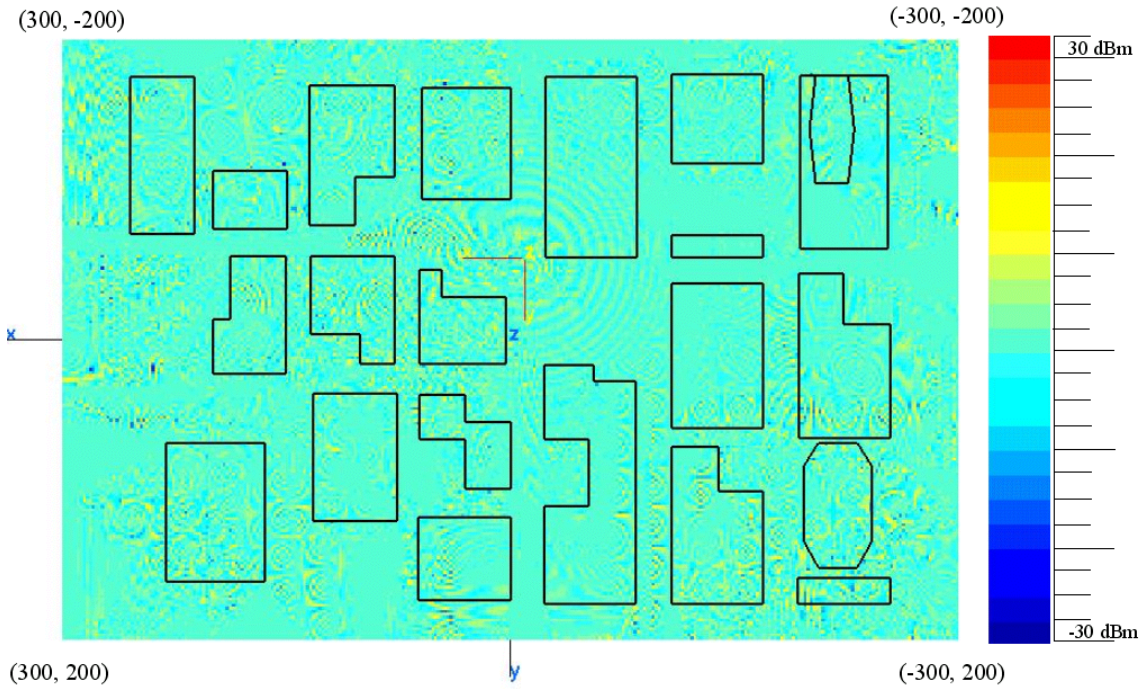

Figure 49. Frequency difference, 2.4 GHz – 2.4125 GHz

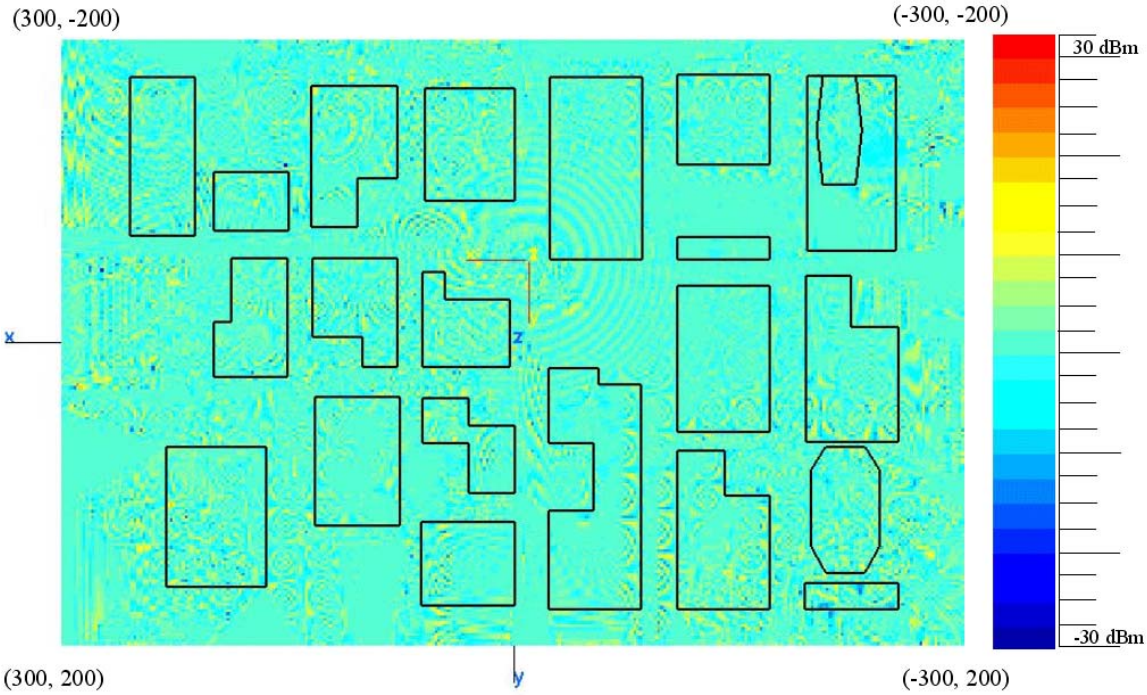

Figure 50. Frequency difference, 2.4 GHz – 2.425 GHz

In this frequency range, most of the variations are in tens of dB. The results for this simulation group are summarized in Table 14.

Center Frequency	Simulation Frequency (GHz)	Power Difference (dB)		Graph Range (dB)	
		Min	Max	Min	Max
2.4 GHz	2.375	-23.0209	20.6258	-30	30
2.4 GHz	2.3875	-20.7410	23.5810	-30	30
2.4 GHz	2.4125	-20.9500	20.3000	-30	30
2.4 GHz	2.425	-24.2500	22.1900	-30	30

Table 14. Frequency difference results for 2.4 GHz

4. Simulations of the 5.0 GHz Frequency Band

In this section 5 GHz is taken as the center frequency, with all other parameters kept constant. Indoor propagation is decreased by a considerable amount while outdoor propagation is approximately the same as at 2.4 GHz. Figures 51 to 55 show the results for the 5.0 GHz center frequency band.

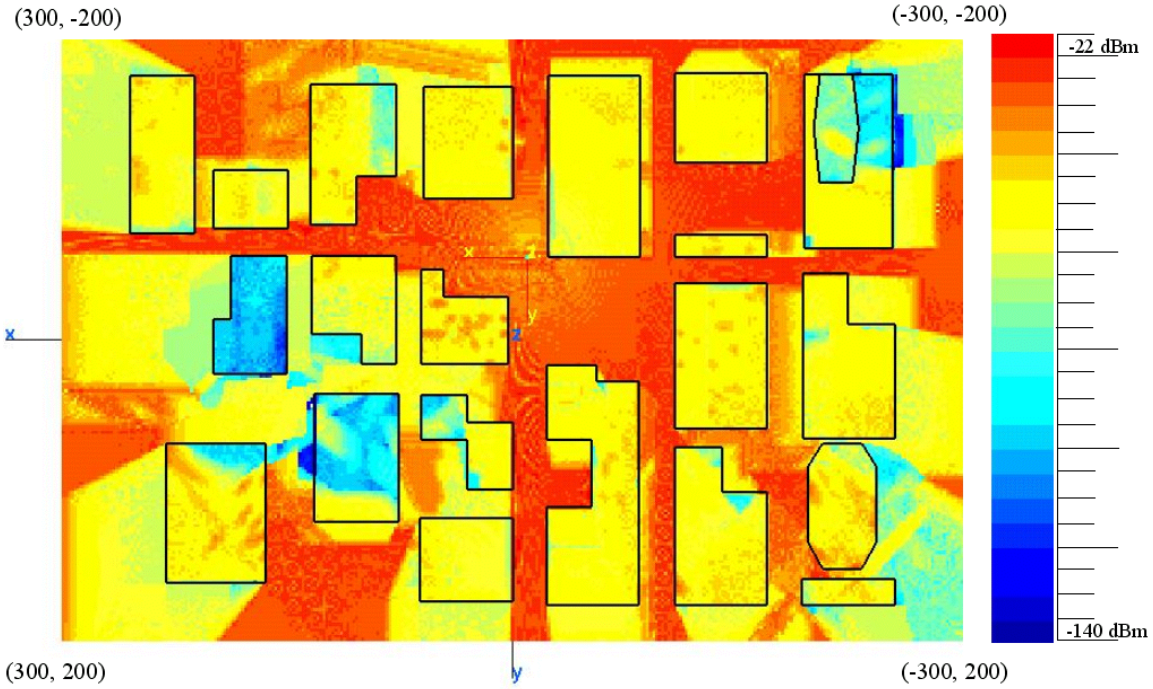

Figure 51. Vertical polarized antenna, 4.975 GHz

For the corridor along the x and y axes the signal levels are high because of the direct contribution. The building at point (150 m, 0 m) is in the shadowed region and therefore signal levels inside of this building are low (nearly –100 dB values).

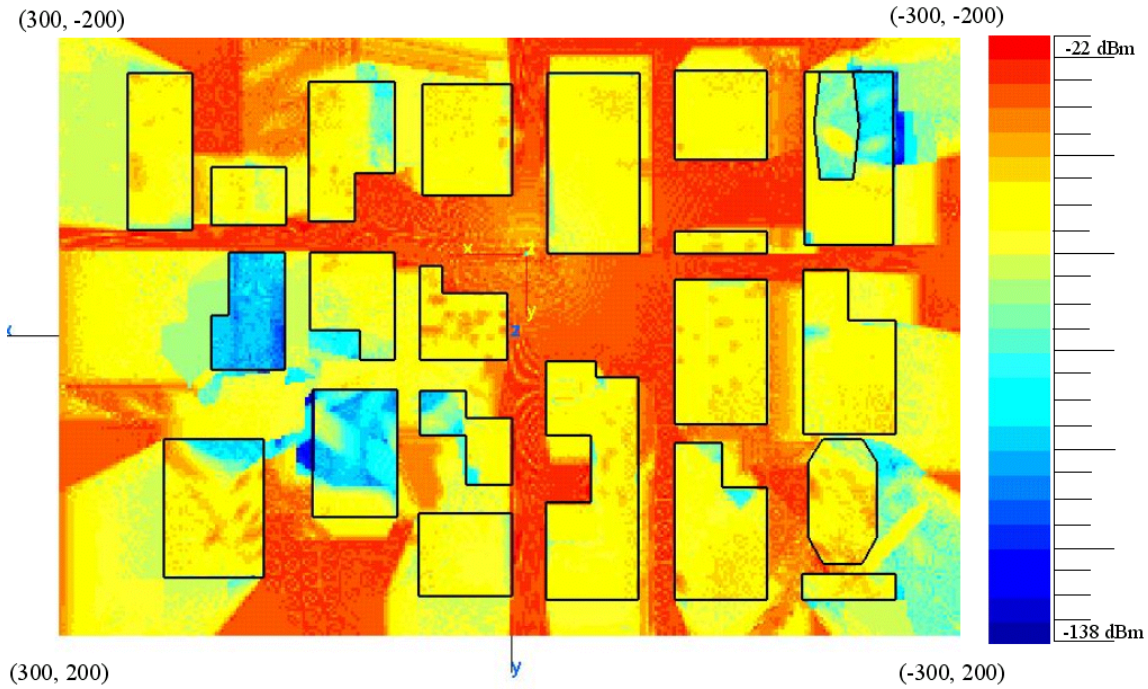

Figure 52. Vertical polarized antenna, 4.9875 GHz

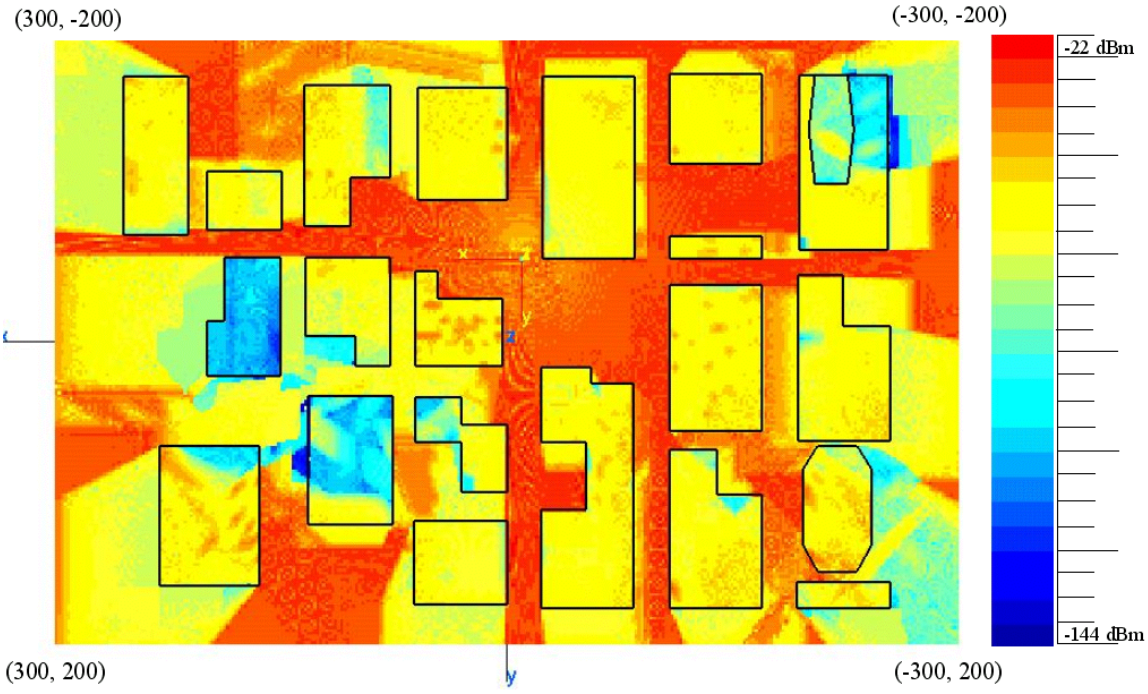

Figure 53. Vertical polarized antenna, 5.0 GHz

In this frequency band, changes between diffraction patterns take place over very short distances. Hot spots are seen at this frequency. Reflection from the walls of the

buildings gives a significant amount of contribution to the signal level at some places that are in line of sight shadows.

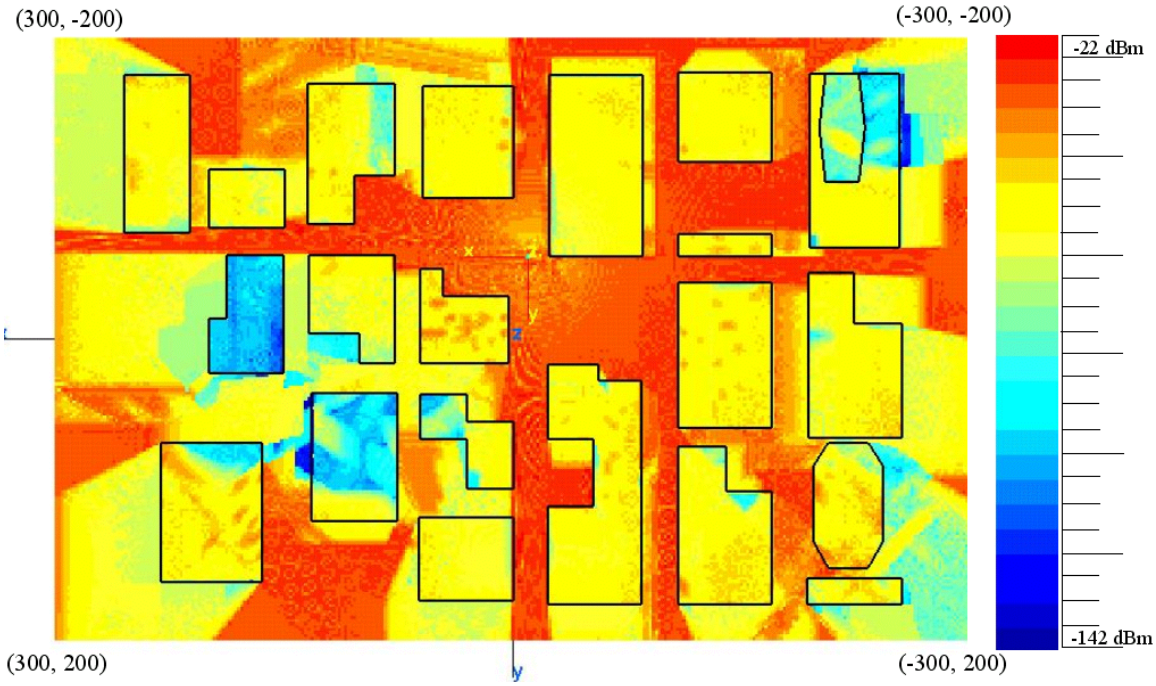

Figure 54. Vertical polarized antenna, 5.0125 GHz

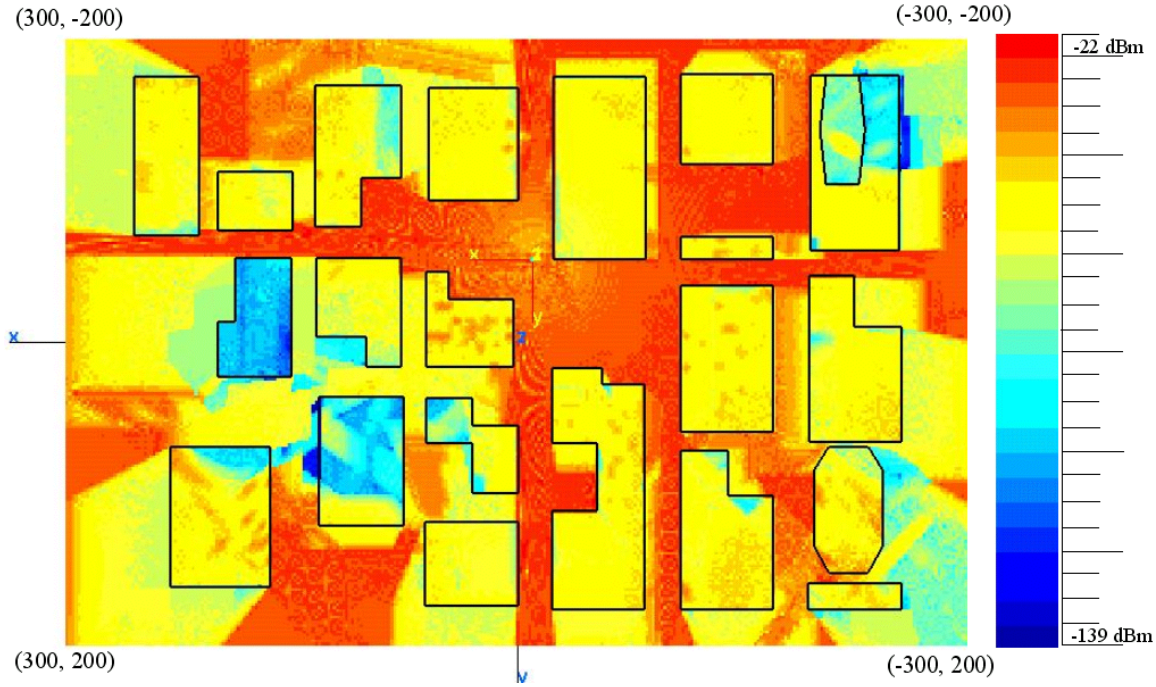

Figure 55. Vertical polarized antenna, 5.025 GHz

The difference plots for the 5.0 GHz band are shown in Figures 56 to 59. Most of the variations are in the –5 dB to 5 dB range. Small diffraction patterns are visible at numerous locations throughout the observation plane. A summary of results for this simulation is shown in Table 15.

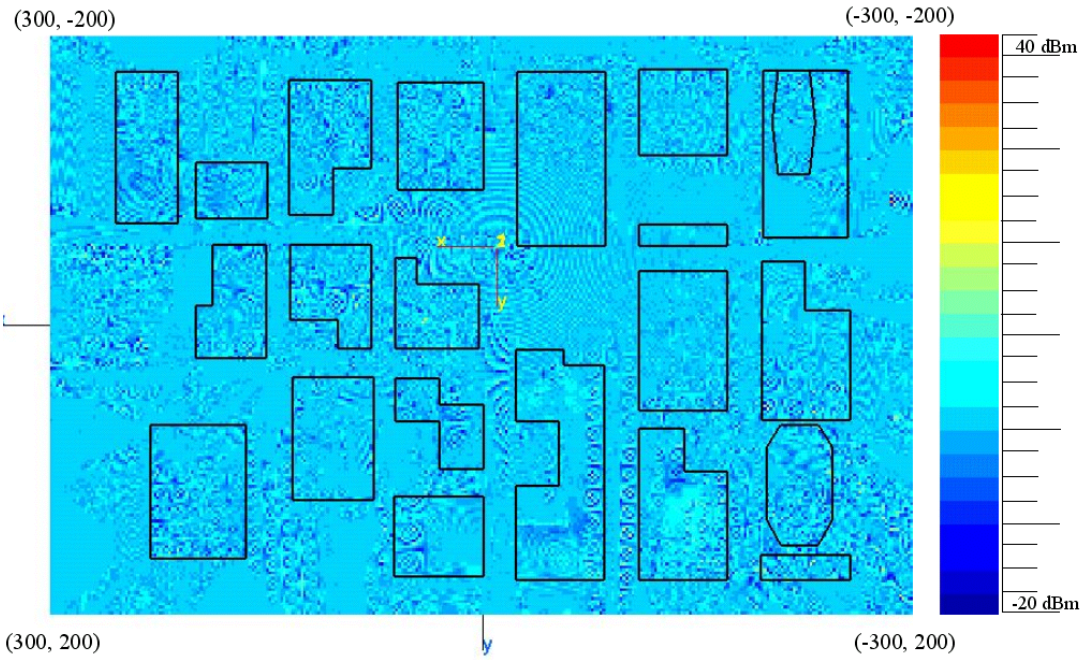

Figure 56. Frequency difference, 5.0 GHz – 4.975 GHz

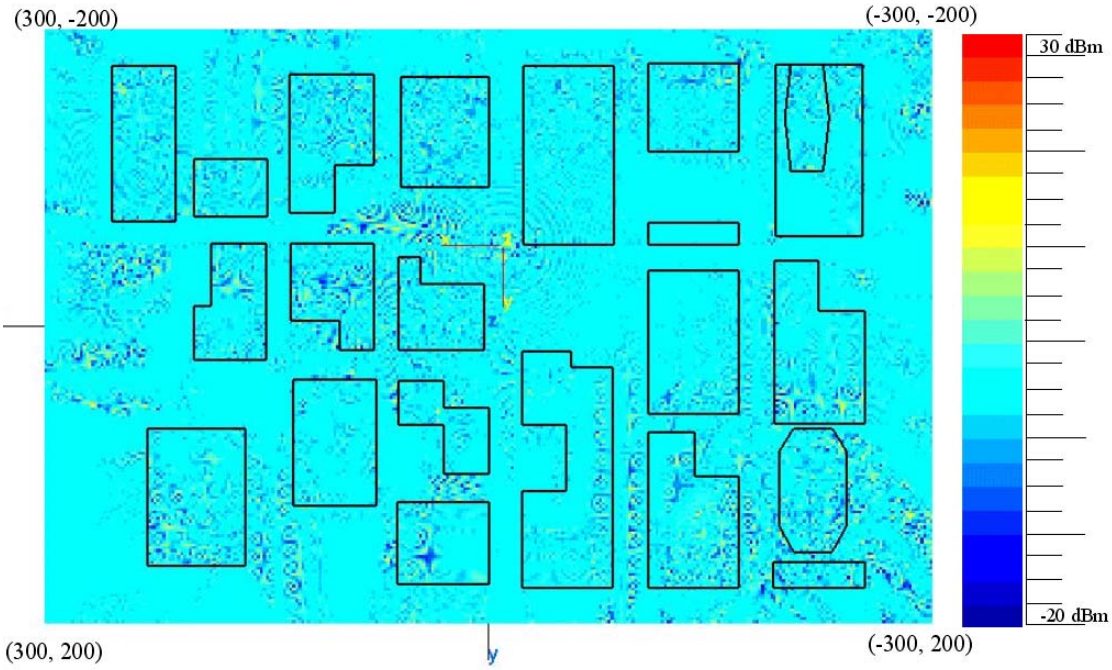

Figure 57. Frequency difference, 5.0 GHz – 4.9875 GHz

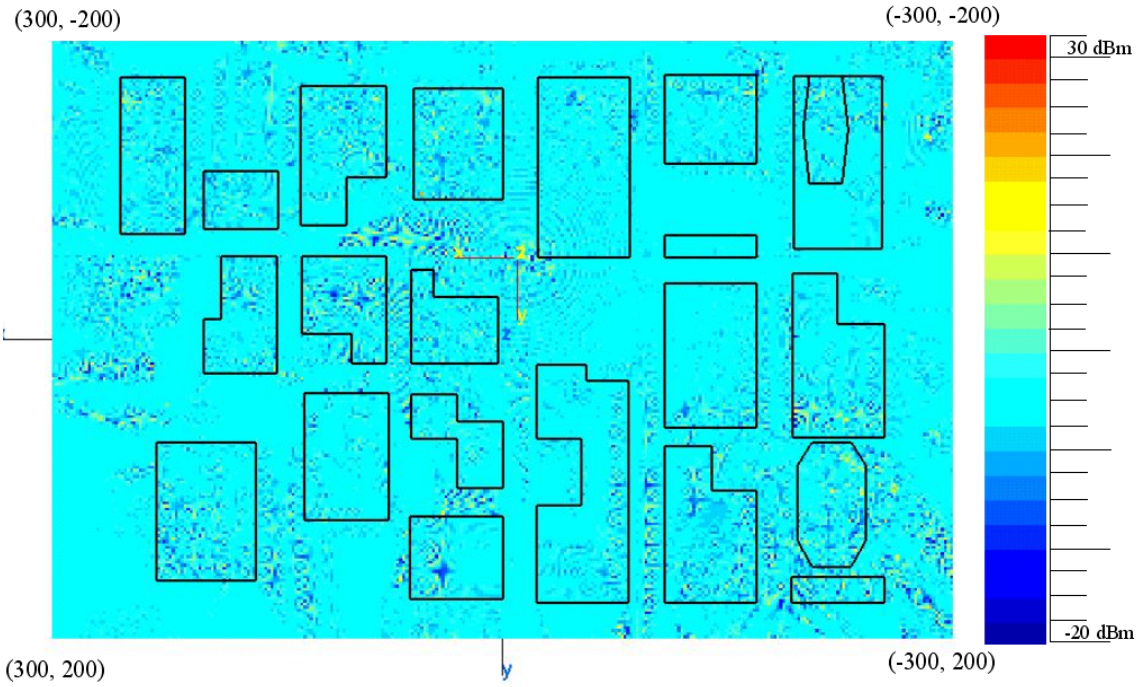

Figure 58. Frequency difference, 5.0 GHz – 5.0125 GHz

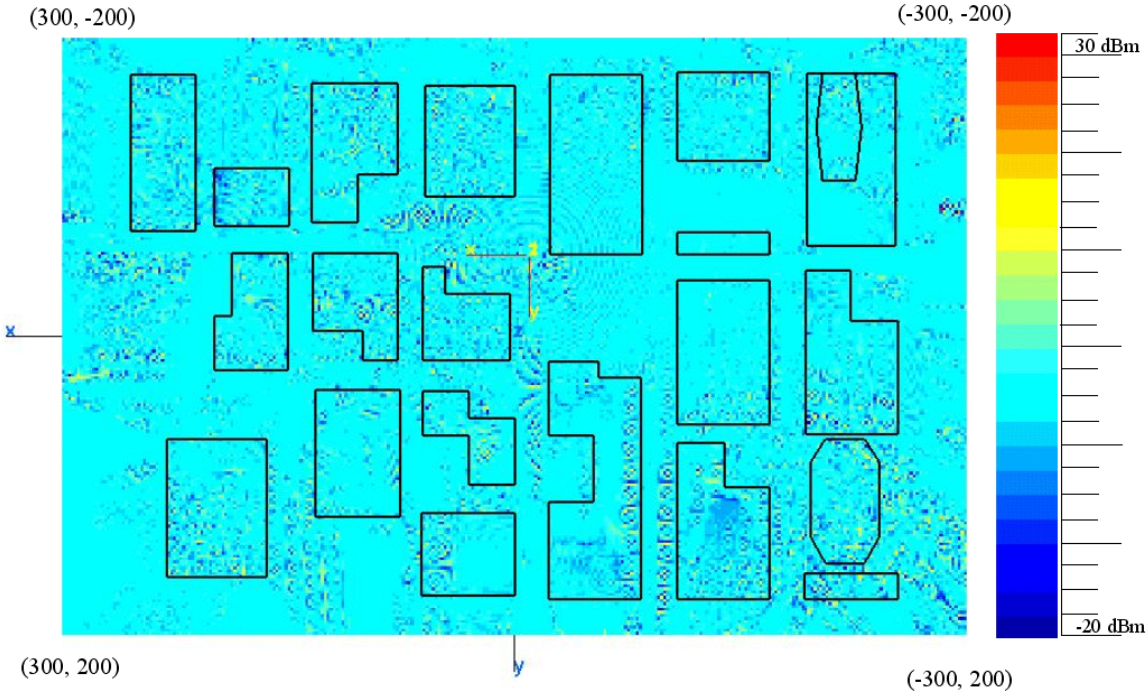

Figure 59. Frequency difference, 5.0 GHz – 5.025 GHz

Center Frequency	Simulation Frequency (GHz)	Power Difference (dB)		Graph Range (dB)	
		Min	Max	Min	Max
5 GHz	4.975	-19.6672	32.7834	-20	40
5 GHz	4.9875	-19.0729	22.7070	-20	30
5 GHz	5.0125	-18.6791	21.0420	-20	30
5 GHz	5.025	-19.5236	29.3287	-20	30

Table 15. Frequency difference results for 5.0 GHz

5. Frequency Simulation Conclusions

Data links at frequencies 900 MHz, 2.4 GHz and 5.0 GHz were simulated for 50 MHz bandwidths. Lower frequencies have a higher signal level indoors compared to the higher frequencies. The differences within each band are tens of dB at most.

E. SIMULATIONS FOR DIFFERENT POLARIZATIONS

In this section, the polarization of the antenna was changed from vertical to horizontal. The Urbana input files for this change are modified in the antenna description part. The antenna rotation vectors are changed to $\hat{x}_{ant} = -\hat{z}$, and $\hat{z}_{ant} = \hat{x}$ relative to the main coordinate system. The antenna is still located at point (0 m, − 50 m, 150 m) in the main coordinates. A 50 MHz bandwidth is used as it was for the vertical case. The antenna altitude is kept constant at z = 150 m. Ray trace parameters and the observation plane are also kept constant.

The polarization simulation results are summarized in Table 16. Minimum and maximum power values for horizontal polarization are very close to those of the vertical polarization.

Horizontal Polarization Simulations for various frequencies (BW=50MHz)					
Polarization Type	Center Frequency	Simulation Frequency (GHz)	Dipole Length (Half-wave) (m)	Power (dB)	
				Min	Max
Horizontal Dipole X(0 0 -1) Z(1 0 0) Oriented	900 MHz	0.875	0.17143	-94	-14.9
		0.8875	0.16901	-92	-15.1
		0.9	0.16667	-95	-14.6
		0.9125	0.16438	-92	-14.8
		0.925	0.16216	-91	-14.8
Horizontal Dipole X(0 0 -1) Z(1 0 0) Oriented	2.4 GHz	2.375	0.06316	-118.2	-15.54
		2.3875	0.06283	-116.02	-15.1
		2.4	0.06250	-113.64	-14.82
		2.4125	0.06218	-116.45	-15.55
		2.425	0.06186	-112.75	-15.43
Horizontal Dipole X(0 0 -1) Z(1 0 0) Oriented	5.0 Ghz	4.975	0.03015	-146.25	-15.62
		4.9875	0.03008	-142.75	-15.24
		5	0.03000	-148	-15.3
		5.0125	0.02993	-148.4	-15.14
		5.025	0.02985	-143	-15.3

Table 16. Horizontal polarization simulation parameters

1. Polarization Difference Simulation for 900 MHz

For the center frequency of 900 MHz, the horizontal polarized antenna signal contours are shown in Figure 60. The signal level is very high along *y*-axis due to the "urban canyon" effect.

Horizontal polarized antenna simulations are only shown for the center frequencies. The signal levels are between –10 dBm and –100 dBm for 900 MHz.

Comparisons with vertical polarization will be done at the same frequencies, as presented in Section D. The antenna rotation vector is set to $\hat{x}_{ant} = -\hat{z}$, and $\hat{z}_{ant} = \hat{x}$. Straight and level flight of the UAV is assumed. To compare the results for different polarizations, the program ***f2fd.x*** is used. Figure 61 shows a comparison for polarizations at 900 MHz.

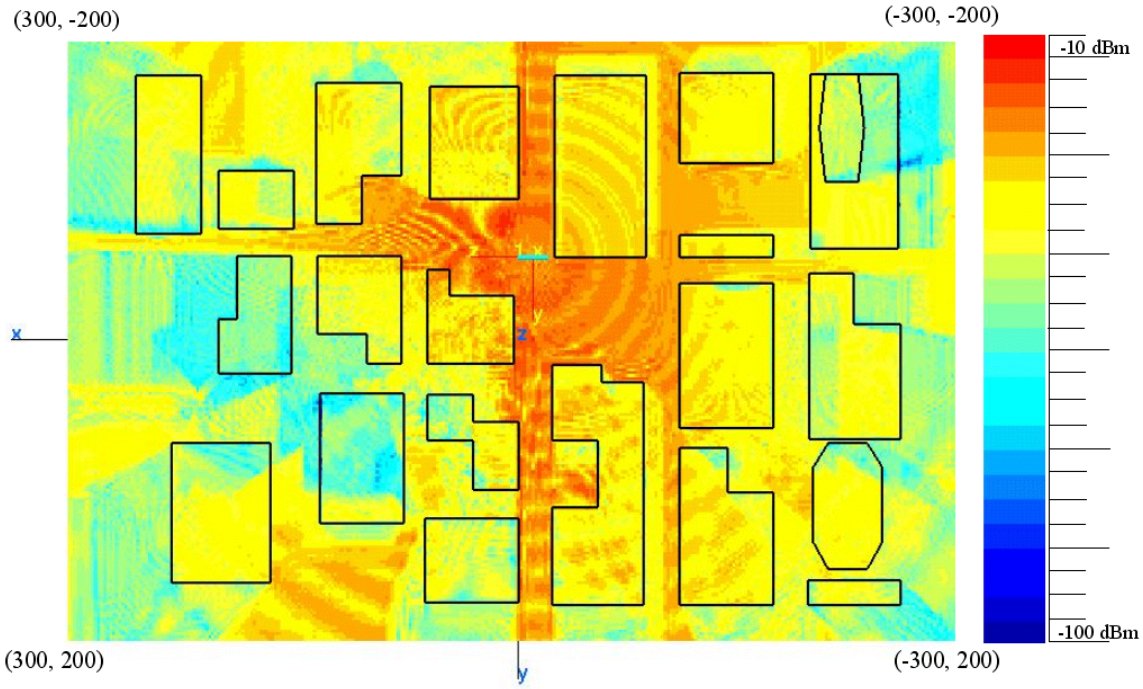

Figure 60. Horizontal polarized antenna, 900 MHz

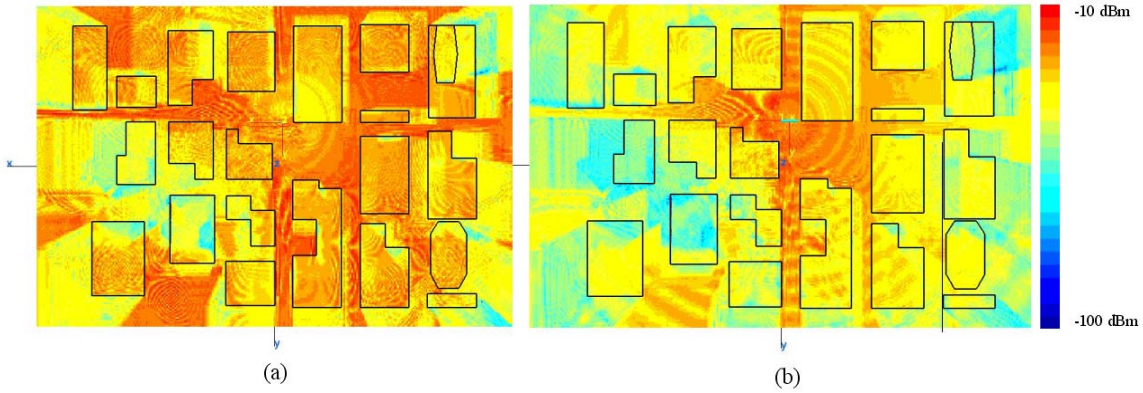

Figure 61. Polarization comparison for 900 MHz (a) vertical and (b) horizontal

Vertical polarized antennas give better results in most cases. Along the corridor created by the buildings, vertical signal levels are high compare to the horizontal polarization result. With polarization diversity there may be some cases where varying antenna polarization can be used to establish a more reliable link. Figures 62 to 66 shows difference plots for the 900 MHz band. Table 17 summarizes the results for the 900 MHz frequency band.

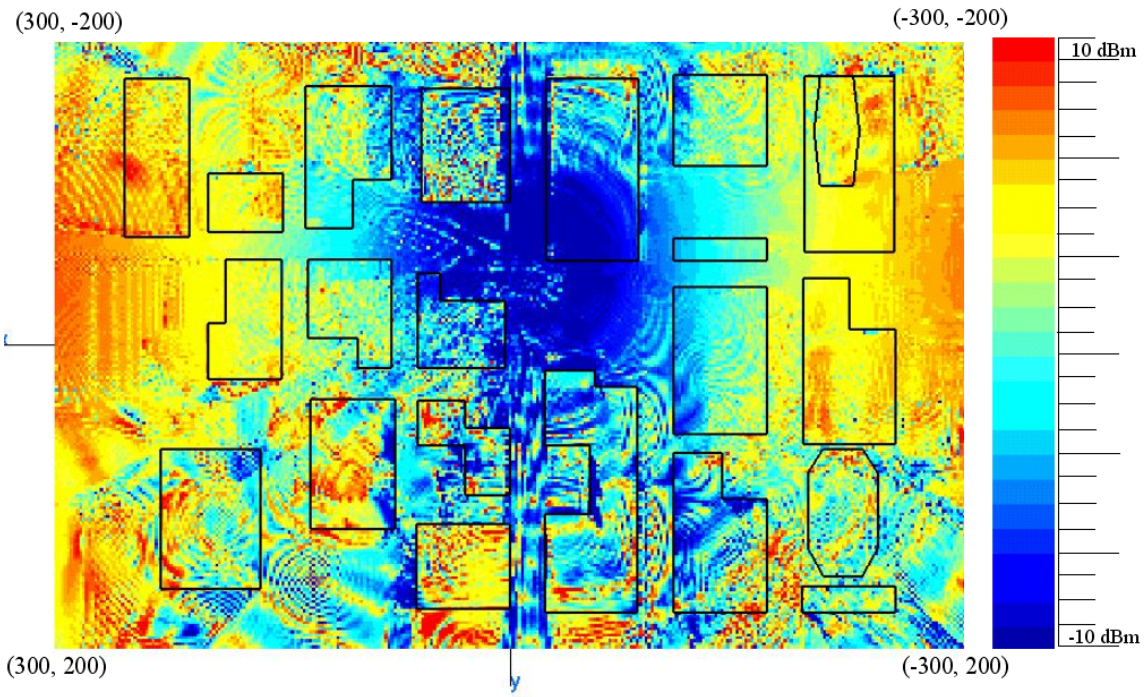

Figure 62. Polarization difference, 875 MHz

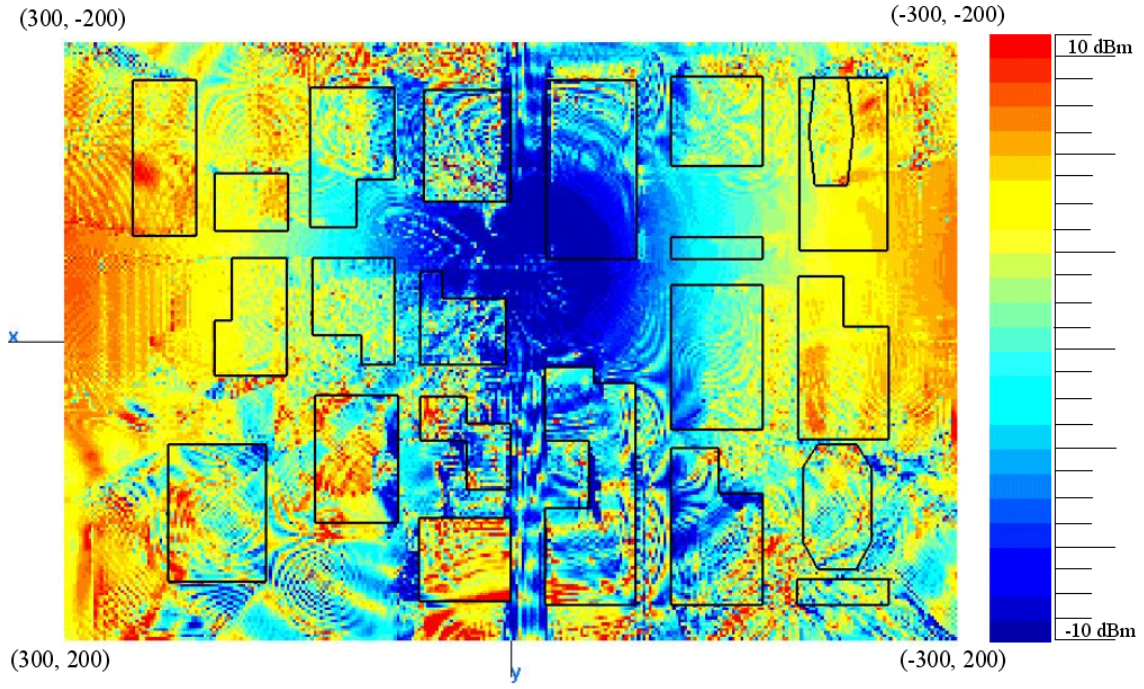

Figure 63. Polarization difference, 887.5 MHz

Below the antenna, the signal difference is observed to be very large compared to far out regions of city model. This is due to the antenna null rotation for vertical polarization.

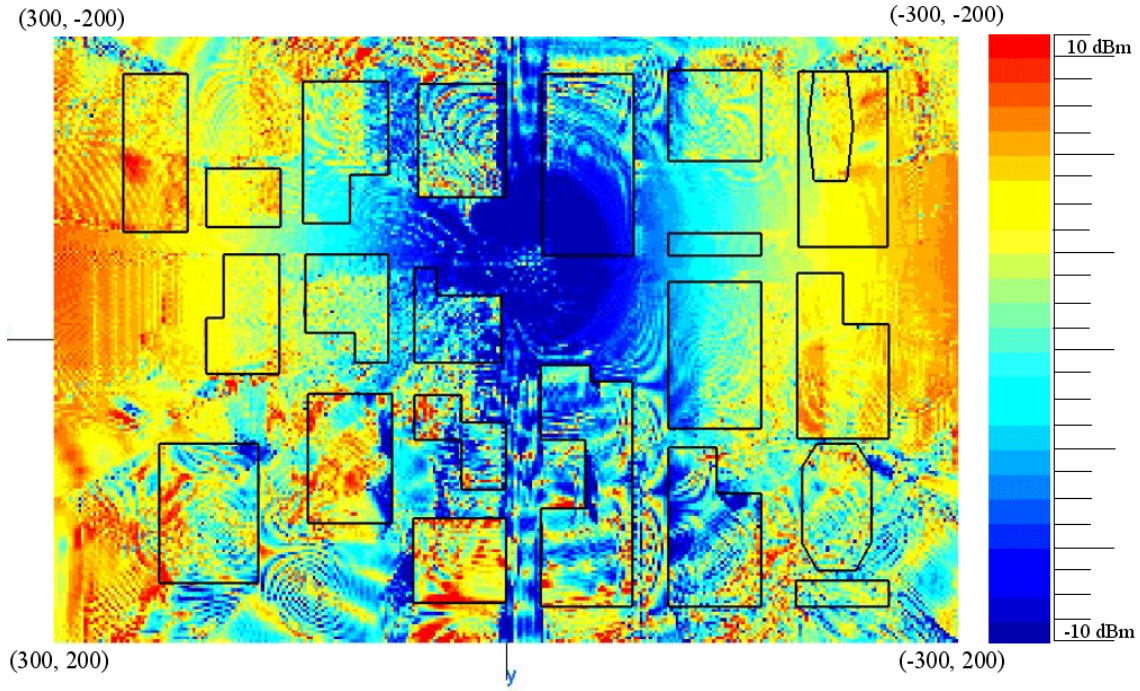

Figure 64. Polarization difference, 900 MHz

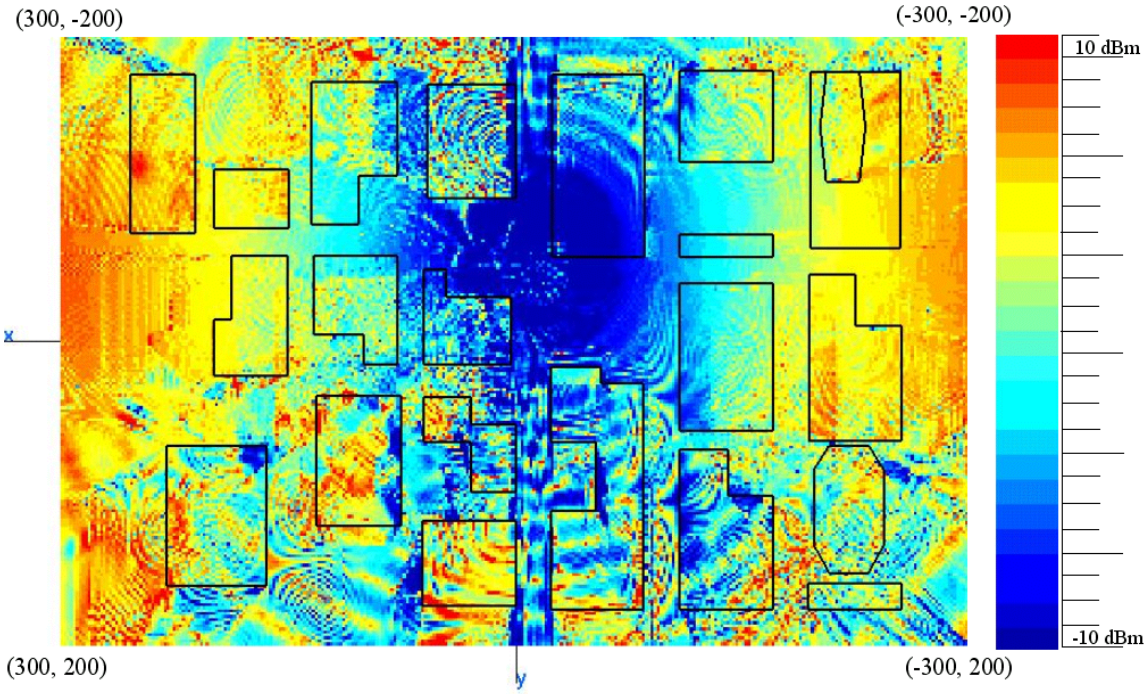

Figure 65. Polarization difference, 912.5 MHz

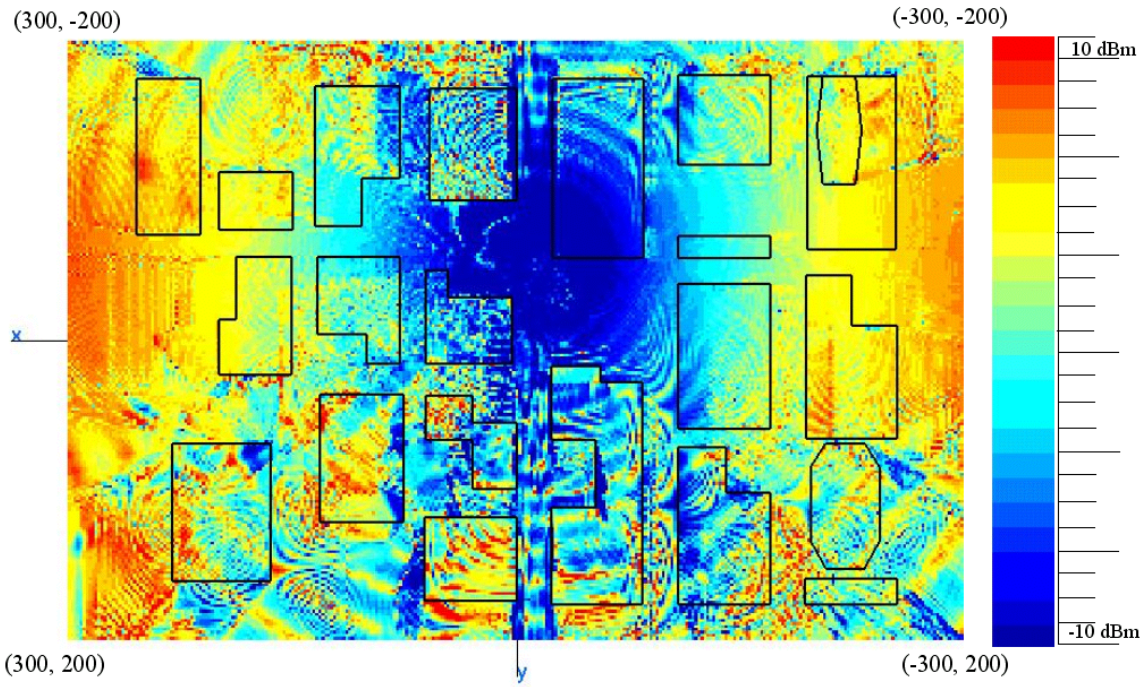

Figure 66. Polarization difference, 925 MHz

900 MHz Center Frequency Polarization Differences						
Polarization Type	Polarization Type	Simulation Frequency (GHz)	Power Difference (dB)		Graph Range (dB)	
			Min	Max	Min	Max
Vertical Dipole X(100) Z(001) Oriented	Horizontal Dipole X(00-1) Z(100) Oriented	0.875	-26.92	24.65	-10	10
		0.8875	-28.81	24.46	-10	10
		0.9	-26.81	25.42	-10	10
		0.9125	-26.2	22.94	-10	10
		0.925	-25.96	25.91	-10	10

Table 17. Polarization results for 900 MHz frequencies.

2. Polarization Difference Simulations for 2.4 GHz

This section presents data for a horizontally polarized antenna for the 2.4 GHz center frequency. Figure 67 is shown as a sample plot of this frequency band. Figure 68 is a comparison between vertical and horizontal polarizations. Figures 69 to 73 are power difference plots for frequencies between 2.375 GHz and 2.425 GHz respectively.

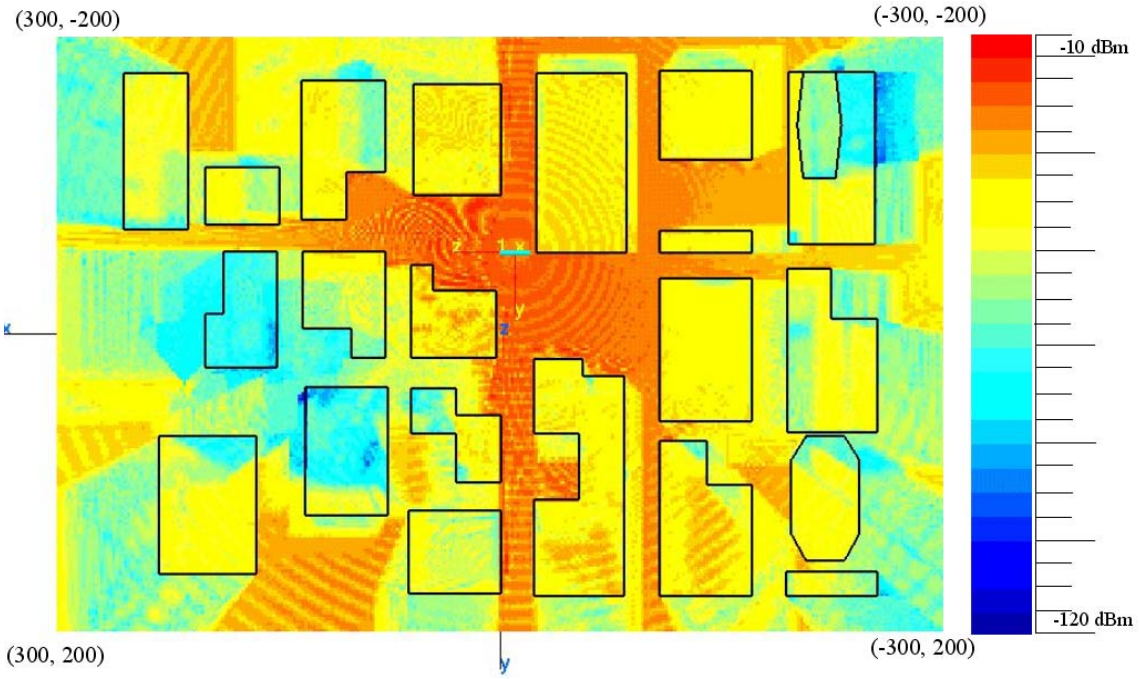

Figure 67. Vertical polarized antenna, 2.4 GHz

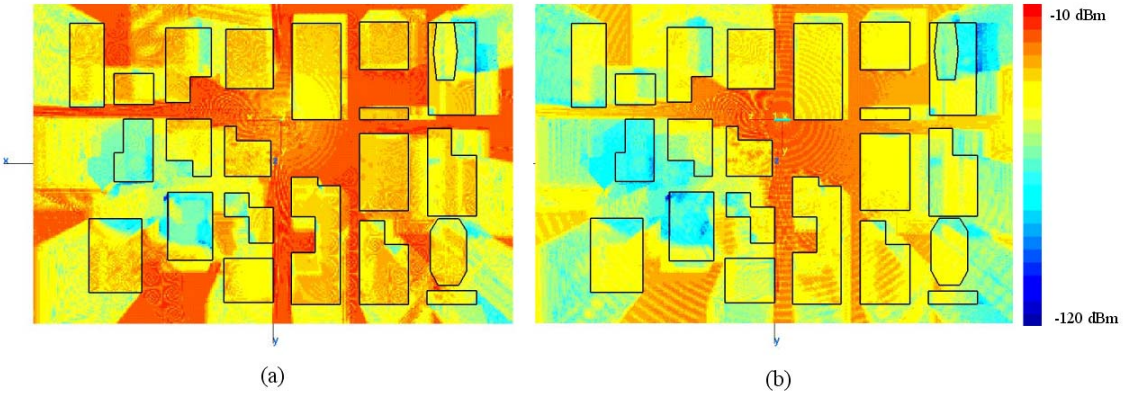

Figure 68. Polarization comparison for 2.4 GHz (a) vertical and (b) horizontal

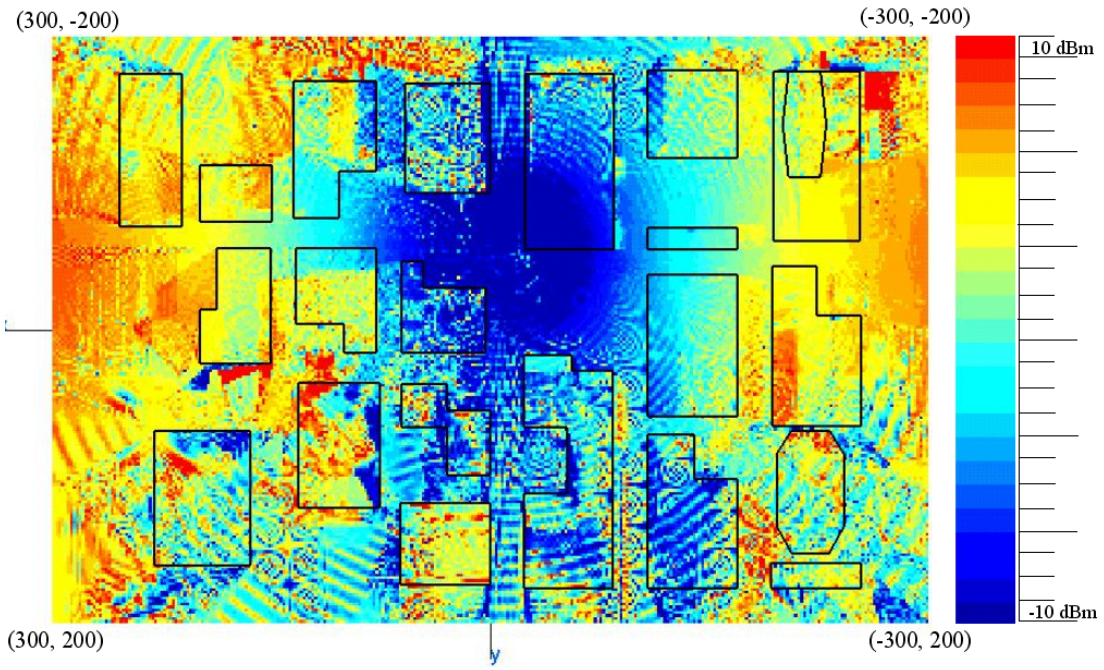

Figure 69. Polarization difference, 2.375 GHz

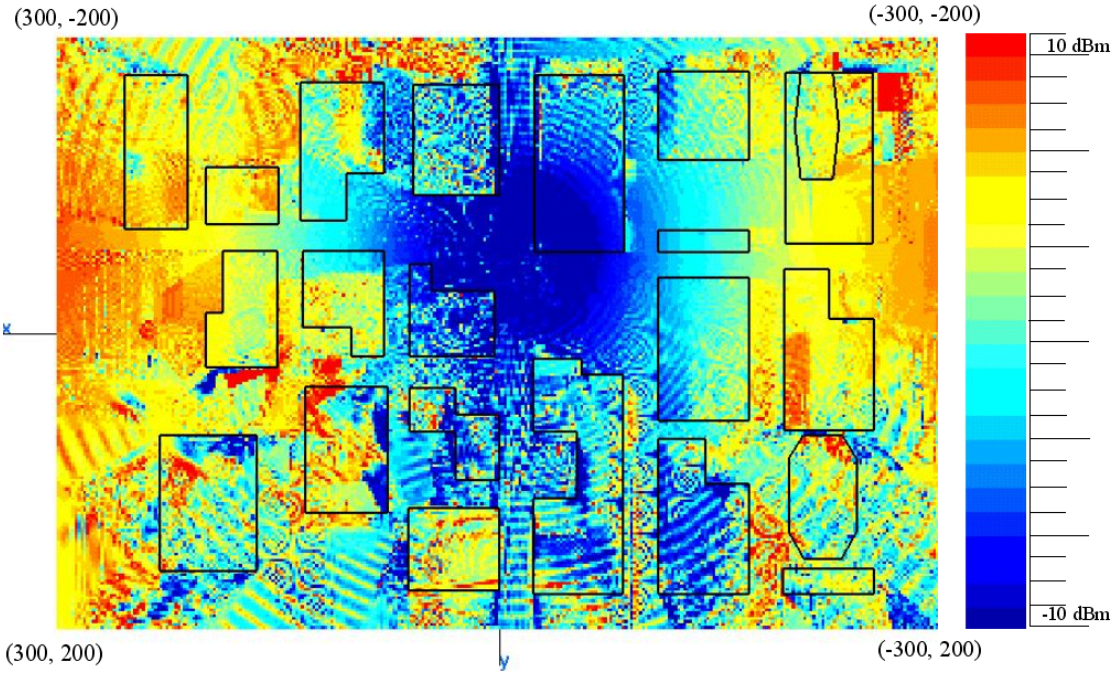

Figure 70. Polarization difference, 2.3875 GHz

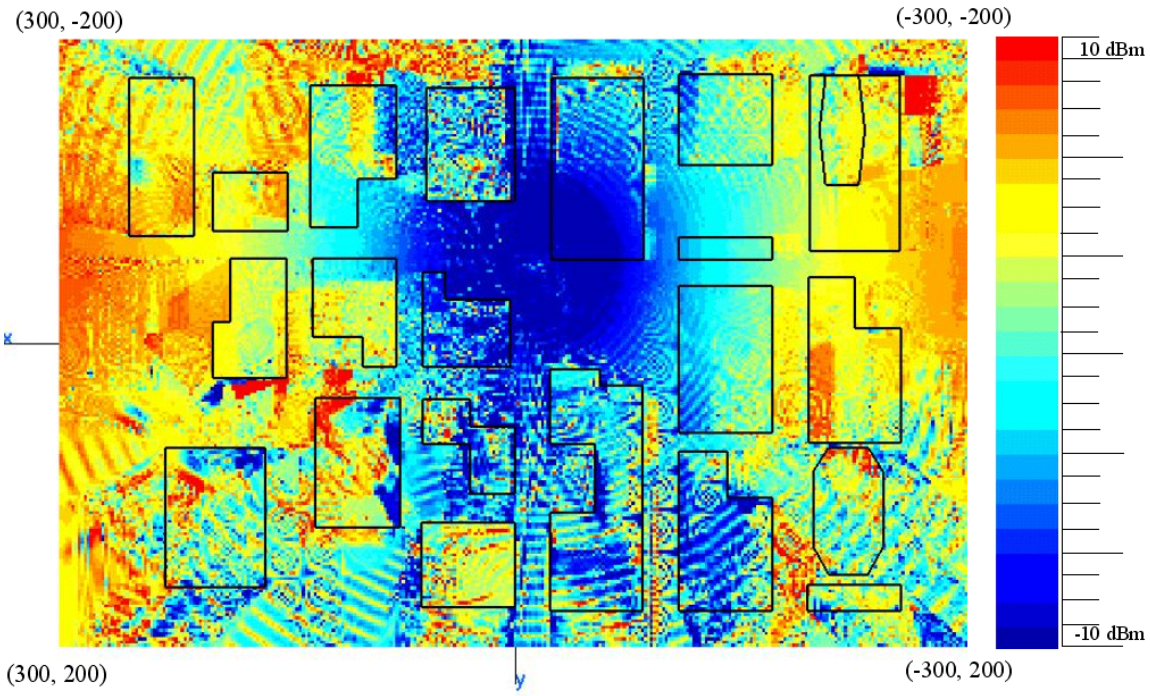

Figure 71. Polarization difference, 2.4 GHz

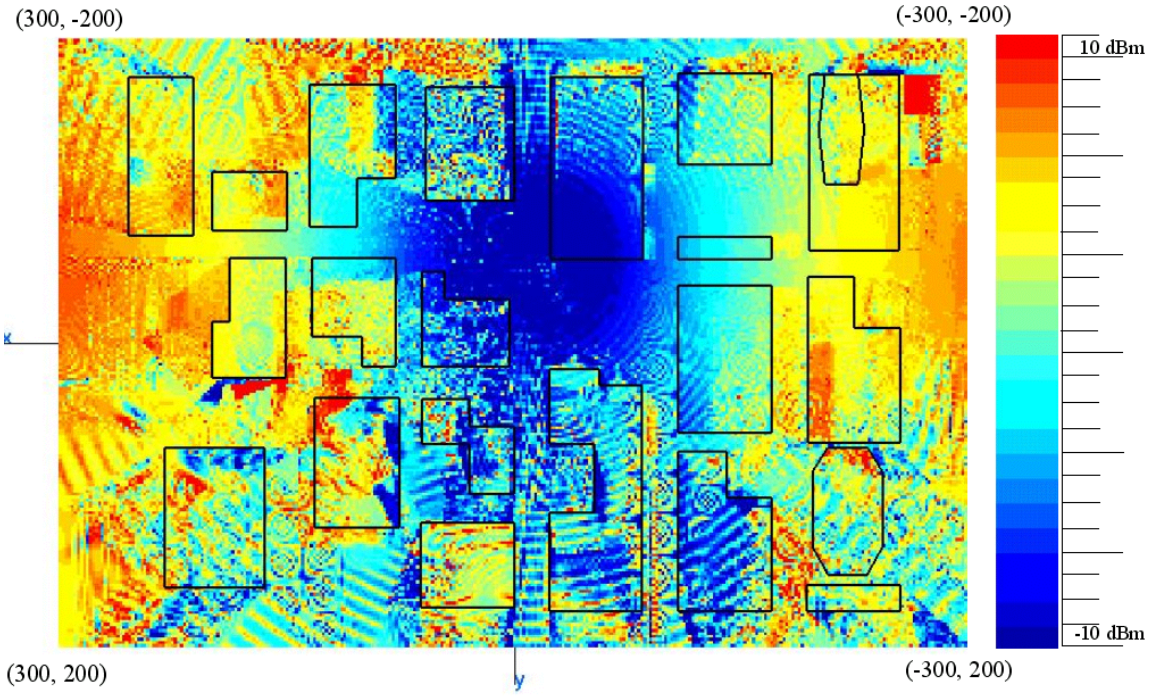

Figure 72. Polarization difference, 2.4125 GHz

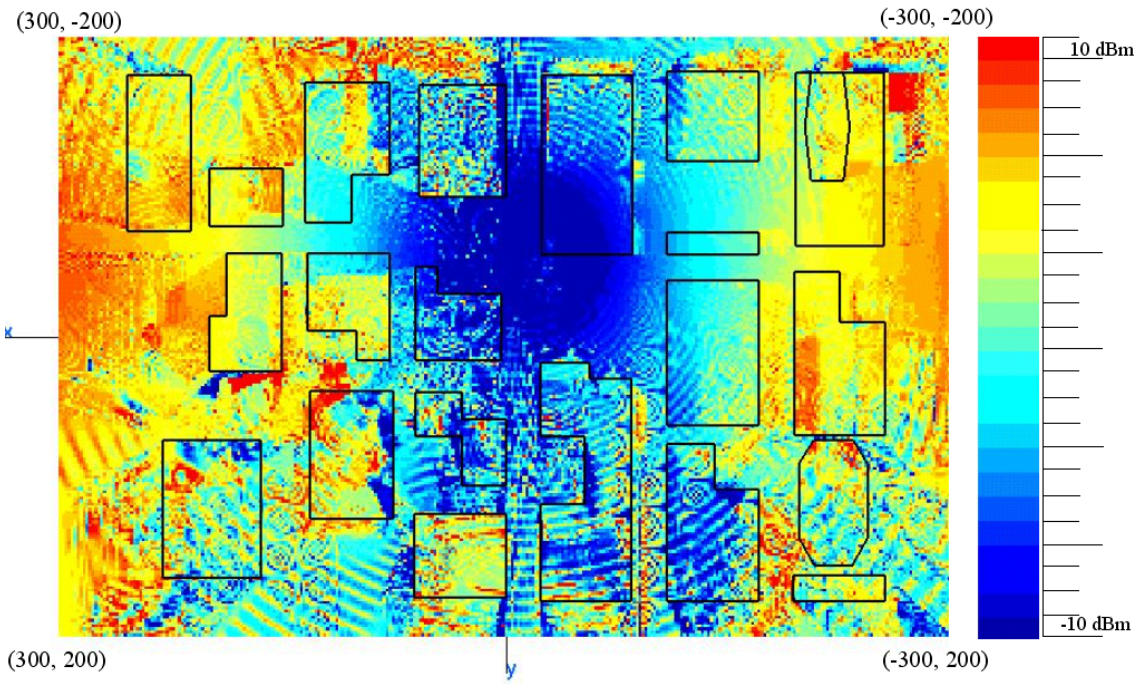

Figure 73. Polarization difference, 2.425 GHz

In regions near the antenna, the signal level differences originating from the change in polarization are very large due to the rotation of the antenna pattern null. In some far out areas of the observation plane, it is possible to see hot spots and low spots very close to each other. A summary for the 2.4 GHz simulations is given Table 18.

2.4 GHz Center Frequency Polarization Differences						
Polarization Type	Polarization Type	Simulation Frequency (GHz)	Power Difference (dB)		Graph Range (dB)	
			Min	Max	Min	Max
Vertical Dipole X(100) Z(001) Oriented	Horizontal Dipole X(00-1) Z(100) Oriented	2.375	-34.77	26.21	-10	10
		2.3875	-30.92	27.3	-10	10
		2.4	-31.22	27.6	-10	10
		2.4125	-31.27	27.23	-10	10
		2.425	-28.5	28.07	-10	10

Table 18. Polarization results for 2.4 GHz frequencies.

3. Polarization Difference Simulations for 5.0 GHz

For the center frequency 5.0 GHz, a sample horizontally polarized antenna signal contour is shown in Figure 74. For every frequency in this band, Urbana was run and the difference plots generated for antenna polarization. Only the center frequencies for

horizontally polarized antenna cases are included. Comparison between vertical and horizontal polarization is illustrated in Figure 75 for 5.0 GHz.

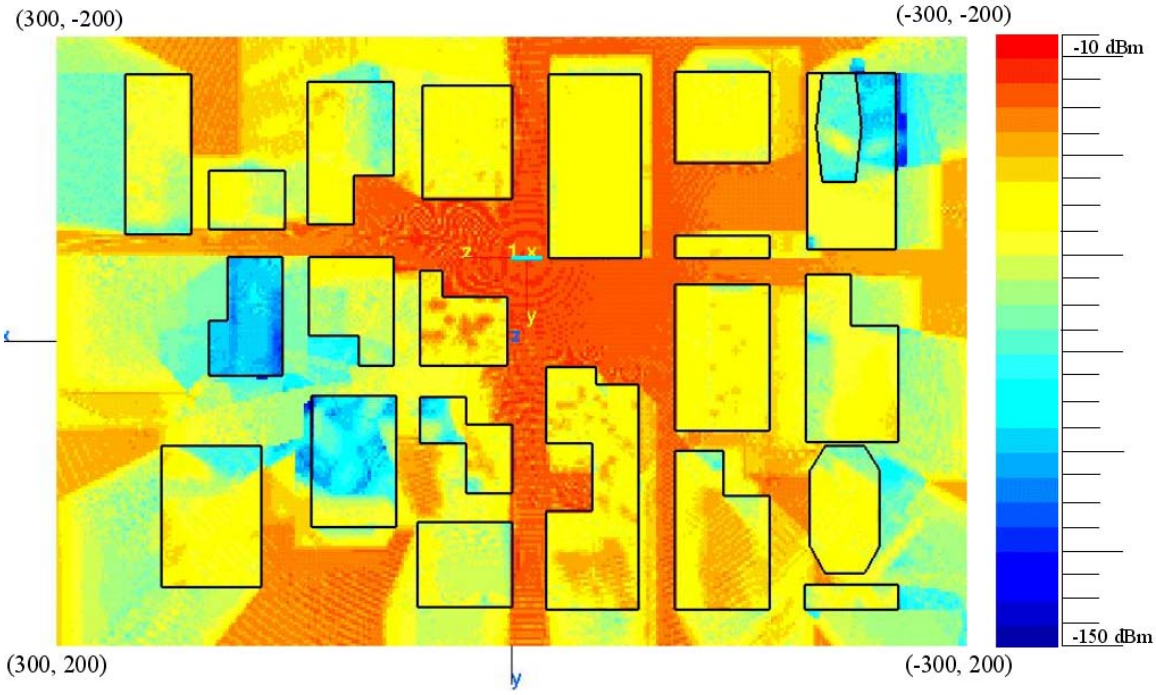

Figure 74. Horizontal polarized antenna, 5.0 GHz

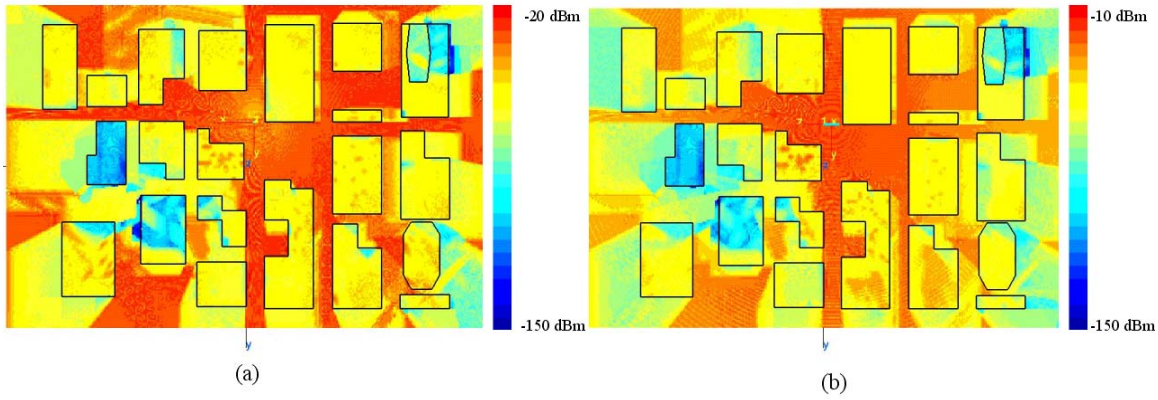

Figure 75. Polarization comparison for 5.0 GHz (a) vertical and (b) horizontal

In this frequency band, vertical and horizontal have very similar signal levels. Figures 76 to 80 shows difference plots for frequencies from 4.975 GHz to 5.025 GHz.

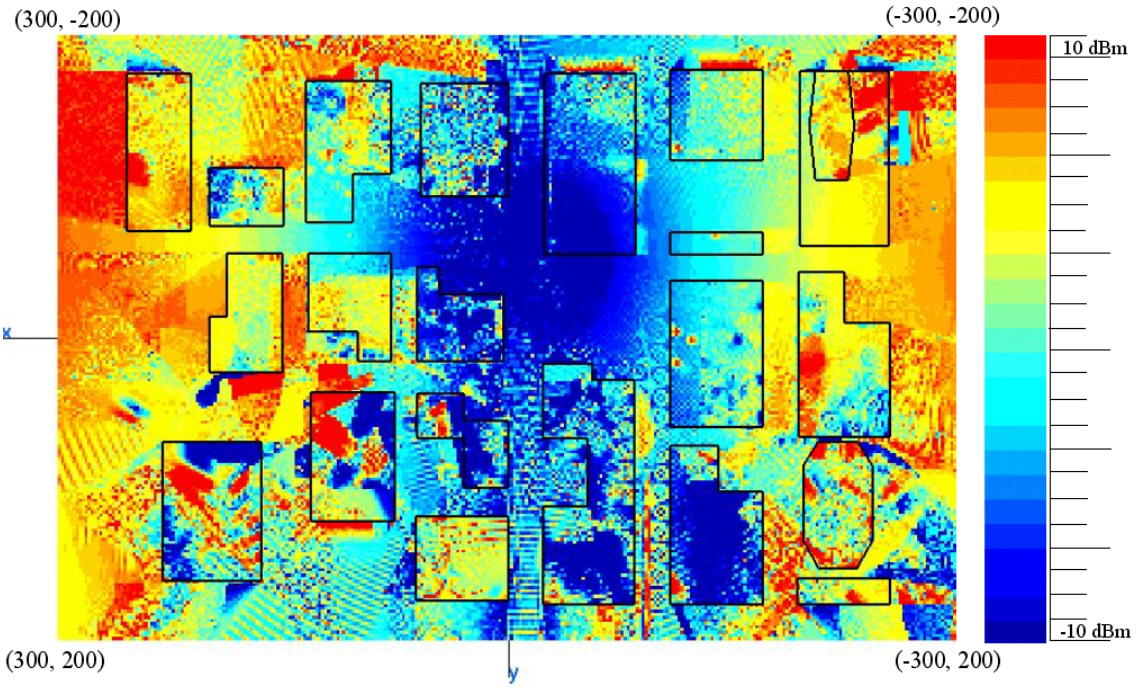

Figure 76. Polarization difference, 4.975 GHz

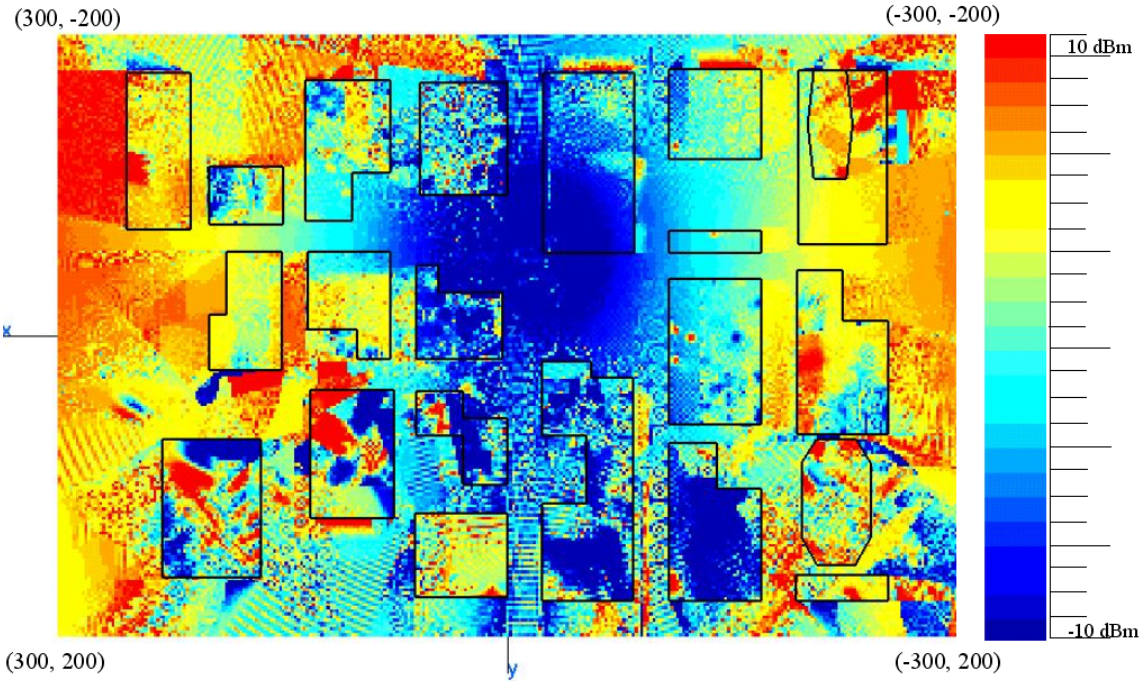

Figure 77. Polarization difference, 4.9875 GHz

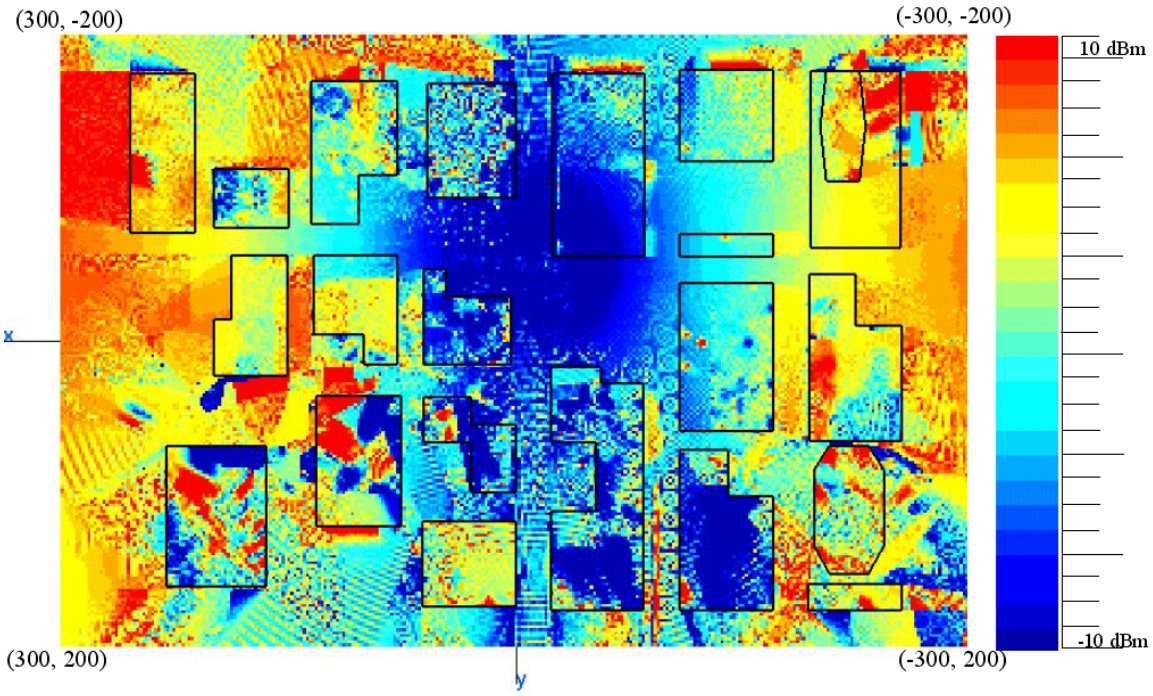

Figure 78. Polarization difference, 5.0 GHz

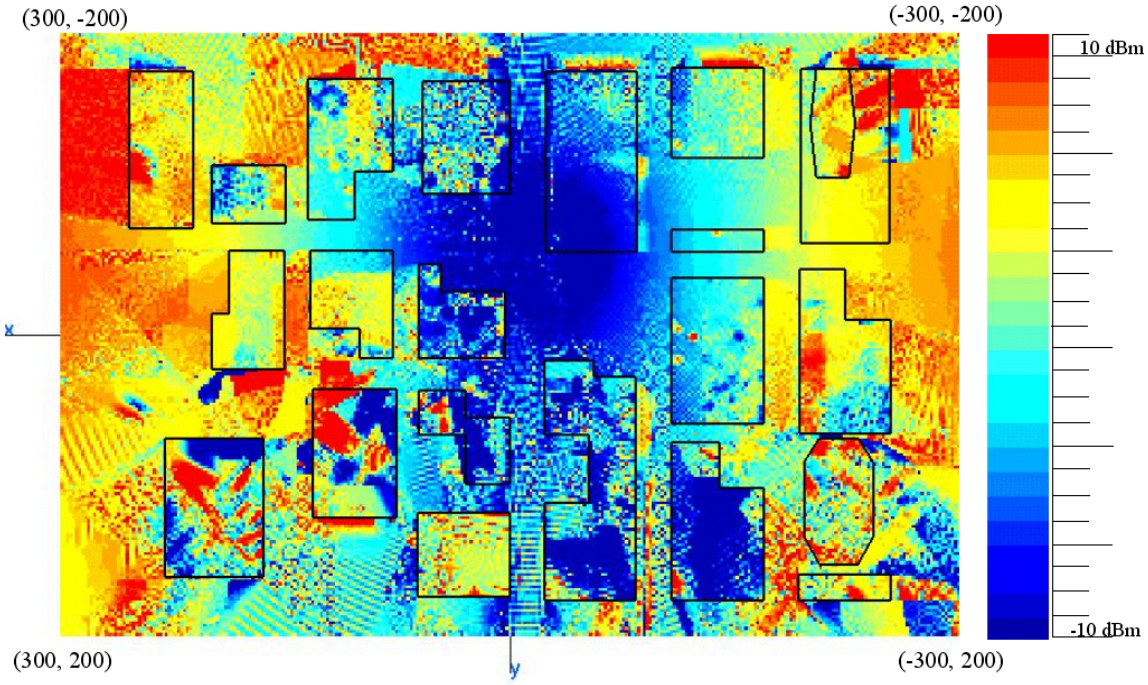

Figure 79. Polarization difference, 5.0125 GHz

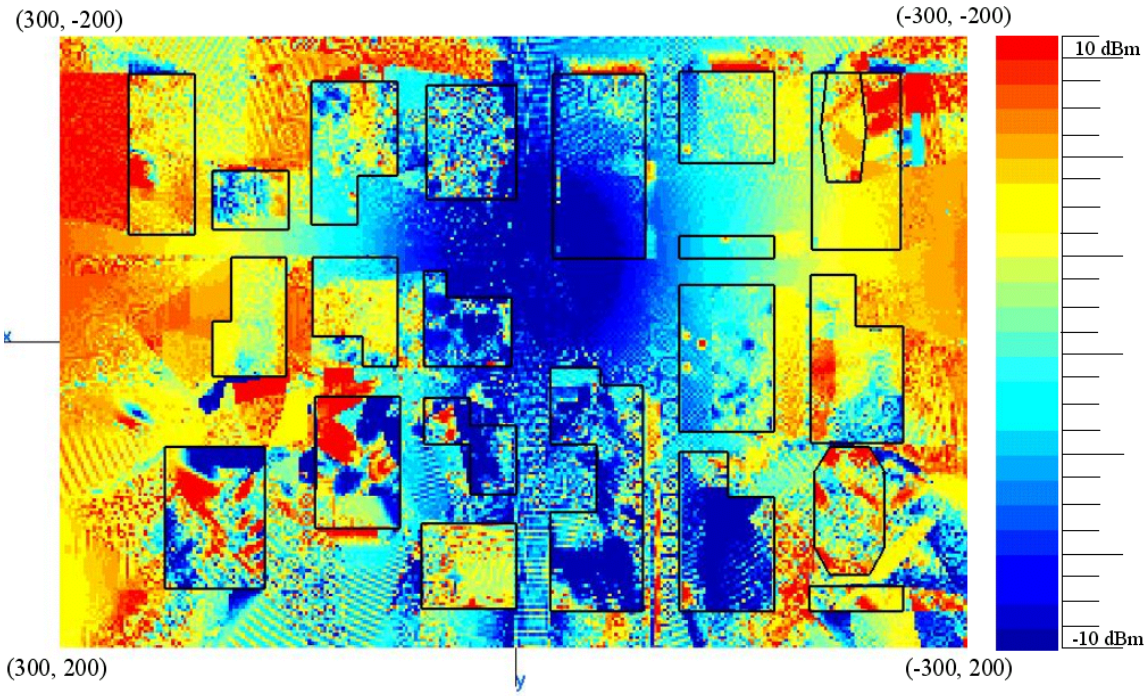

Figure 80. Polarization difference, 5.025 GHz

Again, it is observed that in this 5.0 GHz range, in regions near to the antenna, the signal level difference is high. In some far region areas of the observation plane, it is possible to see hot spots and low spots very close to each other. Reflection and diffraction have a great effect on signal level at these points. The summary for the 5.0 GHz simulations is given in Table 19.

5 GHz Center Frequency Polarization Differences						
Polarization Type	Polarization Type	Simulation Frequency (GHz)	Power Difference (dB)		Graph Range (dB)	
			Min	Max	Min	Max
Vertical Dipole X(100) Z(001) Oriented	Horizontal Dipole X(00-1) Z(100) Oriented	4.975	-32.7	32.15	-10	10
		4.9875	-37.09	33.12	-10	10
		5	-33.95	36.97	-10	10
		5.0125	-33.23	32.04	-10	10
		5.025	-31.55	32.31	-10	10

Table 19. Polarization results for 5.0 GHz frequencies.

F. NOISE BANDWIDTH AND EFFECTIVE BANDWIDTH

In this section, a small area from the city model is selected, and the behavior of the signal level versus frequency is examined over a 50 MHz bandwidth. Observation points are created, again with two meters separation. The coordinates of this region are:

$$(x_{\max}, y_{\max}) = (-250.00 \text{ m}, -90.00 \text{ m})$$

$$(x_{\min}, y_{\min}) = (-300.00 \text{ m}, -92.00 \text{ m})$$

A total of 52 observation points were created. Observation point 1 is at location (-300 m, -92 m) and observation point 52 is at point (-250 m, -90 m). A vertical polarized transmitting antenna with 1 W power is selected for all of the simulations. A height of $z = 4$ m is selected as the observation plane. Figure 81 shows an expanded view of simulation observation area.

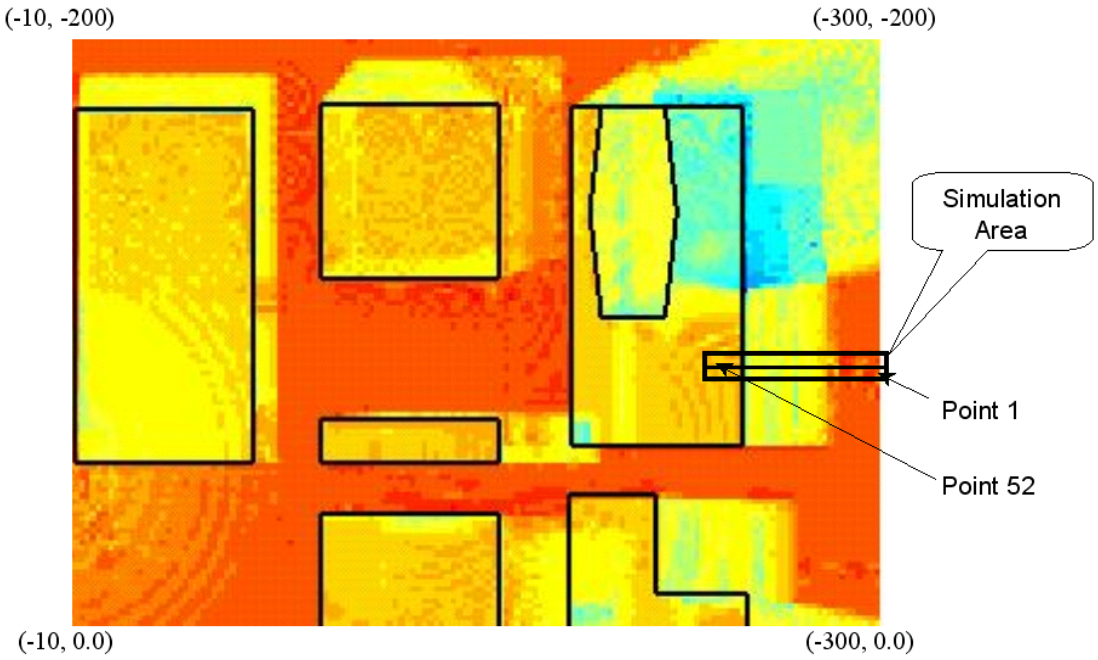

Figure 81. Simulation area for noise and effective bandwidth, 2.4 GHz.

When the frequency of the transmitter is changed, there is a noticeable change in the signal contours. In particular, the location of the hot spots (localized areas of high signal level) changes with the frequency. The 2.4 GHz frequency band is used for calculation in this section. A set of output files are created at frequencies of 2.375 GHz,

2.3875 GHz, 2.4 GHz, 2.4125 GHz, and 2.425 GHz. These files are used for the noise and effective bandwidth calculation as described in the next section. The total electric field values (vertical component) are calculated from the **Urbana** output field files for every frequency at each observation point. Calculated field values vs. observation points are shown in Figure 82.

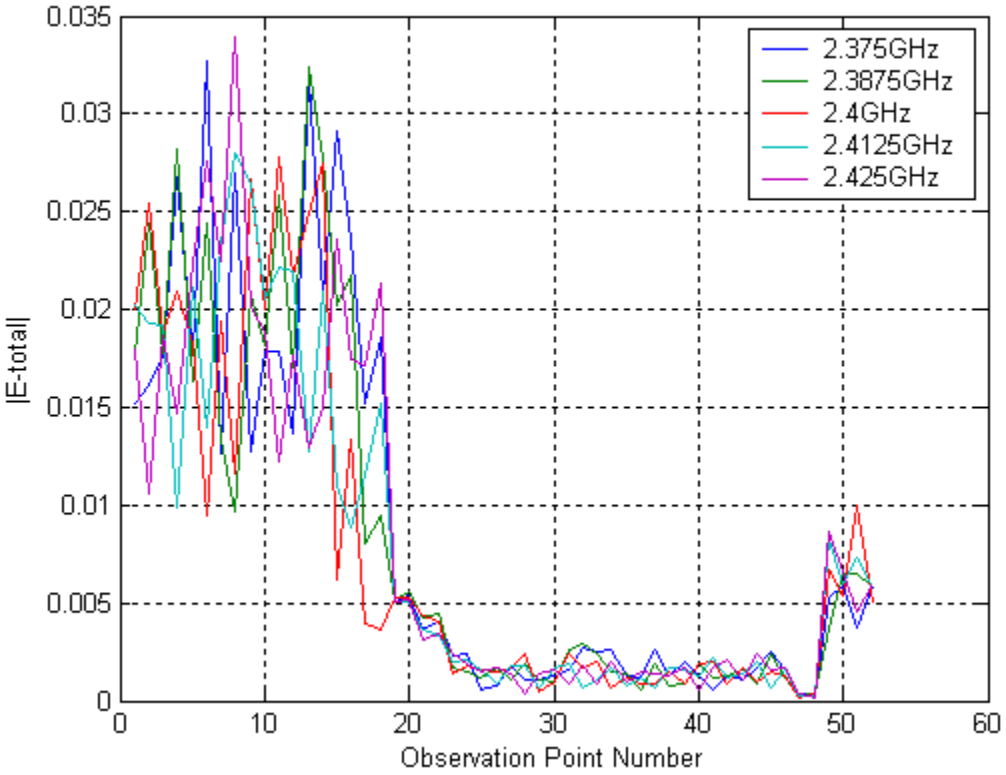

Figure 82. Magnitude of the total field values vs. observation points for 2.4 GHz frequency band.

At some observation points it is clearly seen that E-total is changing rapidly with the change in frequency, while at other observation points values are almost constant. Figure 83 shows E-total values for randomly selected 6^{th} and 14^{th} observation points. It is clearly seen from the figures that observation points have different E-total values for different frequencies originating from multipath in the small city environment.

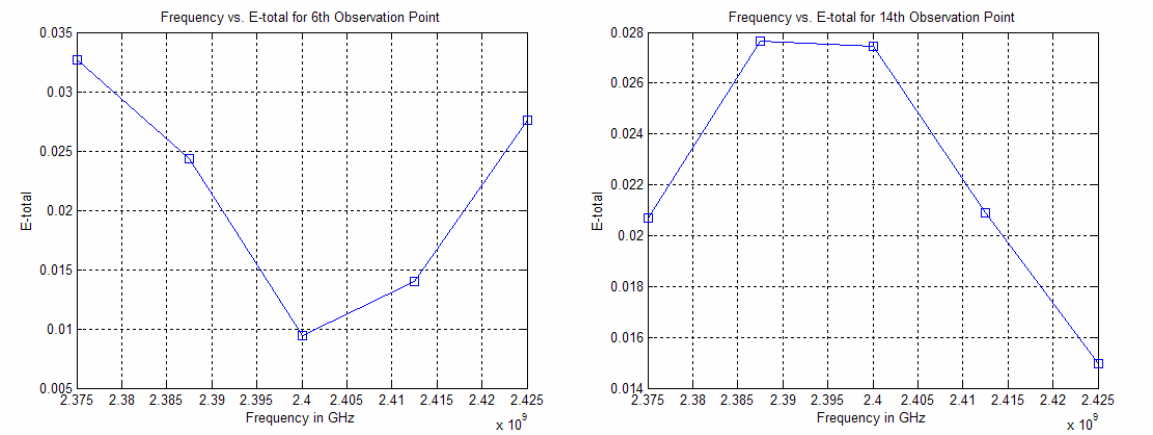

Figure 83. E total values for 6th and 14th observation points.

1. Noise Bandwidth Calculations

At microwave frequencies, the noise with which the signal competes is usually generated within the receiver itself [30]. This is called thermal noise and its magnitude is directly proportional to the bandwidth and absolute temperature of the ohmic portions of the input circuit. The available thermal-noise power in watts generated at the input of a receiver of bandwidth B_n (hertz) at a temperature T (degrees Kelvin) is described in Reference [30] as:

$$N_0 = \text{Available thermal noise power} = kTB_n \tag{4.1}$$

where k =Boltzmann's constant = 1.38×10^{-23} J/deg. The bandwidth B_n is called the noise bandwidth and defined as:

$$B_n = \frac{\int_0^{\infty} |H(f)|^2 df}{|H(f_0)|^2} \tag{4.2}$$

where $H(f)$ is the frequency response function of the filter and f_0 is the frequency of the maximum response. Noise bandwidth is not the same as more familiar half-power or 3 dB bandwidth.

To calculate noise bandwidth for observation plane created in this section, *.field files from all frequency bands are imported into Matlab. A numerical integration is performed using the "trapezoidal rule." Figure 84 shows the noise bandwidth values at every observation point.

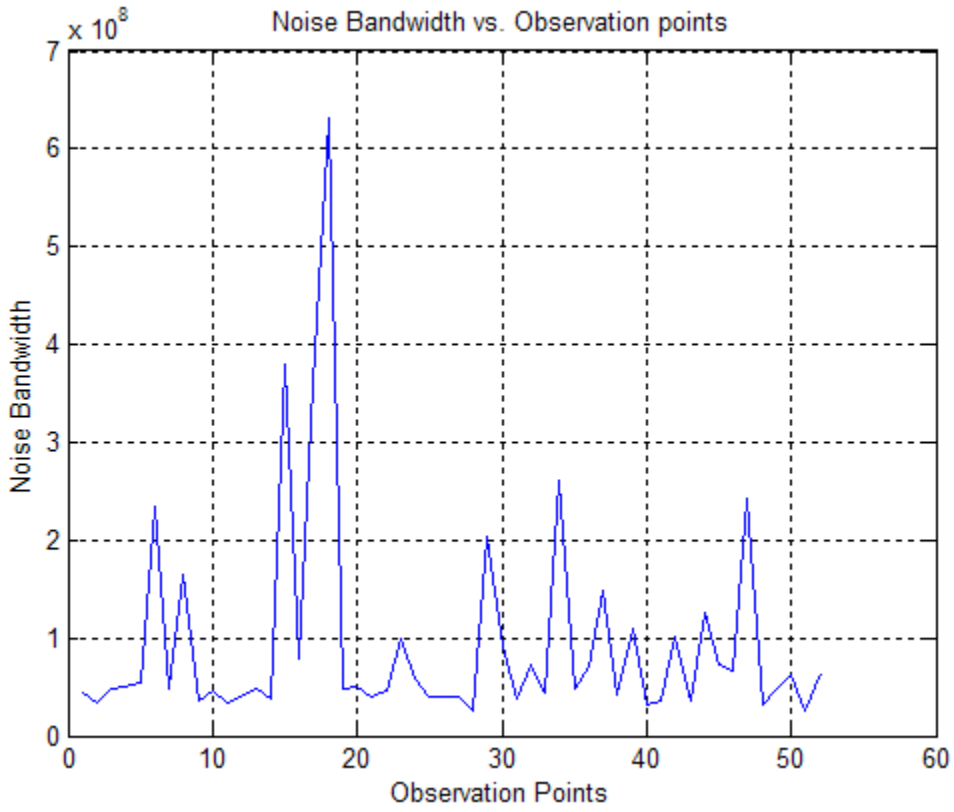

Figure 84. Noise bandwidth values for every observation points.

It is clear that observation points 15 and 18 have greater noise bandwidth according to the simulation. Recall that a 50 MHz bandwidth is used in the simulations, but these points show that some regions have greater noise bandwidth and therefore smaller SNR values. Most of the points have a noise bandwidth close to 50 MHz, which is the value for a constant $H(f)$.

2. Effective Bandwidth Calculations

The effective bandwidth β is different from other bandwidths encountered in electronic engineering [30]. It is not related to either the half-power bandwidth or noise bandwidth. The more the spectral energy is concentrated at the two ends of the band, the larger will be β. The effective bandwidth is also called rms bandwidth and is defined as:

$$\beta^2 = \frac{\int_{-\infty}^{\infty} (2\pi f)^2 |H(f)|^2 \, df}{\int_{-\infty}^{\infty} |H(f)|^2 \, df} \tag{4.3}$$

where, the mean value of $H(f)$ is at $f = 0$, and $H(f)$ is the video spectrum with negative and positive frequencies. Effective bandwidth calculations for the observation points is shown in Figure 85. The mean value of 87 MHz is found for observation plane. This is the value obtained for a constant $H(f)$. The values are not changing significantly at other observation points.

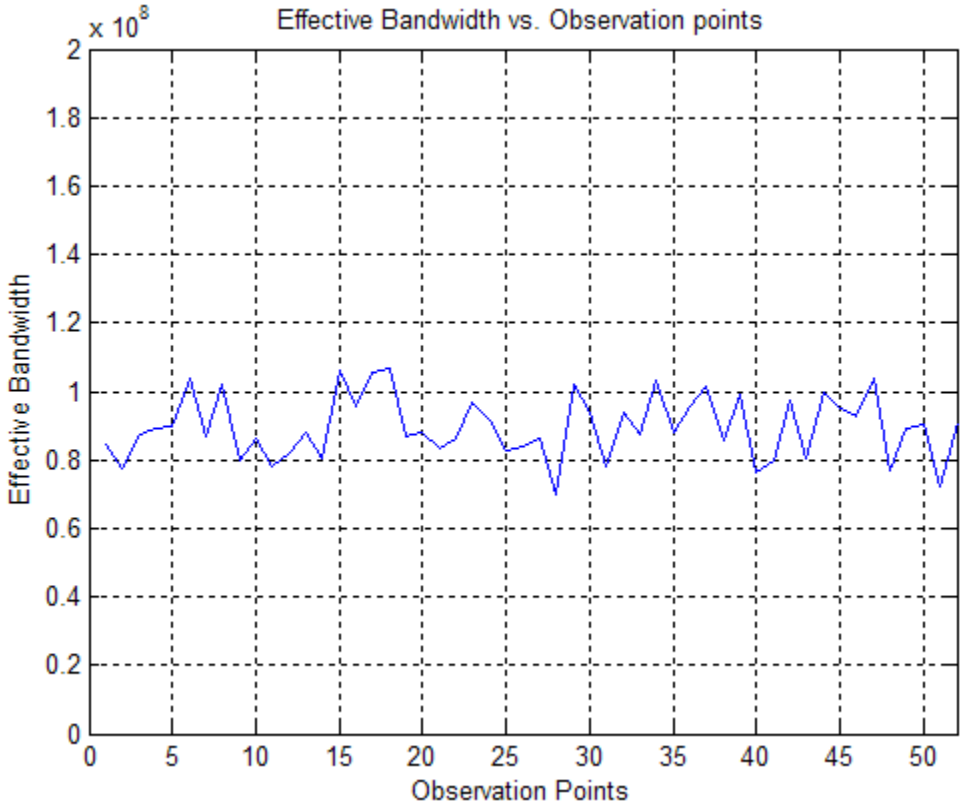

Figure 85. Effective bandwidth values for every observation points.

V. SUMMARY AND CONCLUSION

A. SUMMARY

In the near future, wars may no longer be fought in big open areas, but in built up urban areas. Reliable communication and data links between troops and commanders are necessary for command and control. More and more, air support and reconnaissance missions are highly dependent on UAVs, which are replacing piloted aircraft in this role.

In an operational environment, communication and data links are susceptible to jamming and interference. Besides these hostile actions, multipath propagation can result in a complete loss of command and control signals, which can limit the operational area or even cause loss of the vehicle. On the other hand, diffraction at corners of walls and buildings causes illumination behind walls and into shadowed regions can help in extending propagation by creating constructive interference at some places.

This research investigated frequency and polarization diversity for urban UAV communication and data links using **Urbana**. Several scenarios were developed to approximate operational situations in the small city environment. Variations in the simulation included material coatings of the building walls, observation points, operating altitude, operating frequency, and transmitting antenna polarization.

B. CONCLUSIONS AND FUTURE WORK

This research has examined the frequency and polarization diversity for UAV communication and data links in a city environment. The results show that high frequencies are attenuated more rapidly in lossy materials like concrete, wood and glass commonly found in city environment. However higher frequencies have an advantage of higher data rates compared to lower frequency bands. At the same time, higher frequencies are more susceptible to attenuation due to weather conditions. This causes a shorter operational range that translates to a smaller RF spread radius, and thus lowers the susceptibility to detection, jamming and interference. In addition to this, increasing the frequency results a decrease in outdoor-to-indoor propagation. Diffraction has a strong

impact on the signal level in a city environment. It is possible that a shadowed region may have good signal strength due to reflections from surfaces and diffraction from edges.

Increasing the operating altitude generally gives more uniform coverage because building shadows are smaller. However, high altitudes make the UAV more visible, vulnerable to fire, and consume more fuel.

Vertical polarized antennas generally give better results than horizontal polarized antennas except in the pattern null directly below the UAV. Along corridors created by the buildings, vertical signal levels are high compared to horizontal. This is probably due to the larger number of vertical edges in a dense urban environment. The configuration of a street bounded by high-rise buildings is referred as an urban canyon. This effect can be used to advantage when positioning a UAV for communication because of the high signal levels.

The signal level is not dramatically different for the two polarizations once the effects of the antenna pattern are removed. However, with polarization diversity there may be some cases where varying antenna polarization can be used to establish a more reliable link.

The propagation channel was examined for a 50 MHz bandwidth about the frequencies of 900 MHz, 2.4 GHz and 5 GHz. As expected, the multipath effects varied with frequency. At a fixed observation point the signal level can vary up to 20 dB over the band. The equivalent noise bandwidth and effective bandwidth were calculated for several observation points. The effects of fading could be seen in the noise bandwidth, which increased significantly at some observation points. An increase in noise bandwidth decreases the signal-to-noise ratio. Reduced SNR will degrade the bit error rate, but exactly how much depends on the type of modulation that is used.

Future work might include the investigation of space diversity analysis for the UAV linkage in the presence of jamming. Simulations involving directional antenna beams, and a comparison of predicted signal contours with physical measurements would also be beneficial.

With directional antenna models, simulations can be performed and the effectiveness of the angle and space diversity techniques can be investigated. Directional antennas have small beam widths and are less susceptible to multipath interference. Effects of directional antenna beams can be a topic of investigation and research.

THIS PAGE INTENTIONALLY LEFT BLANK

APPENDIX

A. MATLAB CODES

The following is a list of Matlab codes, which are used in the research. They include plot of reflection coefficients versus incident angle, plot of free space path loss versus frequency, half-wave dipole power radiation pattern, observation plane generation, and noise and effective bandwidth calculation from **Urbana** field files.

```
% Reflection coefficients vs. incident angle plots
%--------------------------------------------------------------------------------
clear;clc;

% parameters

E_r = [3 20 25 81];
theta_i = linspace(0,pi/2,1000);
theta_deg = theta_i.*180./pi;

% calculation and plotting
% for parallel and perpendicular reflection coefficients.

for i =1:4

   Per_ref_coef =(cos(theta_i)-(sqrt((E_r(i))-
(sin(theta_i)).^2)))./(cos(theta_i)+(sqrt((E_r(i))-(sin(theta_i)).^2)));
   Par_ref_coef =((-E_r(i).*cos(theta_i))+(sqrt((E_r(i))-
(sin(theta_i)).^2)))./((E_r(i).*cos(theta_i))+(sqrt((E_r(i))-(sin(theta_i)).^2)));
   plot(theta_deg,abs(Per_ref_coef),'r-.');grid on;
   hold on;
   plot(theta_deg,abs(Par_ref_coef),'-');

end
title('Reflection Coefficients for Parallel and Perpendicular Polarization vs. Incident
Angle');
legend('perpendicular','parallel');
ylabel('Reflection Coefficient');
xlabel('Incident Angle(deg)');
text(2,0.3,'Dry Ground');
text(2,0.6,'Ceramic Slab');
```

```
text(2,0.7,'Wet Ground');
text(2,0.83,'Water');
%-------------------------------------------------------------------------------


% Free space path loss calculation
%-------------------------------------------------------------------------------

clc; clear;

% parameters

c = 3e8;
f = linspace(900e6,5.8e9,1000);
d = 1000;  % 1 km fixed distance

% calculation & plot

lamda = c./f;
path_loss_db = 20.*log10((4*pi*d)./lamda);
plot(f,path_loss_db);
grid on;
xlabel('Frequency in Hz.');
ylabel('Path Loss in dB (Lp)');
%-------------------------------------------------------------------------------



% Half-wave dipole power radiation pattern
%-------------------------------------------------------------------------------

clc;clear;

% parameters & calculations

theta = linspace(0,2*pi,1000);
el_f = sin(theta);                          % element factor
pat_f = cos((pi/2)*cos(theta))./sin(theta).^2;  % pattern factor
field_pat = el_f.*pat_f;                    % far-field pattern
p_pat = abs(field_pat).^2;                  % power pattern

% half-power beam width calculations
s=1;
for i = 1:1000
   if (field_pat(i) >0.705)&(field_pat(i) <0.709)
      a(s)= theta(i)*180/pi;
```

```
        hppoints(s)= i;
        s=s+1;

    end
end
polar(theta,p_pat);
hold on;
polar(theta(hppoints(1)),p_pat(hppoints(1)),'r*');
polar(theta(hppoints(2)),p_pat(hppoints(2)),'r*');
hpbw = a(s-1)-a(1);
title('Power Pattern for Half-wave Dipole');
xlabel(['HPBW = ' num2str(hpbw) ' Degrees.']);
%--------------------------------------------------------------------------------



% Observation points generation
%--------------------------------------------------------------------------------
clc;
clear;
i = 1;
z = 4;
for x = -300:2:300;
    for y = -200:2:200;
        M(i,:) = [x, y, z];
        i = i + 1;
    end
end
save obvpoint M -ASCII;
%--------------------------------------------------------------------------------


% Urbana (E-total & Noise bandwidth & Effective Bandwidth calculations ) from files.
%--------------------------------------------------------------------------------
clear;clc;
DataArray =[];

%loading file
cd ('H:\thesis template\matlab codes');
name=input('Enter root name of the file (without .field and number): ','s');
for m=1:1:5;

    n=int2str(m);
    fname=[name,n,'.field'];
    fid=fopen(fname);
```

```
% discard first 6 lines (comments and headings)
   for i=1:6
      linedat=fgetl(fid);
   end
   irow=0;

% read edge data in blocks
   disp('reading input file .....')
   n=1;
   while feof(fid)==0
       irow=irow+1;
       linedat=fgetl(fid);
       B=sscanf(linedat,'%f');
       A(irow,1:11)=transpose(B);
   end
   disp(['data read, number of rows =',num2str(irow)])

% Ex, Ey, Ez values are taken from input matrix
   for k=1:52;
      Ex(k)=A(k,6)+j*A(k,7);
      Ey(k)=A(k,8)+j*A(k,9);
      Ez(k)=A(k,10)+j*A(k,11);

      AbsEx(k)=abs(Ex(k));
      AbsEy(k)=abs(Ey(k));
      AbsEz(k)=abs(Ez(k));

      Etotal(k)=sqrt(AbsEx(k).^2+AbsEy(k).^2+AbsEz(k).^2);
   end

   fclose(fid);
   DataArray(m,:)=Etotal;
end

% plotting e-total vs. observation points for every frequency.
x=1:52;
figure(1);
plot(x,DataArray(1,:),x,DataArray(2,:),x,DataArray(3,:),x,DataArray(4,:),x,DataArray(5,:
));
xlabel('Observation Point Number');
ylabel('|E-total|');
legend('2.375GHz','2.3875GHz','2.4GHz','2.4125GHz','2.425GHz');
grid;

% plotting frequency vs. e-total for selected observation points
freq_data=transpose(DataArray);
```

```
obv = input('Enter an observation point number for E-total calculation :');
obvstr=num2str(obv);
figure(2)
f=2.375e9:.0125e9:2.425e9;
plot(f,freq_data(obv,:),'s-');
title(['Frequency vs. E-total for ',obvstr,'th Observation Point']);
xlabel('Frequency in GHz');
ylabel('E-total');
grid;


% for test simulation (comment for real data values)
% freq_data =ones([52,5]);


% interpolating frequency file to middle for calculations
for i =1:length(freq_data)
   for k =1:4
      freq_data_new(i,k) =.5*(freq_data(i,k)+freq_data(i,k+1));
   end
end

% noise bandwidth and effective bandwidth calculations for every observation points
for i=1:length(f)-1
   fre(i)=0.5*(f(i)+f(i+1))-2.4e9;
end
df=0.0125e9;
w =2*pi.*fre;


for i =1:length(freq_data_new)
   NoiseBW(i)=sum((freq_data_new(i,:).^2).*df)/(freq_data(i,3).^2);
   for k= 1:4
      EffBW2num(i,k)= w(k)^2.*freq_data_new(i,k).^2*df;
      EffBW2denum(i,k) = freq_data_new(i,k).^2*df;
   end
   EffBW2numsum(i)=sum(EffBW2num(i,:));
   EffBW2denumsum(i)=sum(EffBW2denum(i,:));
end
EffBWsqr = EffBW2numsum./EffBW2denumsum;
EffBW = sqrt(EffBWsqr);


% plotting noise bandwidth
figure(3);
plot(NoiseBW);
```

```
grid;
title('Noise Bandwidth vs. Observation points');
xlabel('Observation Points');
ylabel('Noise Bandwidth');


% plotting effective bandwidth
figure(4);
plot(EffBW);
axis([0 52 0 2e8]);
grid;
title('Effective Bandwidth vs. Observation points');
xlabel('Observation Points');
ylabel('Effective Bandwidth');
%--------------------------------------------------------------------------------
```

B. URBANA INPUT SCRIPT FILE

The following is a listing of the sample **Urbana** input file for small city simulation:

```
--- input Urbana v 2.5
#
# ********************************
# A---scatterer file,length & freq
# ********************************
#--- name of scatterer file in ACAD format (e.g. wall.facet)
filename.facet
#--- length unit:1=inch, 2=cm, 3=meter, 4=mm, 5=mil
3
#--- uniform freq (GHz): start freq, end , nstep
#    (nstep=0 means: just do first freq. CAUTION: antenna patterns are
#     assumed to be indep. of freq and is calculated at end freq)
0.875 0.875 0
#
# *********************************
# B--- Antenna Description and List
# *********************************
#
#---Enter method of describing antennas.
#   (1 = here, 2 = file):
2
#---If described in file, enter file name:
filename.antenna
#---If described here, fill in sections B1, B2, B3.
#   If described in file, use dummy data in sections B1, B2, B3
#   (specify one dummy antenna type, dummy antenna origin,
#    and one dummy item in antenna list).
#
# ************************
# B1: Define Antenna Types
# ************************
#
#   Two lines for each type.
#     Line1: type ID, ant code
#     Line2: parameters
#
#   Type ID must start from 1 and increment by 1 thereafter
#
#   Ant Code   meaning           parameters
#   --------   ---------------   ----------------------------
#      1       pattern file      filename(ascii)
```

```
#     2       dipole            length(real)
#
#   Antenna Types list:
#
#   Enter number of antenna types:
1
#   Type #1
1 2
0.1714
#
# ***********************************************
# B2: Enter origin of antenna coord in main coord
# ***********************************************
#
0. 0. 0.
#
# ***********************
# B3: Create Antenna List
# ***********************
#
#   Three lines for each antenna.
#     Line1: Type ID, location (x,y,z), power (watts), phase(deg)
#     Line2: Local x-axis in main coord.
#     Line3: Local z-axis in main coord.
#
#   Enter number of antennas:
1
#
#   Antenna #1
1  -10 -55 150 1. 0.
1. 0. 0.
0. 0. 1.
#
# **********************
# C---Observation points
# **********************
#--- Observation points defined with respect to main coord. system 7.
#    Enter method of specifying list of points.
#    (1 = here, 2 = file):
2
#--- If points are listed here, enter number of points (kobtot):
1
#--- If listed here (1 above), List xyz of points in main coord 7
#    (one point at a line). If 2 above, include one dummy line.
1.          2.              -11.00
#--- If points listed in file (2 above), enter name of file.
```

```
observationplane.list
#--- Include direct Tx to observer contribution.
#   If you turn on the direct contribution from the transmitter to the
#   observation point, computed result will be the total field, which is
#   the incident + scattered field.   For propagation analysis, this is
#   the preferred setting.  Otherwise, the result only includes the
#   scattered field.
#
#   Include direct contribution from transmitter to observation point (rx)
#   (1 = yes, 0,2 = no):
1
#--- Compute received power into Rx antenna.
#   Urbana always computes field levels at the observation point.
#   If you specify an Rx antenna, Urbana will also compute the received
#   power and record the results in the (runname).couple file.
#   This causes a moderate but slow-down when using the SBR method (below).
#
#   Include Rx antenna (1 = yes, 0,2 = no):
0
#--- Rx antenna specification
#   Remaining entries in Section C can be ignored if not including
#   an Rx antenna.
#   Enter antenna type (1 = pattern file, 2 = dipole):
1
#   Each antenna type requires additional parameters.
#   List of expected parameters follows.  Choose one.
#
#   Type  Description     Expected Parameter(s)
#   1     Pattern File    File Name (e.g., beam.antpat)
#   2     Dipole          Length (in prevailing unit)
#
#   Enter parameter(s) on next line:
dummy.antpat
#--- Rx antenna orientation
#   Enter local x-axis of Rx in global coordinates
1. 0. 0.
#   Enter local z-axis of Rx in global coordinates
0. 0. 1.
#
# ****************************
# D---Theoretical consideration
# ****************************
#--- Choose method of computation
#   0 = compute fields in the ABSENCE of the scatterer
#   1 = compute fields by SBR
#   2 = compute fields by GO
```

```
2
#--- If SBR, select a PO integration scheme at bounce points
#    1 = do integration at first & last bounce points only
#    2 = do so at all bounce points (GTD formulation)
1
#--- Edge diffraction
#    SBR can be enhanced with PTD edge diffraction.
#    GO can be enhanced with GTD edge diffraction.
#    Add edge diffraction (0,2=no, 1=ILDC (SBR or GO), 3=UTD (GO only)
3
#--- If edge diffraction switched on, enter name of edge file
#    (e.g., wall.edge or dummy if edge not included).
filename.edge
#--- Choose method of ray launch
#    1 = by (baby) facet, achieving a uniform first bounce surface density
#    2 = uniform angular distribution (burst launch)
#    (If computation by GO, must select 2 = burst launch)
2
#--- If ray launch by (baby) facet (1 above), enter ray density:
#    # rays/wavelength (normally 5-10)
5.
#--- If burst ray launch (2 above), enter angular interval (deg).
#    (Typically 0.25 - 2.0 deg)
2.
#--- max permissible ray bounces (normally 5-10)
7
#--- max-voxdepth = max depth of BSP tree (normally 20)
#    max-voxl = max facets in each voxel(normally 10)
#    (Larger voxdepth & smaller voxl lead to faster ray tracing
#     but more computer memory)
20,10
#--- ICOAT for absorbing facets
888
#--- IQMATRIX for divergence factor
#     1 = calculated by Q-matrix
#     2 = ignored except for the spherical wave spread
2
#--- IF using Q-matrix, name target curvature file(e.g. wall.curv)
dummy.curv
#--- IPEC=1 if all pec,  =2 if coating present
2
#--- For PEC scatterer, give the magnitude of reflection coeff
#    (use 1.0 for ideal PEC, use less for rough PEC--fudging)
1.0
#--- IF PEC, the rest coating info is dummmy
#--- material reflection is done through a look-up table
```

```
#    specify the freq interval in GHz for the table e.g. 0.25
#    (dummy if input freq less than 51)
0.2
********************
E---coating material
********************
---- number of materials
     (NOT including pec, which is identified by ICOAT=0)
     (NOT including absorbing facets:  ICOAT=28 or 888)
     (If 3 material, urbana reads only ICOAT=1-3)
3   <----NCOTOT
--- for each material, identify its boundary type:
   iboundary = 1 if impedance boundary
               2 if layered slabs with PEC backing
               3 if penetrable layered slabs with air backing
               4 if penetrable FSS Tx/Refl table supplied by user
               5 if same as 2 except using freq-dep ramlib.d
               6 if antenna refl table supplied by user
               7 if layers over semi-infinite ground
for each material, given info by following the templates
^^^ ICOAT=1 ^^^^^^^^^^^^^^^^^^^^^^^^^^^^^^^^^^^^^^^^^^^^^^^^^^^^^^^^^^^^^^^^
--- iboundary
3
--- number of layers over air backing
   (1st layer is farthst fr incid field and innermost)
1
--- thick,epsilon(c),mu(c),resistivity(ohm)
0.30000 (10.1,0.5) (1.0,0.0) 1.e+30
^^^ ICOAT=2 ^^^^^^^^^^^^^^^^^^^^^^^^^^^^^^^^^^^^^^^^^^^^^^^^^^^^^^^^^^^^^^^^
--- iboundary
2
--- number of layers over PEC backing
   (1st layer is farthst fr incid field and innermost)
2
--- thick,epsilon(c),mu(c),resistivity(ohm)
0.0300 (2.5,-0.000) (1.6,-0.000) 1.e+30
0.0500 (3.0,-0.000) (1.0,-0.000) 1.e+30
^^^ ICOAT=3 ^^^^^^^^^^^^^^^^^^^^^^^^^^^^^^^^^^^^^^^^^^^^^^^^^^^^^^^^^^^^^^^^
--- iboundary
7
--- number of layers over half-space (semi-infinite ground)
   (1st layer is farthst fr incid field and innermost)
1
--- thick,epsilon(c),mu(c),resistivity(ohm)
0.1000 (3.000,-0.0) (1.0,-0.0) 1.e+30
--- epsilon(c),mu(c) of semi-infinite ground
```

(3.00,-0.00) (1.0,-0.00)

(End of regular input file. Leave a few blank lines)

'OPTIONAL ADVANCE FEATURES' (Do not change letters in quotations)
The line above must be placed at the end of the regular urbana
input. Advance features are designed for special applications or
for testing codes. They are not needed by general usages.

ADVANCE1: ADD GTD-TYPE BLOCKAGE CHECK

In regular urbana computation, blockage check is mostly done by
PTD principle. For interior scattering in a confined region, use of
GTD principle may be more appropriate.
Option to use GTD principle: 1=yes,   2=no (regular case)
2

ADVANCE2: SIMPLE TERRAIN BLOCKAGE MODEL

For GO method, terrain generates 100% blockage, and blocked rays leave
no energy behind a hill. With this feature, LOS rays and UTD edge
diffraction rays can pass through terrain, with some attenuation.
Attenuation is measured in dB per hill. Each hill is identified
by two passages through two terrain facets.
Can only be used with GO method (and UTD edge option).
Use simple terrain model: 1 = yes, 2 = no (regular case)
2
Enter coating code range of terrain facets (e.g., 1, 2):
1 1
Enter amount of attenuation per hill (dB, > 0):
5.

ADVANCE3: APPROXIMATE DOUBLE DIFFRACTION MODEL

For GO + UTD method, only single diffraction is considered.
With this feature, double diffraction is approximated by identifying
surfaces which block the single diffraction, such as building walls.
If one or two facets block the path from the single diffraction point
to the transmitter, the diffraction is still included, but with attenuation.
Works best if "diffracting facets", marked by their coating code, are
always associated with enclosed structures with well defined edges.
Use double diffraction model: 1 = yes, 2 = no (regular case)
2
Encounter coating code range of diffracting facets (e.g., 5, 10):
2 2

```
# Enter amount of attenuation for second diffraction (dB, > 0);
10.
# ----------------------
# ADVANCE4: ACCELERATION
# ----------------------
# For large scenes, run time grows both with the number of field
# observation points and the number of edges.  Normally, all combinations
# of lit edges and observation points are considered.  This feature
# accelerates the processing by limiting the scope of considered edge
# interactions to region around the LOS path from the transmitter
# to the observation point.  For example, to run a 5 km by 5 km scene,
# one may choose a 250 m interaction radius.  For each observation
# point, edges are ignored that lie outside an ellipse whose foci are the
# Tx and the observation point and whose major axis is the LOS distance
# plus 500 m (radius x 2).
# This feature can also be used to automatically filter edge files
# whose domain far exceeds the domain of ovservation points.
# Only use this feature for terrestrial simulations where the scene
# is nominally parallel to the x-y plane.
#
# Use large scene acceleration: 1 = yes, 2 = no (regular case)
2
# Enter radius of interaction
250.
# ---------------------------
# ADVANCE5: MULTI-DIFFRACTION
# ---------------------------
# Subsitute for Adv. #3.  Uses ray rubber-banding algorithm to find
# path from transmitter to receiver.
# Can only be used with GO. Cannot be used in conjunction with Adv. #3.
# If UTD switched on above, will take measures not to double count
# single diffraction mechanims.
# Use multi-diffraction model: 1 = yes, 0,2 = no
2
# Enter coating code range of diffracting facets (e.g. 5, 10):
2 2
# Enter maximum number of rubber-band points ( also used in Advance6 )
1
# Check multiple crawl planes instead of just vertical one: 1 = yes, 0,2 = no
0
# ---------------------------
# ADVANCE6: REFLECTION-DIFFRACTION
# ---------------------------
# If UTD switched on above, will take measures not to double count
# single diffraction mechanims.
# Use reflection-diffraction model: 1 = yes, 0,2 = no
```

```
2
# Do more than just single diffractions: 1 = yes, 0,2 = no
# Allow rubber-banding to both transmitter and receiver: 1 = yes, 0,2 = no
1 0
# Choose crawl plane selection mode: 0 = always vertical, 1 = initial edge,
#                                    2 = adaptive from edge to edge
1
# -----------------------------------
# ADVANCE7: GREEN'S FUNCTION (GF) FILE
# -----------------------------------
# By default, for SBR and no-target methods, a GF file IS NOT produced.
# Also, by default, for GO, a GF file IS produced.
# Use this feature to explicitily activate or de-activate generation
# of the GF file, which is needed by the re-processor for its activities.
# Activate GF file: 0 = no, 1 = yes, 2 = default activation behavior
2
# If yes, enter buffer scale factor.  Increasing scale factor reduces
# the number of GF file dumps to disk during a run, but costs memory.
# Recommend 2 - 5 for GO method, 1 for no-target method,
# and 100 - 10000 for SBR method.
2
```

LIST OF REFERENCES

[1] K. C. Wong, *Survey of Regional Developments: Civil Applications,* University of Sidney, February 8, 2001.

[2] E. Bone, C. Bolkcom, *Unmanned Aerial Vehicles: Background and Issues for Congress,* Congressional Research Service, Library of Congress, April 25, 2003.

[3] R. Janaswamy, *Radiowave Propagation and Smart Antennas for Wireless Communications,* Kluwer Academic Publishers, 2001.

[4] S. Loredo, L. Valle, and R. P. Torres, "Accuracy analysis of GO/UTD radio-channel modeling in indoor scenarios at 1.8 and 2.4 GHz," *IEEE Antennas and propagation Magazine,* Vol.43, No. 5, pp 37-51,October 2001.

[5] D. C. Jenn, Lecture notes for EC3630, Radio wave Propagation, available at www.nps.navy.mil/jenn/EC3630list.html, accessed on May 2004.

[6] E. K. Wesel, *Wireless Multimedia Communications,* Addison-Wesley Wireless Communication Series, 1998.

[7] D. C. Jenn, *Radar and Laser Cross Section Engineering,* AIAA Education Series, Washington, 1995.

[8] J. B. Andersen, T. S. Rappaport, and S. Yoshida, "Propagation measurements and models for wireless communication channels," *IEEE Communication Magazine,* Vol.33, No.1, pp 42-49, January 1995.

[9] F. T. Ulaby, "*Fundamentals of Applied Electromagnetics,*" Prentice Hall, Upper saddle River, New Jersey, 2001.

[10] W. L. Stutzman, G. A. Thiele, "*Antenna Theory and Design*," John Wiley and Sons, New York, 1998.

[11] W. S. Ament, "Towards a theory of reflection by a rough surface," *Proc IRE,* vol. 41, pp. 142-146, 1953.

[12] E. E. Johnson, R. I. Desourdis, G. D. Earle, S. C. Cook, J. C. Ostergaard, "Advanced High-Frequency Radio Communications," *Artech House,* Norwood, 1997.

[13] R. B. Steven, "Antenna Polarization Considerations in Wireless Communications Systems," white paper, Cushcraft Corporation, 1 November 2001.

[14] Taga, T., "Analysis for mean effective gain of mobile antennas in land mobile radio environments," *IEEE Trans. Veh. Tech.,* Vol. VT-39, No.2, pp. 117-131, May 1990.

[15] K. Siwiak, "Radiowave Propagation and Antennas for Personal Communications," *Artech House*, Norwood, 1998.

[16] www.iec.org/online/tutorials/smart_ant/topic03.html accessed on June 15, 2004.

[17] N. Benvenuto and L. Tomba, "Performance Comparison of Space Diversity and Equalization Techniques for Indoor Radio Systems," *IEEE Trans. Veh. Tech*., Vol 46, no.2, pp.358-368,May 1997.

[18] K. Tsunekawa, "Diversity Antennas for Portable Telephones," *IEEE Veh. Tech Conf.,* 1989, pp.50-56.

[19] A. M. D. Turkmani, A. A. Arowojolu, P. A. Jefford, and C. J. Kellet, "An Experimental Evaluation of the Performance of Two-branch Space and Polarization Diversity Schemes at 1800 MHz," *IEEE Trans. Veh. Tech.,* Vol. 44, no.2, pp. 318-326,1995.

[20] J. Walfisch and H. L. Bertoni, "A theoretical model of UHF propagation in urban environments," *IEEE Trans. Antennas Prop.,* Vol. 36, pp. 1788–1796, December 1988.

[21] A. G. Longley and P. L. Rice, "Prediction of tropospheric radio transmission loss over irregular terrain-a computer method," *ESSA Technical Report ERL 79-IOTS 67,* Washington, DC, July 1968.

[22] K. Bullington, "Radio propagation for vehicular communications," *IEEE Trans. on Vehicular Tech.,* Vol. VT-26, No.4, pp. 295-308, November 1977.

[23] W. C. Y. Lee, *Mobile Communication Engineering*, New York, NY. McGraw-Hill Book Co., 1989.

[24] F. Ikegami, S. Yoshida, T. Takeuchi, and M. Umehira, "Propagation factors controlling mean field strength on urban streets," *IEEE Trans. on Antennas and Propagation,* Vol. AP-32, pp. 822-829, December 1984.

[25] J. D. Parsons, *The Mobile Radio Propagation Channel,* New York, NY, John Wiley & Sons, Inc., 1989.

[26] Y. Okumura, E. Ohmori, T. Kawano, and K. Fukuda, "Field strength and its variability in VHF and UHF land-mobile service," *Rev. Elec. Commun. Lab*., Vol. 16, pp. 825–873, September–October 1968.

[27] M. Hata, "Empirical formula for propagation loss in land mobile radio services," *IEEE Trans. on Vehicular Technology,* Vol. VT-29, No. 3, pp. 317-325. August 1980.

[28] www.saic.com/products/software/urbana/, accessed on July 13, 2004.

[29] W. L. W. Lock, "Effects of Radio Wave Propagation in Urbanized Areas on UAV-GCS Command and Control," Masters Thesis, Naval Postgraduate School, Monterey, CA, December 2003.

[30] M. I. Skolnik, *Introduction to Radar Systems 3rd ed.,* McGraw-Hill, New York, NY, 2001.

THIS PAGE INTENTIONALLY LEFT BLANK

INITIAL DISTRIBUTION LIST

1. Defense Technical Information Center
   Ft. Belvoir, Virginia

2. Dudley Knox Library
   Naval Postgraduate School
   Monterey, California

3. Chairman
   Information Sciences Department
   Monterey, California

4. Professor David C. Jenn
   Department of Electrical and Computer Engineering
   Monterey, California

5. Professor Daniel C. Schleher
   Information Sciences Department
   Monterey, California

6. 1st. Lt. Fatih Pala
   Turkish Air Force
   Ankara, Turkey